COMPUTERIZED ANALYSIS OF
SHELLS—GOVERNING EQUATIONS†

DAVID BUSHNELL

Applied Mechanics Laboratory, Lockheed Palo Alto Research Laboratory, 3251 Hanover Street,
Palo Alto, CA 94304, U.S.A.

Abstract—This paper opens with a general discussion of terms in an energy functional which might be the basis from which equations governing stress, stability, and vibration analyses are derived. The energy expression includes strain energy of the shell and discrete stiffeners, kinetic energy of the shell and stiffeners, constraint conditions with Lagrange multipliers, and other terms arising from the change in direction of applied loads during deformation. Brief discussions are included of the coupling effect between bending and extensional energy needed for the analysis of layered composite shells or elastic–plastic shells, nonlinear terms, and the form that the energy expression takes upon discretization of the structure.

A section follows in which the energy formulation for stress, stability, and vibration analyses of an elastic curved beam is given, including thermal effects, moderately large rotations, boundary conditions, and distributed and concentrated loads. The matrix notation and type of discretization are introduced here which will later be used for the analysis of shells of revolution. Terms in the local element stiffness, mass, and load-geometric matrices are derived in terms of nodal point displacements, and it is shown how these local matrices are assembled into global matrices. The purpose of the section is to demonstrate the procedure for derivation of the analogous equations and quantities for shells of revolution or more complex structures.

The next section is on elastic shells of revolution. It opens with a summary of what computer programs exist for stress, buckling, and stability analyses of such structures. The assumptions on which these programs are based are listed and the various components of the energy functional, such as strain energy of the shell and discrete rings, are identified and derived in terms of nodal point displacements. Included are a derivation of the constitutive law for anisotropic shell walls and a formulation of nonlinear constraint conditions, which are required for the treatment of segmented or branched shells with meridional discontinuities between segments or branches. Derivations of terms in the global stiffness and load-geometric matrices and the force vector are given, with tables tracing the origin of each term. The computational strategy for calculation of critical bifurcation buckling loads in the presence of prebuckling nonlinearities is given, with an example of buckling under axial compression of a very thin cylinder. This is a simple problem to formulate but a difficult one to solve numerically, owing to the existence of closely spaced eigenvalues corresponding to nonsymmetric buckling at loads close to the load corresponding to nonlinear axisymmetric collapse. A description of various pitfalls encountered in the search for the lowest bifurcation buckling load is given, including estimates of the critical number of circumferential waves in the buckling mode. Computerized formulations and run times are compared for various discretization methods, including finite difference energy models and standard finite element models, with an example showing comparisons of rate of convergence with increasing nodal point density and computer times required to form stiffness matrices.

Hybrid bodies of revolution are discussed next. By "hybrid" is meant a body of revolution with both one-dimensionally and two-dimensionally discretized regions. The formulation is particularly useful for the stress, buckling, and vibration analyses of branched shells or ring-stiffened shells in which one is particularly interested in local effects within a distance equal to a shell wall thickness of a branch or ring. An appropriate strategy for the solution of nonlinear problems with simultaneous geometric nonlinearity and path-dependent material properties is described, including the development of the incremental constitutive law for the tangent stiffness method of treatment of elastic–plastic structures. The two-dimensionally discretized regions are modeled with use of 8-node isoparametric quadrilaterals of revolution. Details are presented on the formulation of constraint conditions for compatibility at junctions between rotationally symmetric shell segments (one-dimensionally discretized regions) and solid segments (two-dimensionally discretized regions).

The paper closes with a summary of linear equations for general shells. Surface coordinates, the first and second fundamental forms, and the definition of a shell are introduced, and the assumptions corresponding to Love's first approximation are identified. The differences in commonly used or referenced formulations are listed, including differences with regard to kinematic relations, expressions for total strain anywhere in the thickness of the shell wall, and expressions for stress and moment resultants. Comments are offered on which theory is the most suitable for engineering estimates.

GOVERNING EQUATIONS—AN INTRODUCTORY SUMMARY

The majority of computerized analyses of thin shells are based on an energy formulation, important exceptions being the programs for shells of revolution by Cohen[1], Kalnins[2], and Svalbonas[3] based on forward integration. Energy expressions can be used to demonstrate the kinds of terms that should be included in a reasonably comprehensive computer program intended to be widely used for the analysis of stress, buckling, and vibration of practical engineering shell structures.

STRAIN ENERGY

If the displacement method is used, the strain energy of the shell is expressed in terms of the strains and changes in curvature of the reference surface, which is not necessarily the middle surface or the neutral surface

$$U_{shell} = \frac{1}{2} \int_S (e^T C e + 2Ne) \, dS \tag{1}$$

where dS is the elemental area of the reference surface. The six element vector e represents the reference surface strains e_1, e_2, e_{12}, and changes in curvature κ_1, κ_2, κ_{12}; and C is a 6×6 symmetric matrix of coefficients which depends on the location of the wall material relative to the reference surface, on the details of the wall construction, on the temperature, and, if plasticity is present and the tangent stiffness method is used[4], on the stress–strain curve and flow law of the material. The quantity N is a vector containing thermal expansion effects, creep strains, and plastic strains. If plasticity is present or if the material properties depend on the temperature, the elements of C and N at a point on the reference surface must in general be determined by numerical integration through the thickness. Stricklin et al.[5] and Bushnell[4] point out that Simpson's rule should be used for the integration. Jones[6], Ashton et al.[7], and Ashton and Whitney[8] derive C for laminated wall construction.

Coupling between bending and extensional behavior

If the middle surface is the reference surface, and if the properties of the wall are symmetric with respect to this surface, then all those elements of C are zero through which stress resultants N_1, N_2, N_{12} cause changes in curvature κ_1, κ_2, κ_{12}, and through which moment resultants M_1, M_2, M_{12} cause normal strains of the reference surface. Generally, however, there exists coupling of bending and extensional behavior which cannot be eliminated by a shifting of the reference surface. Three common examples are shells reinforced in one direction by stiffeners that are eccentrically located with respect to the shell's neutral surface, shells stressed into the plastic region by a combination of stretching and bending, and nonuniformly heated shells constructed of temperature-dependent material. In the first example the neutral surface with regard to bending and stretching in one direction is in a different plane from the neutral surface with regard to bending and stretching in an orthogonal direction. In the second and third examples the location of the neutral surface changes with strain and temperature distribution. In all three of the examples it is not possible to choose *a priori* a reference surface location in order to eliminate coupling between extensional and bending terms in the energy expression. In

addition, it is often advantageous not to have to choose the middle surface as a reference surface, since practical monocoque shell structures often have variable wall thicknesses and doublers which make the middle surface difficult to describe mathematically and which cause its position to change abruptly in space. Coupling between bending and stretching energy is also present in shells with composite walls such as layered orthotropic, fiberwound, or semisandwich corrugated construction.

One of the first requirements of a computer program for shell analysis, therefore, is to permit arbitrary location of the reference surface with respect to the wall material and to include in the mathematical model the energy coupling between changes in curvature and normal strains of this surface. If the engineer is interested in performing analyses of many different kinds of shell structures, he is advised to obtain a computer program or programs which include coupled membrane and bending behavior. The traditional finite element model of a shell in which membrane and bending behavior are introduced through separate elements is not generally adequate.

Kinematic relations and nonlinear terms

In eqn (1) the strain vector e can be expressed in terms of displacement and rotation components and derivatives of these quantities. Kinematic relations have been given by many authors. The nonlinear strain-displacement equations of Love[9], Novoshilov[10], or Sanders[11] are acceptable as a basis for the displacement method. In general, non-linearities need not be retained in the change-in-curvature-displacement relations as long as the largest reference surface rotations are less than about 20°, which is usually the case. The normal strains e_1, e_2 and in-plane shear strain e_{12} can always be written so that the highest order nonlinearities are quadratic.

There is a good physical explanation for the need to retain nonlinear terms in the strain-displacement but not in the curvature-displacement relations. If a thin shell deflects a large amount, let us say an amplitude many times the thickness, the strains are usually small even though the deflections are rather large. Hence, the linear terms in the strain-displacement relations will tend to cancel each other, and the nonlinear terms will become significant for much smaller displacements than they would have if the linear terms had not tended to cancel. The linear terms in the expressions for the change in curvature, however, do not tend to cancel, and the wall rotations must be large indeed before nonlinear terms have to be included in these expressions.

Discretization—a brief summary

Finite element method. By far the majority of computer programs for shell analysis are based on the finite element method. Gallagher[12–14] gives surveys of the use of finite elements for linear and nonlinear analysis of general shells. Brombolich and Gould[15] present such a survey for shells of revolution. A detailed description of the various elements with evaluation will therefore not be presented here. Gallagher encapsulates the state-of-the-art as of 1972: "Three alternative forms of finite element representation of this curved shells are popular: (1) in 'faceted' form via the use of flat elements, (2) by means of isoparametric solid elements which have been specialized to represent curved thin shells, and (3) via the theories formulated directly for shallow or deep curved shells"[13].

Until about 1970 finite element experts using the dis-

placement method were insistent that the displacements of adjacent elements be fully compatible at the common boundary. Maintenance of slope and displacement compatibility does have the advantage of guaranteeing that convergence of displacements is monotonic from below and that eigenvalues for bifurcation buckling and modal vibrations converge monotonically from above (assuming that in the case of vibrations a consistent mass matrix is used). However, the enforcement of full interelement compatibility results in an overestimation of the stiffness of the structure, which tends to decrease the rate of convergence as the nodal point density is increased. Wilson[16] introduces incompatible displacement functions in order to improve the convergence properties.

A major drawback of incompatible elements used in bifurcation buckling analysis is the tendency of the discretized model to yield spuriously low buckling eigenvalues. For example, an engineer may wish to set up a discretized model in which the nodal points are locally concentrated in order that local buckling near some stress concentration be accurately predicted. However, because of the unfortunate property of convergence from below, this model may yield a physically unreasonable prediction of buckling in some areas where the compressive stresses are lower but the nodal point density is sparse. This spurious mode and others would likely prevent calculation of the local mode for which the locally dense mesh was originally established. The problem of spurious buckling modes becomes especially severe in cases for which an intuitive grasp of the expected behavior is weak.

Finite difference energy method. A few shell analyses have been performed and computer programs written based on the finite difference energy method, in which the displacement derivatives appearing in *e* (eqn 1) are replaced by finite difference expressions. Johnson[17] was the first to perform such an analysis with use of an arbitrary quadrilateral finite difference mesh. A widely used computer program based on this approach is BOSOR4, which treats stress, buckling, and vibration of axisymmetric shells[18].

A good test case. Bushnell[19] presents a comparison of the finite element method and the finite difference energy method, showing that in certain cases the finite difference energy method is actually a rapidly convergent kind of finite element method in which the element

displacements and rotations are incompatible at interelement boundaries. Figures 1 and 2, taken from [19], show the results of a convergence study involving a free hemisphere pinched by a $\cos 2\theta$ pressure distribution. This rather ill-conditioned problem is a very good test of various methods of discretization. The problem is ill-conditioned because small forces cause large displacements. Thus, the predicted reference surface strains are very small differences of relatively large numbers. The dotted line in Fig. 2 is obtained with use of a half-station finite difference energy method, which is equivalent to a finite element method based on linear functions for *u* and *v* and a quadratic function for *w*. Detailed descriptions of the finite elements are given in [19, 20]. Users and developers of computer programs for shell analysis and for general structures are urged to employ this case in order to determine the adequacy of the shell elements in the finite element libraries of their programs.

Discretized kinematic relations. With use of a discretization method, analytical kinematic relations $e = L(d)$, where L is a nonlinear differential operator and d is the displacement vector, can be expressed in the algebraic form

$$e_i = B_L d_i + d_i^T B_{NL} d_i. \tag{2}$$

The vector e_i represents reference surface strains and changes in curvature at some point i; d_i is the local nodal point displacement vector associated with i; and B_L and B_{NL} are $6 \times m$ matrices dependent on the local reference surface geometry and mesh spacing at i. The number of columns m of B_L and B_{NL} depends on how many nodal degrees of freedom are used in the discrete model. If eqn (1) is expressed in discrete form, and if the r.h.s. of eqn (2) is substituted into it, the strain energy expression for the thin shell becomes a quartic algebraic form in the d_i if C and N are independent of d_i.

Stiffener strain energy

Many practical shell structures are reinforced by stiffeners. Depending on the configuration these might be "smeared out" or treated as discrete elastic structures.

"Smeared" stiffeners. If there exists a regular pattern of reasonably closely spaced stiffeners, their contribution to the wall stiffness of the shell or plate might be modeled by an averaging of their extensional and bend-
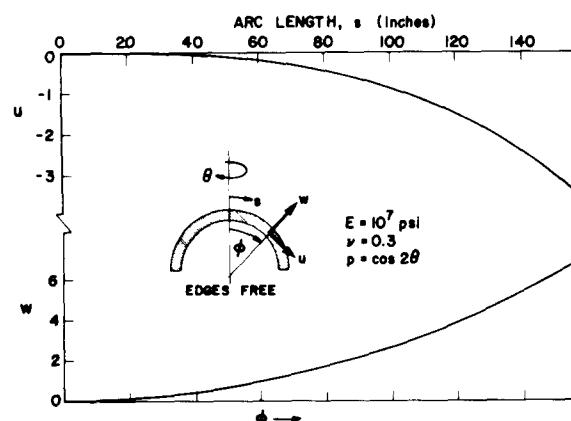

Fig. 1. Meridional and normal displacements at $\theta = 0$ of a hemisphere with a free edge subjected to pressure $p = \cos 2\theta$ (from Bushnell[19]).
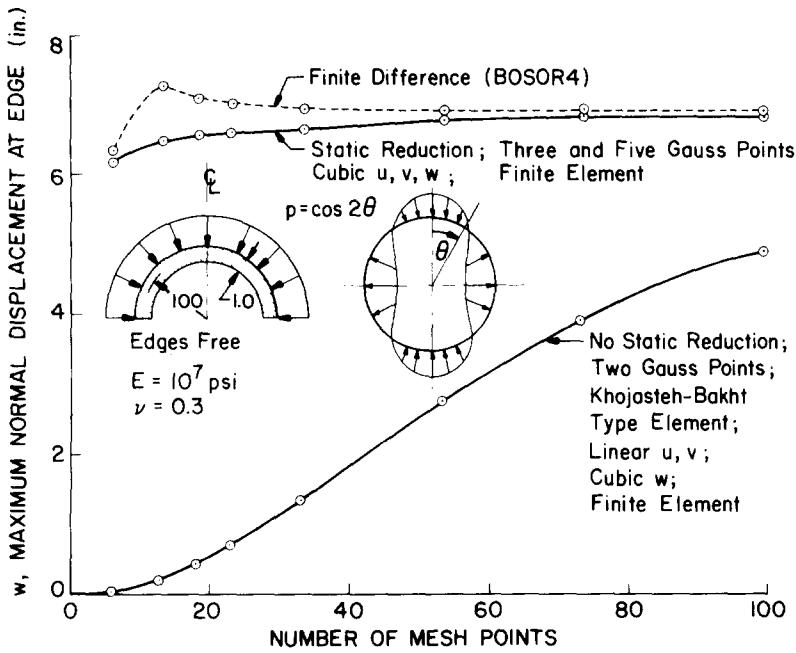
Fig. 2. Comparison of convergence of finite element method with finite difference energy method (from Bushnell[19]).

ing rigidities over arc lengths equal to the local spacings between them. Thus, the actual wall is treated as if it were orthotropic. This "smearing" process accounts for the fact that the neutral axes of the stiffeners do not in general lie in the plane of the reference surface of the shell wall. Predictions of buckling loads and vibration frequencies of stiffened cylinders have been found to be very sensitive to this eccentricity effect. A general rule of thumb for deciding whether to smear out the stiffeners or to treat them as discrete is that for smearing there should be about 2–3 stiffeners per half-wavelength of the deformation pattern. It may be appropriate to smear out stiffeners in a buckling or vibration analysis but, because of local stress concentrations caused by the stiffeners, not in a stress analysis. The stiffeners can be smeared as an analytical device to suppress local buckling and vibration modes. In order to handle problems involving smeared stiffeners, a computerized analysis must include coupling between bending and extensional energy as described earlier. The paper by Baruch and Singer[21] is a classic in the field of stiffened shell analysis.

Discrete stiffeners. If the stiffeners are so far apart that significant variations of displacement and stress occur between them, then they cannot be averaged over the entire shell surface but must be treated as discrete one-dimensional bodies. The standard approach is to assume that the cross section of the stiffener does not deform but that it translates and rotates in a fashion compatible with the shell to which it is attached. If plane sections of the stiffener remain planar and normal to the reference axis, the strain energy can be written in a form analogous to that for the shell:

$$U_{\text{stiffner}} = \frac{1}{2} \int_L (e_r^T \bar{G} e_r + 2N_r e_r) \, dL \tag{3}$$

where dL is the incremental length along the reference axis of the stiffener. The four-element vector e_r

represents the reference axis normal strain e_{r1}, changes in curvature κ_{r1}, κ_{r2} in two orthogonal planes, and twist κ_{r12}. $\bar{G}$ is in general a full 4×4 symmetric matrix of coefficients which depends on the location of the stiffener material relative to the reference axis, on details of the stiffener construction, on the temperature, and if plasticity is present and the tangent stiffness method is used, on the stress–strain curve and the flow law of the stiffener material. The vector N_r is analogous to N in eqn (1). If plasticity is present or if the material properties of the stiffener are temperature dependent, the elements of $\bar{G}$ and N_r at a point on the reference axis must in general be determined by numerical integration over the stiffener area. The reference axis strain e_{r1}, changes in curvature κ_{r1}, κ_{r2}, and twist κ_{r12} can be expressed in terms of the displacement and rotation components and derivatives of these quantities referred to the stiffener reference axis. With appropriate discretization, the stiffener strain vector e_r can be expressed in algebraic form as

$$e_{ri} = B_{Lr} d_{ri} + d_{ri}^T B_{NLr} d_{ri} \tag{4}$$

in which all quantities are analogous to those in eqn (2). Since the reference axis of the stiffener does not in general lie in the plane of the reference surface of the shell, the local displacement vector d_{ri} must be expressed in terms of the local shell reference surface displacement d_i

$$d_{ri} = E d_i \tag{5}$$

so that eqn (4) in terms of the dependent variables d_i becomes

$$e_{ri} = B_{Lr} E d_i + d_i^T E^T B_{NLr} E d_i. \tag{6}$$

If eqn (3) is expressed in discrete form and if the r.h.s. of

eqn (6) is substituted into it, the strain energy expression for the stiffener becomes a quartic algebraic form which is added to the shell strain energy.

LOADING

Two aspects of loading are of particular interest when thin shells are involved: (1) "live" load or following loads vs "dead" or constant-directional loads; and (2) loading by means of enforced displacement vs loading by prescribed external forces.

Live loads

A "live" or following load is a load the direction of which changes as the shell surface rotates. The expressions for work done by the external forces distributed over the shell surface and along the discrete stiffeners are, respectively

$$W_{shell} = \int_S (pd + d^T Pd)\, dS \tag{7}$$

$$W_{stiffener} = \int_L (qd_r + d_r^T Qd_r)\, dL. \tag{8}$$

The second terms in each integrand represent the live load effect. This effect should be included if the deflections or rotations are moderately large or, in modal vibration of bifurcation buckling problems, if the half-wavelength of the mode is the same order of magnitude as the smallest principal radius of curvature. Two examples in which the live load effect is significant are the bifurcation buckling or nonlinear collapse of a very long cylinder under external pressure and that of a ring under external radial compression. Inclusion of the live load effect lowers the predicted failure loads by about 30% in these cases.

Displacement vs force loading

Loading may be applied by means of a controlled displacement distribution (such as uniform end shortening of a cylinder) or by means of a controlled force distribution (such as uniformly applied axial force). A given thin shell structure may behave very differently under these two loading conditions. If a boundary displacement is imposed, a significant amount of stress

redistribution can occur. Flexible or "soft" parts of the structure deform considerably with more load subsequently being taken up by the stiff or "hard" parts. Figures 3 and 4 show shells for which this type of behavior occurs. At an axial load of about 200 lb the flat portions of the pear-shaped cylinder shown in Fig. 3 begin to bend. The load initially carried by these portions is transferred to the curved parts, which absorb an increasing percentage of the total load until these also buckle, resulting in a decreased load-carrying capacity. A similar phenomenon occurs in the case of the axially compressed cylinder with an elliptical cross section shown in Fig. 4. The perfect cylinder ($\xi = 0$) buckles at point A in a mode Δw shown in insert (a). However, significant post-buckling load-carrying capacity is exhibited at B and finally at C because the load initially carried by the flatter portions of the cross section ($S = 2.2$) has been transferred to the more highly curved portions ($S = 0$). Less stress redistribution can take place if the boundary forces are imposed, leading in general to earlier failure than for cases in which boundary displacements are imposed.

KINETIC ENERGY

In thin shell analysis it is not necessary to include rotatory inertia of the shell wall. There is a stronger case for including rotatory inertia of the discrete stiffeners, however. The kinetic energy of the shell and the stiffeners has the analytical form

$$K.E. = \frac{1}{2}\int_S \dot{d}^T m\dot{d}\, dS + \frac{1}{2}\int_L (\dot{d}_r^T m_r\dot{d}_r + \dot{\omega}_r^T I_r\dot{\omega}_r)\, dL \tag{9}$$

in which (˙) indicates differentiation with respect to time, m is the mass/area of the shell reference surface, m_r is the mass/length of discrete stiffener reference axis, ω_r is the rotation vector of the stiffener reference axis, and I_r is a matrix of rotatory inertia components of the stiffener referred to its reference axis. As before, various transformations are used in order to express all quantities in terms of the shell wall displacements. Whether or not the mass matrix is diagonal depends, of course, on the discretization model and the choice of nodal degrees of freedom.
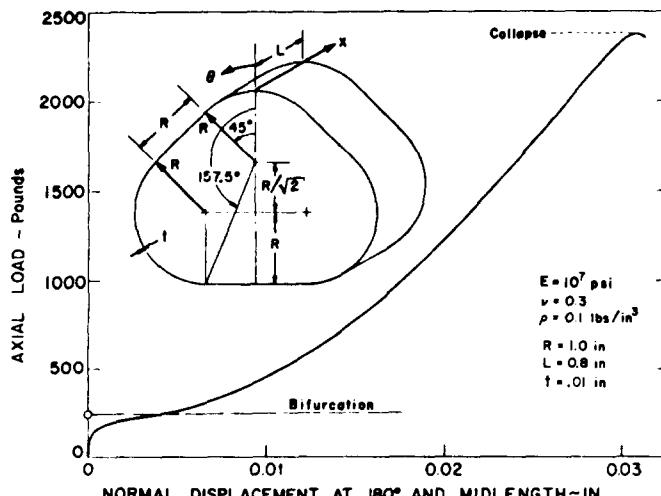

Fig. 3. Noncircular cylinder subjected to uniform end shortening (from Almroth and Brogan[22]).
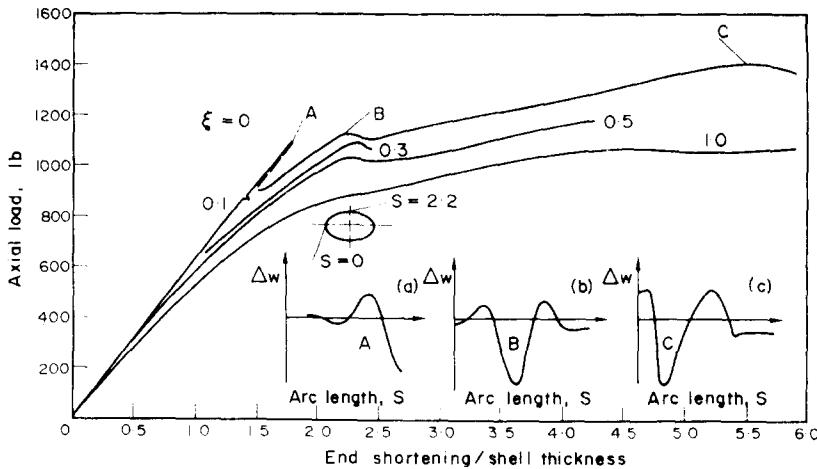
Fig. 4. Load-deflection curves for axially compressed perfect and imperfect elliptic cylinders (from Bushnell *et al.*[23]).

BOUNDARY AND OTHER CONSTRAINT CONDITIONS

The energy minimization problem (displacement method) is subject to constraint conditions corresponding to behavior at the boundaries of the shell or other locations within the domain where certain relationships between nodal point displacements are postulated to hold. These conditions may be linear or nonlinear. Two types of nonlinearity may exist: the first may result from continually changing geometry as loads are varied; the second may result from a sudden change in behavior as one part of a structure contacts another.

The constraint conditions might be introduced into the analytical model by means of Lagrange multipliers or by appropriate elimination of rows and columns of stiffness matrices. If the Lagrange multiplier method is used, a general nonhomogeneous, nonlinear constraint condition might assume the form

$$U_c = \lambda[d_a - T_L d_b - d_b{}^T T_{NL} d_b - d_0] \qquad (10)$$

in which U_c denotes an energy-like term pertaining to constraint conditions; λ is a vector of Lagrange multipliers; d_a and d_b are displacement vectors at different points, a and b, in the structure; and d_0 is an applied displacement.

A total energy expression H can be constructed from the r.h.s. of eqn (1)–(10). For a branched, segmented stiffened shell of revolution, the expression H might include:

- strain energy of shell segments, including smeared stiffeners (1)
- strain energy of discrete rings (3)
- potential energy of applied loads (7), (8)
- kinetic energy of shell segments (9)
- kinetic energy of discrete rings (9)
- constraint conditions for boundaries (10)
- constraint conditions for junctions between shell segments (10)

With appropriate substitutions of discretized displacement components q for continuous variables and numerical integration over the shell reference surface and over the lengths of discrete stiffeners, a non-

homogeneous quartic functional

$$H = \int_{t_1}^{t_2} f(q, \dot{q}; t) \, dt \qquad (11)$$

can be obtained in which the coefficients as well as the displacements may be time dependent. (Note that damping as well as fluid or soil structure interaction effects have been omitted in the above development.) Numerical solutions for problems involving linear and nonlinear static stress, bifurcation (eigenvalues) buckling, modal vibration with prestress, and linear and nonlinear dynamic response can be based on this functional. Through minimization with respect to the nodal point variables q, a set of simultaneous algebraic equations is generated. The nature of these equations and the best numerical methods for their solution depend on the type of problem that is being solved.

SECTION 2

ANALYSIS OF A CURVED BEAM

The foregoing discussion will be illustrated by a one-dimensional example—a curved beam shown in Fig. 5. The total energy expression H is given by

$$H = U - W + U_c - T \qquad (12)$$

in which U_s = strain energy; W = work done by external loads; U_c = constraint conditions (Lagrange multiplier formulation); and T = kinetic energy.

STRAIN ENERGY

The strain energy in the beam is given by

$$U_s = \frac{1}{2} \int_{vol} \sigma \epsilon_s \, dV \qquad (13)$$

in which σ is the stress and ϵ_s is the strain that produces σ:

$$\epsilon_s = \epsilon - \alpha T. \qquad (14)$$
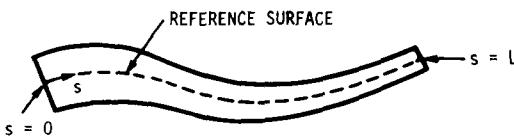
Fig. 5. Curved beam of developed length, L.

The quantity ϵ is the total strain and T is the temperature rise above the zero-stress state.

It is assumed that plane sections remain plane, normal sections remain normal, and the beam deforms only in the plane of the paper. Displacements and coordinates are shown in Fig. 6.

The total strain $\epsilon(s, z)$ can be expressed in terms of the strain and change in curvature of the reference surface:

$$\epsilon(s, z) = e(s) - z\kappa(s) \tag{15}$$

and the reference surface quantities e and κ can be expressed in terms of the displacements:

$$e = du/dx + w/R + \frac{1}{2}\beta^2$$

$$\kappa = d\beta/ds \tag{16}$$

where

$$\beta = dw/ds - u/R \tag{17}$$

$R(s)$ is the local radius of curvature of the reference surface of the beam, and β is the rotation as shown in Fig. 7.

The stress σ is given by

$$\sigma = E(\epsilon - \alpha T) \tag{18}$$

where E is the modulus of elasticity and α is the coefficient of thermal expansion.
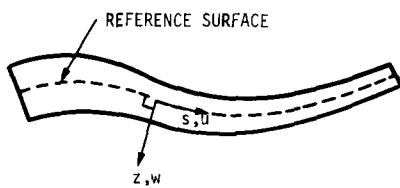
Fig. 6. Coordinates (s, z) and displacements (u, w).
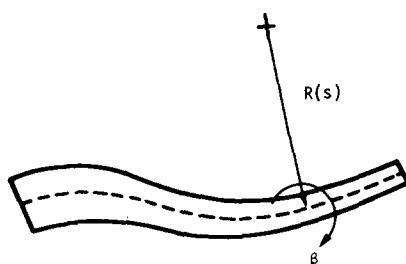
Fig. 7. Local radius of curvature $R(s)$ and rotation β.

Using eqns (14), (15) and (18), and assuming that the beam is of unit depth normal to the plane of the paper, one can write eqn (13) in the form

$$U_s = \frac{1}{2} \int_s \int_z \left(\lfloor e, \kappa \rfloor \begin{bmatrix} E & -Ez \\ -Ez & Ez^2 \end{bmatrix} \begin{Bmatrix} e \\ \kappa \end{Bmatrix} \right.$$
$$\left. - 2E\alpha T \lfloor 1, -z \rfloor \begin{Bmatrix} e \\ \kappa \end{Bmatrix} + E\alpha^2 T^2 \right) dz\,ds \tag{19}$$

in which $\lfloor \rfloor$ denotes a row vector, $[\ ]$ a matrix, and $\{\}$ a column vector.

The quantity $\lfloor e, \kappa \rfloor$ denotes a row vector with two elements, e and κ. Equation (19) is derived in Fig. 8.

Integration with respect to z, and neglect of the term $E\alpha^2 T^2$, which does not contain any dependent variables, leads to

$$U_s = \frac{1}{2} \int_s \left(\lfloor e, \kappa \rfloor \begin{bmatrix} C_{11} & C_{12} \\ C_{12} & C_{22} \end{bmatrix} \begin{Bmatrix} e \\ \kappa \end{Bmatrix} + 2\lfloor N^T, M^T \rfloor \begin{Bmatrix} e \\ \kappa \end{Bmatrix} \right) ds \tag{20}$$

in which

$$C_{11} \equiv \int_z E\,dz; \quad C_{12} \equiv -\int_z Ez\,dz; \quad C_{22} \equiv \int_z Ez^2\,dz$$

$$N^T = -\int_z E\alpha T\,dz; \quad M^T \equiv \int_z E\alpha Tz\,dz. \tag{21}$$

The strain energy can be expressed in terms of the displacements and their derivatives with use of eqns (16) and (17).

EXTERNAL LOADING

Suppose that the beam is submitted to loading as shown in Fig. 9(a). The reference surface is considered to be loaded by constant-directional distributed pressure p_n and traction p_t, and constant-directional end loads, V, H and M.

The work done by the applied loads shown in Fig. 9(a) is

$$W = \int_s (p_t u + p_n w)\,ds + Hu_L^* + Vw_L^* + M\beta_L \tag{22}$$

provided the loads act in a constant direction as the beam deforms.

In matrix notation, eqn (22) becomes

$$W = \int_s \lfloor p_t, p_n, 0 \rfloor \begin{Bmatrix} u \\ w \\ \beta \end{Bmatrix} ds + \lfloor H, V, M \rfloor \begin{Bmatrix} u_L^* \\ w_L^* \\ \beta_L \end{Bmatrix}. \tag{23}$$

CONSTRAINT CONDITIONS

Suppose the beam is supported as shown in Fig. 10. The terms in U_c (eqn 12) are

$$U_c = \lambda_{01} u^*(0) + \lambda_{02} w^*(0) + \lambda_{03}\beta(0)$$
$$+ \lambda_{L1} 0 + \lambda_{L2} w^*(L) + \lambda_{L3} 0 \tag{24}$$

or in matrix notation

$$U_c = \lfloor \lambda_{01}, \lambda_{02}, \lambda_{03} \rfloor \begin{Bmatrix} u^* \\ w^* \\ \beta \end{Bmatrix}_0 + \lfloor \lambda_{L1}, \lambda_{L2}, \lambda_{L3} \rfloor \begin{Bmatrix} 0 \\ w^* \\ 0 \end{Bmatrix}_L. \tag{25}$$

$$U_s = \frac{1}{2}\int_{vol} \sigma \epsilon_s \, dV \qquad (13)$$

$$\epsilon_s = \epsilon - \alpha T \qquad (14)$$

$$\epsilon = e - z\kappa \qquad (15)$$

$$\sigma = E(\epsilon - \alpha T) \qquad (16)$$

$$U_s = \iint_{s,z} \frac{E}{2}(e - z\kappa - \alpha T)^2 \, dz\,ds$$

$$U_s = \iint_{s,z} E\left(\lfloor 1, -z\rfloor \begin{Bmatrix} e \\ \kappa \end{Bmatrix} - \alpha T\right)^2 dz\,ds$$

$$U_s = \iint_{s,z}\left[\overset{A}{E\left(\lfloor 1, -z\rfloor \begin{Bmatrix} e \\ \kappa \end{Bmatrix}\right)^2} - \overset{B}{2E\alpha T\lfloor 1, -z\rfloor\begin{Bmatrix} e \\ \kappa \end{Bmatrix}} + E\alpha^2 T^2\right] dz\,ds$$

$$U_s = \iint_{s,z}\left[\overset{B^T}{\lfloor e, \kappa\rfloor}\overset{A^T}{\begin{Bmatrix}1\\-z\end{Bmatrix}}E\overset{A}{\lfloor 1,-z\rfloor}\overset{B}{\begin{Bmatrix}e\\\kappa\end{Bmatrix}} - 2E\alpha T\lfloor 1,-z\rfloor\begin{Bmatrix}e\\\kappa\end{Bmatrix} + E\alpha^2 T^2\right]dz\,ds$$

$$\int_z \begin{bmatrix} E & -Ez \\ -Ez & Ez^2 \end{bmatrix} dz \cong \begin{bmatrix} C_{11} & C_{12} \\ C_{12} & C_{22} \end{bmatrix} \qquad \int_z 2E\alpha T\lfloor 1, -z\rfloor \, dz \cong 2\lfloor N^T, M^T\rfloor$$

Fig. 8. Derivation of eqns (19) and (20).

Equation (25) can be written in a more general form

$$U_c = \lfloor\lambda_0\rfloor \overset{3\times3}{[K_A]} \begin{Bmatrix} u^* \\ w^* \\ \beta \end{Bmatrix}_0 + \lfloor\lambda_L\rfloor \overset{3\times3}{[K_B]} \begin{Bmatrix} u^* \\ w^* \\ \beta \end{Bmatrix}_L \qquad (26)$$

where, in the case of eqn (25)

$$\overset{3\times3}{[K_A]} = \begin{bmatrix} 1 & & \\ & 1 & \\ & & 1 \end{bmatrix}; \qquad \overset{3\times3}{[K_B]} = \begin{bmatrix} 0 & & \\ & 1 & \\ & & 0 \end{bmatrix}. \qquad (27)$$

KINETIC ENERGY

The kinetic energy of the beam is

$$T = \frac{1}{2}\int_s [m(\dot{u}^2 + \dot{w}^2) + I_m\dot{\beta}^2]\,ds \qquad (28)$$

in which (˙) denotes differentiation with respect to time, m is the mass/length of reference surface arc, and I_m is the mass moment of inertia of the beam cross section. If one is concerned with modal vibrations

$$(\dot{u}, \dot{w}) = i\Omega\cdot(u, w) \qquad (29)$$

in which Ω is the modal angular frequency.

In matrix form eqn (28) becomes

$$T = -\frac{\Omega^2}{2}\int_s \lfloor u, w, \beta\rfloor \overset{3\times3}{[M]} \begin{Bmatrix} u \\ w \\ \beta \end{Bmatrix} ds \qquad (30)$$

where

$$[M] \equiv \begin{bmatrix} m & 0 & 0 \\ 0 & m & 0 \\ 0 & 0 & I_m \end{bmatrix}. \qquad (31)$$

DISCRETIZATION

Now assume that the beam is modeled as a series of discrete elements, with nodal point displacements distributed as shown in Fig. 11. The continuous dependent variables (u, w) must be expressed in terms of nodal point quantities.

In the special case with the degrees of freedom distributed as shown in Fig. 11 the finite elements are most appropriately chosen to extend between adjacent u-points. The energy in the beam is then given approximately by the sum over the number of elements of the energy density at the midlength of each element times the arc length h_i of that element.

If the nodal point spacing is constant, the energy in the ith finite element in Fig. 11, e.g. is evaluated at w_i. At this point the quantities appearing in eqns (16) and (17) can be written in terms of nodal point displacements as follows:

$$u = (u_{i-1} + u_i)/2$$

$$w = w_i \qquad (32)$$

$$\beta_i = (w_{i+1} - w_{i-1})/(2h_i) - (u_{i-1} + u_i)/(2R_i)$$

$$e_i = (u_i - u_{i-1})/h_i + w_i/R_i + \frac{1}{2}\beta_i^2$$

$$\kappa_i = (w_{i+1} - 2w_i + w_{i-1})/h_i^2 \qquad (33)$$

$$- [(u_i + u_{i-1})/2](1/R_i)' - (u_i - u_{i-1})/(h_iR_i)$$
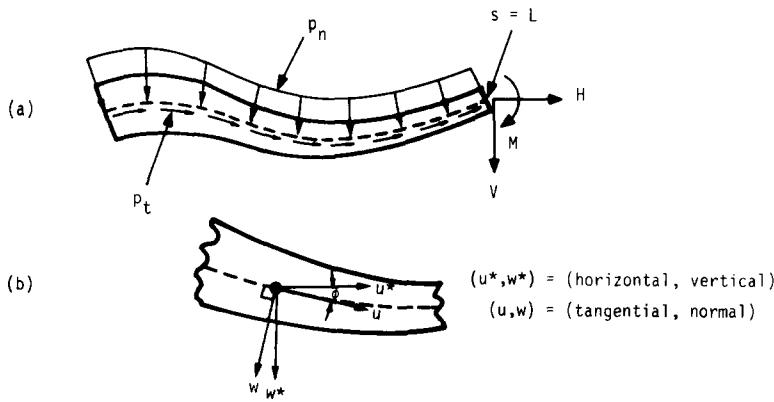
Fig. 9. (a) Loading on the beam; (b) Displacement notation.
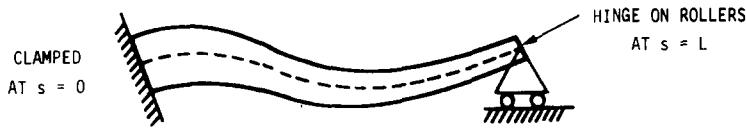
Fig. 10. Boundary conditions.

in which $(\ )'$ denotes differentiation with respect to the reference surface arc length, s.

In matrix form eqns (32) can be written as

$$\left\{\begin{matrix} u \\ w \\ \beta \end{matrix}\right\} = \overset{3\times5}{[D]}\{q\} \tag{34}$$

with

$$\overset{3\times5}{[D]} = \begin{bmatrix} 0 & 1/2 & 0 & 1/2 & 0 \\ 0 & 0 & 1 & 0 & 0 \\ -1/(2h_i) & -1/(2R_i) & 0 & -1/(2R_i) & 1/(2h_i) \end{bmatrix} \tag{35}$$

and

$$\lfloor q \rfloor = \{q\}^T = \lfloor w_{i-1}, u_{i-1}, w_i, u_i, w_{i+1} \rfloor. \tag{36}$$

The reference surface strain and change in curvature are given in matrix form by

$$\left\{\begin{matrix} e \\ \kappa \end{matrix}\right\} = \overset{2\times5}{[B]}\{q\} + \left\{\begin{matrix} \frac{1}{2}\beta_i^2 \\ 0 \end{matrix}\right\}$$

$$= [B]\{q\} + \left\{\begin{matrix} \frac{1}{2}\lfloor q\rfloor\overset{5\times5}{[B_{NL}]}\{q\} \\ 0 \end{matrix}\right\} \tag{37}$$

with

$$\overset{2\times5}{[B]} = \begin{bmatrix} 0 & -1/h_i & 1/R_i & 1/h_i & 0 \\ 1/h_i^2 & \left(-\frac{1}{2}\left(\frac{1}{R}\right)'+\frac{1}{h_iR_i}\right) & -2/h_i^2 & \left(-\frac{1}{2}\left(\frac{1}{R}\right)'-\frac{1}{h_iR_i}\right) & 1/h_i^2 \end{bmatrix} \tag{38}$$

and

$$\overset{5\times5}{[B_{NL}]} = \{\bar{R}\} \overset{5\times1}{\underset{1\times5}{\lfloor \bar{R} \rfloor}} \tag{39}$$

in which the vector $\lfloor \bar{R} \rfloor$ is given by the third row of $[D]$:

$$\lfloor \bar{R} \rfloor = \lfloor -1/(2h_i), -1/(2R_i), 0, -1/(2R_i), +1/(2h_i) \rfloor. \tag{40}$$

In the derivation of the total energy functional H of the ith finite element, matrix formulas for $\lfloor u^*, w^*, \beta \rfloor$, which appears in eqns (23) and (26) are also needed. If the angle between the tangent to the reference surface and the horizontal is ϕ, as shown in Fig. 9, then the vector $\lfloor u^*, w^*, \beta \rfloor$ is related to the vector of nodal point degrees of freedom by

$$\left\{\begin{matrix} u^* \\ w^* \\ \beta \end{matrix}\right\} = \overset{3\times3}{[\bar{T}]}\overset{3\times5}{[D]}\{q\} \tag{41}$$

in which

$$[\bar{T}] \equiv \begin{bmatrix} \cos\phi & -\sin\phi & 0 \\ \sin\phi & \cos\phi & 0 \\ 0 & 0 & 1 \end{bmatrix}. \tag{42}$$

TOTAL ENERGY OF AN ELEMENT

With use of eqns (20) and (37) for U_s; eqns (23), (34) and (41) for W; eqns (26) and (41) for U_c, and eqns (30) and (34) for T, one can form the expression for the total
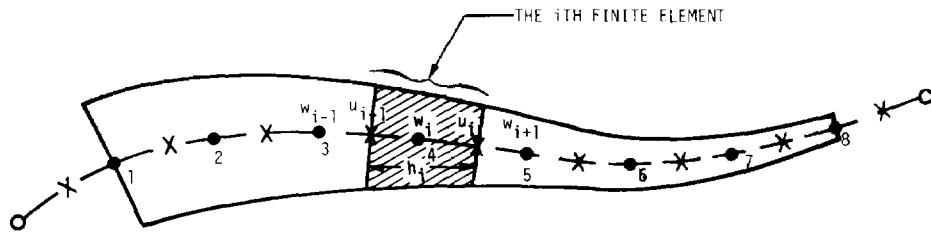
Fig. 11. Discretized model of the curved beam.

"energy" H_i of the ith finite element

$$H_i = U_i - W_i + U_{ci} - T_i \qquad (43)$$

in terms of the nodal point degrees of freedom. The strain energy of the ith finite element is:

$$U_{si} = \frac{h_i}{2}\left[\left(\overset{1\times 5}{\lfloor q \rfloor}\overset{5\times 2}{[B]^T} + \left\lfloor\frac{1}{2}\beta_i^2, 0\right\rfloor\right)\overset{2\times 2}{[C]}\left(\overset{2\times 5}{[B]}\overset{5\times 1}{\{q\}} + \left\{\begin{matrix}\frac{1}{2}\beta_i^2\\0\end{matrix}\right\}\right)\right.$$
$$\left. + 2\lfloor N^T, M^T\rfloor\left(\overset{2\times 5}{[B]}\overset{5\times 1}{\{q\}} + \left\{\begin{matrix}\frac{1}{2}\beta_i^2\\0\end{matrix}\right\}\right)\right]. \qquad (44)$$

The work done by external loads is:

$$W_i = \lfloor p_t, p_n, 0\rfloor[D]\{q\}h_i + \lfloor H, V, M\rfloor[\bar T][D]\{q\}\delta_L{}^i. \qquad (45)$$

The constraint condition "energy" is:

$$U_{ci} = \lfloor\lambda_0\rfloor[K_A][\bar T][D]\{q\}\delta_0{}^i + \lfloor\lambda_L\rfloor[K_B][\bar T][D]\{q\}\delta_L{}^i \qquad (46)$$

and the kinetic energy is:

$$T_i = -(\Omega^2/2)\lfloor q\rfloor[D]^T[M][D]h_i\{q\}. \qquad (47)$$

Note that in eqns (44), (45) and (47) the reference axis arc length increment ds_i has been replaced by the nodal point spacing h_i. The Kronecker deltas appearing in eqns (45) and (46) are defined by

$$\delta_L{}^i = 0 \text{ if } i \neq i_L; \quad \delta_L{}^i = 1 \text{ if } i = i_L$$
$$\delta_0{}^i = 0 \text{ if } i \neq i_0; \quad \delta_0{}^i = 1 \text{ if } i = i_0 \qquad (48)$$

in which i_L means "i at $s = L$"; i_0 means "i at $s = 0$". At the ends of the beam the energy density is multiplied by one-half the spacing between adjacent u-nodes.

LOCAL AND GLOBAL STIFFNESS AND MASS MATRICES

If the nonlinear term $(1/2)\beta^2$ in eqn (33a) is neglected, the strain energy U_k of the kth finite element is simplified:

$$U_k = \frac{1}{2}[\underbrace{\lfloor q\rfloor h_k[B]^T[C][B]\{q\}}_{\substack{5\times 5\\ [K]^k}} + 2h_k\lfloor N^T, M^T\rfloor[B]\{q\}] \qquad (49)$$

The 5×5 matrix $[K]^k = h_k[B]^T[C][B]$ is called the local element stiffness matrix of the unloaded, undeformed finite element. The (i, j)th member of this matrix K_{ij}^k is generated by differentiating U_k with respect to q_i and q_j, or calculating the second variation of U_k:

$$\frac{\partial^2 U_k}{\partial q_i \partial q_j} \equiv K_{ij}^k. \qquad (50)$$

The global stiffness matrix $[K]$ for the entire beam is calculated by assembling or accumulating local element stiffness matrices into a "master" or global array, as shown in Fig. 12. The positions of the filled members of the global stiffness matrix depend on the numbering scheme used for the nodal point degrees of freedom. For the simple example of the beam, the nodal point degrees of freedom are logically numbered in increasing order from left to right, resulting in compact storage of each 5×5 local stiffness matrix within the $N\times N$ global array, where N is the number of degrees of freedom of the entire discretized model. As seen from Fig. 12, this numbering scheme results in a global stiffness matrix which is narrowly banded about the main diagonal. Solving such one-dimensional equilibrium, vibration, or stability problems on the computer requires much less computer time and storage than do problems of higher dimensionality.

Figure 13 shows the lower triangular part of a stiffness matrix for a more complex "branched" one-dimensionally discretized structure. Included in the matrix are terms of the type K_{ij}^k, indicated by x's, boundary condition terms of the type

$$[Q] = [K_A][\bar T][D] \qquad (51)$$

from eqn (46), and juncture condition terms, not yet described, corresponding to stations at which Segment ② is fastened to Segment ①. Although the bandwidth of this stiffness matrix is locally large at structural branch points, the average bandwidth becomes relatively smaller as the nodal point density in the two structural segments is increased, resulting in inexpensive computer runs.

The local mass matrices

$$[M]^k = h_k[D]^T[M][D] \qquad (52)$$

are assembled into a global mass matrix, and the local force vectors (eqn 45)

$$\{F_d\}^k = h_k\lfloor p_t, p_n, 0\rfloor[D] \qquad \left(\begin{matrix}\text{distributed}\\\text{loads}\end{matrix}\right) \qquad (53)$$
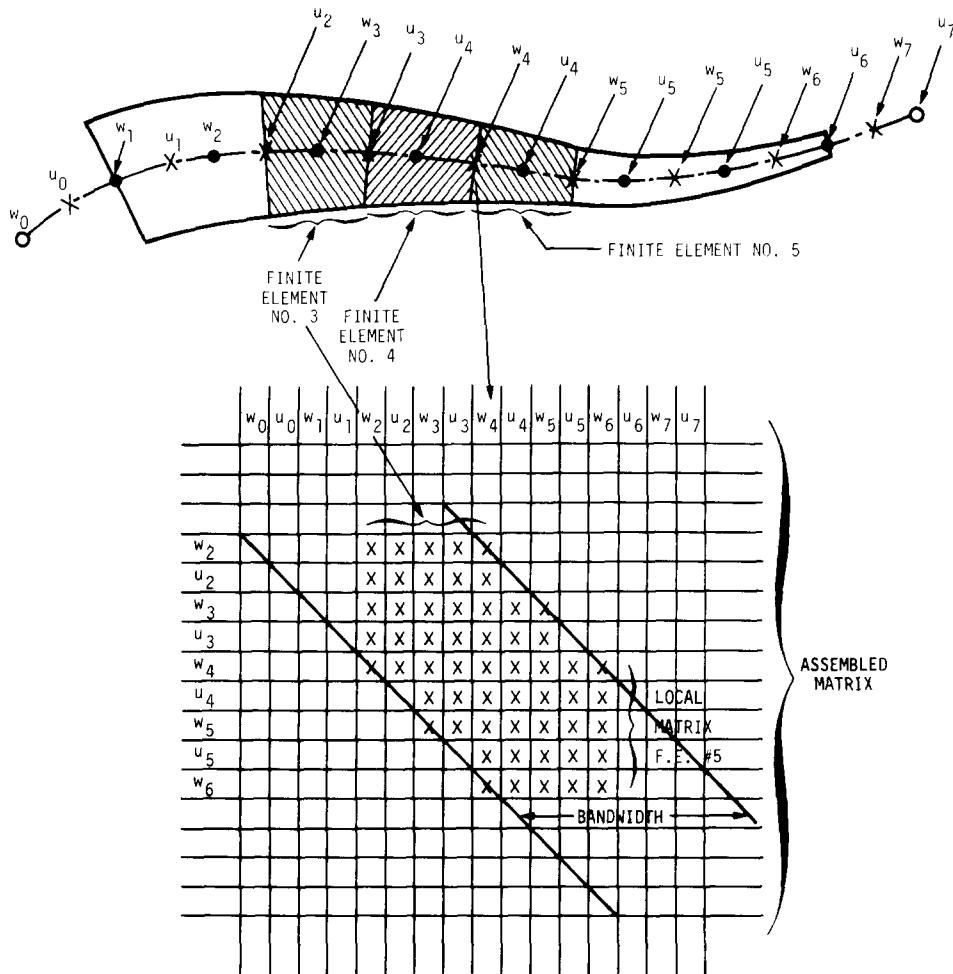
Fig. 12. Local and Assembled matrix architecture.

$$\{F_b\}^k = \lfloor H, V, M \rfloor [\bar{T}][D]\delta_L^{\ k} \quad \begin{pmatrix} \text{boundary or} \\ \text{concentrated} \\ \text{loads} \end{pmatrix}$$

$$(54)$$

are assembled into a global force or "right-hand-side" vector in a manner completely analogous to that just described in connection with the stiffness matrix.

If the discretization scheme shown in Fig. 11 and specified by eqn (32) is used for derivation of the mass matrix, this matrix will have the same form as the stiffness matrix, part of which is shown in Fig. 12. In order to obtain a diagonal mass matrix, one must assign a lumped mass to each displacement degree of freedom. For example, in the interior of the beam shown in Fig. 11, half the mass of element i might be assigned to nodal degree of freedom u_{i-1}, half to u_i and the full mass to w_i. The boundary and segment junction conditions represented by the matrices $[Q]$ and $[D]$ in the global stiffness matrix shown in Fig. 13 would be filled with zeroes in the corresponding global mass matrix.

EQUILIBRIUM, BUCKLING AND VIBRATION

According to the principle of stationary energy, or minimum potential energy, a structure is in equilibrium if

$$\frac{\partial H}{\partial x_i} = 0 \quad i=1,2,\ldots N \qquad (55)$$

where x_i represents a nodal degree of freedom or a Lagrange multiplier, and N is the total number of degrees of freedom in the system including the Lagrange multipliers. The terms in the global matrices governing equilibrium, buckling, or modal vibration can be derived by application of this principle to each finite element of the structural system.

Equilibrium

Because of the appearance of β_i^2 in eqn (44), eqn (55) represents a system of simultaneous nonlinear algebraic equations. These nonlinear algebraic equations are solved with use of the Newton–Raphson method. The first variation $\partial H / \partial x_i$ is expanded in a Taylor series about a known solution, $\{x_0\}$, with retention up to linear terms in $\{\Delta x\}$ only:

$$\partial H / \partial x_i = \partial H(x_0 + \Delta x) / \partial x_i = \partial H(x_0) / \partial x_i + \sum_{j=1}^{N} \frac{\partial^2 H(x_0)}{\partial x_i \partial x_j} \Delta x_j = 0$$

$$(56)$$

$$i = 1,2,\ldots N.$$

Equation (56) is solved for $\Delta x_j, j=1,2,\ldots N$; a new trial solution $\{x_0 + \Delta x\}$ is then available; and the solution of eqn (56) with $\{x_0\}$ replaced by $\{x_0 + \Delta x\}$ is carried out for a new $\{\Delta x\}$. Iterations continue until $|\{\Delta x/x\}|$ is smaller than some prespecified number. (In the discussion of the
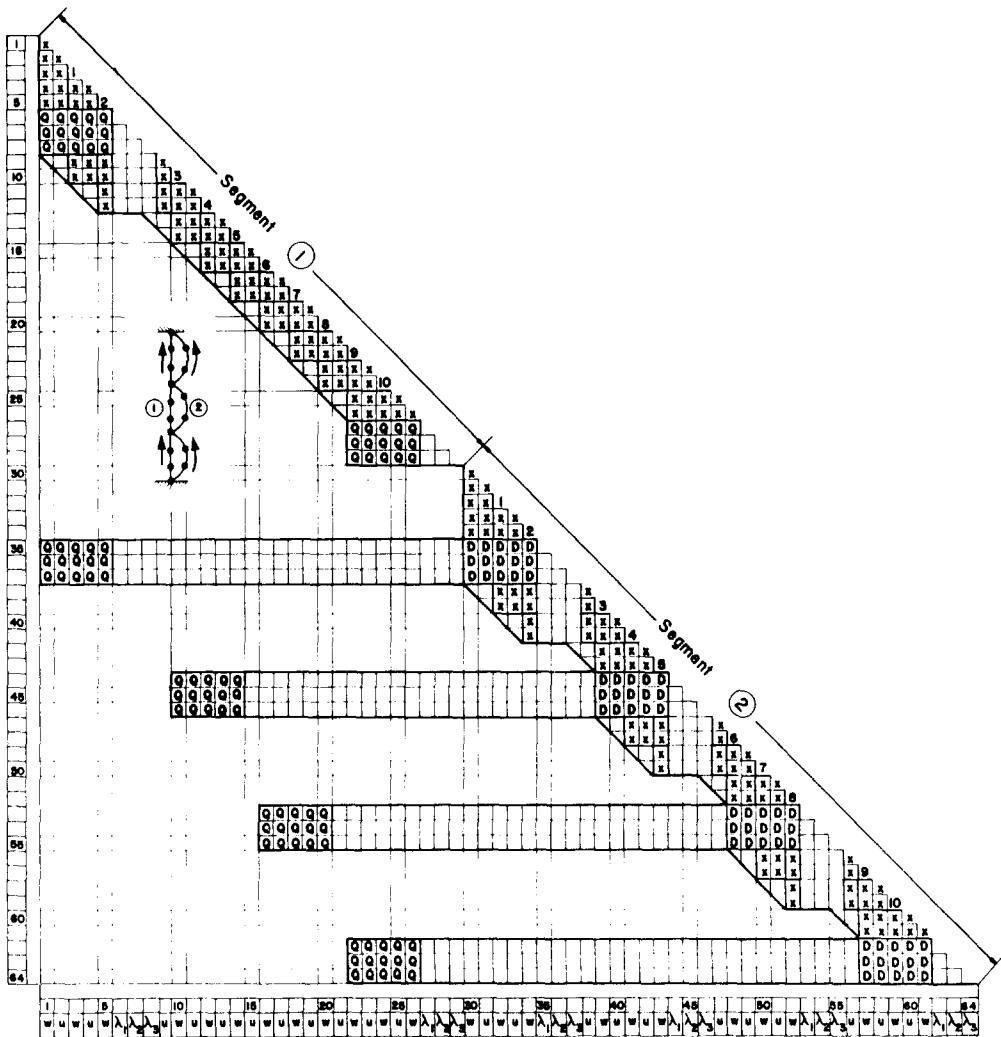
Fig. 13. Stiffness matrix configuration for 2-segment, one-dimensionally discretized structure with intermittent fasteners (from Bushnell[18]).

Newton–Raphson method the kinetic energy is assumed to be omitted from eqn 12.)

Bifurcation buckling

Figure 14 shows a load-deflection curve with a bifurcation point at $(p_{cr}, \|x_0\|)$, in which $\|x_0\|$ is a generalized displacement conjugate to the load p_{cr}.

Since the bifurcation point is on the equilibrium path O–A, it is known that

$$\frac{\partial H(x_0)}{\partial x_i} = 0 \quad i = 1, 2, \ldots N. \tag{57}$$

In order to determine if $\{x_0\}$ is a bifurcation point, one must check to see if

$$\frac{\partial H(x_0 + x^b)}{\partial x_i^b} = 0 \quad i = 1, 2, \ldots N \tag{58}$$

where $\{x^b\}$ is a non-trivial infinitesimal buckling mode. Expansion of H in a Taylor Series about $\{x_0\}$, as before, yields

$$\frac{\partial H(x_0)}{\partial x_i^b} + \sum_{j=1}^{N} \frac{\partial^2 H(x_0)}{\partial x_i^b \partial x_j^b} x_j^b + \text{h.o.t.} = 0 \quad i = 1, 2, \ldots N. \tag{59}$$

Since $\{x_0\}$ is an equilibrium state, the first term of eqn (59) is zero, so that the bifurcation buckling equations become

$$\sum_{j=1}^{N} \frac{\partial^2 H(x_0)}{\partial x_i \partial x_j} x_j^b = 0 \quad i = 1, 2, \ldots N \tag{60}$$

These equations are linear and homogeneous in $x_j^b, j = 1, 2, \ldots N$. A non-trivial solution $\{x^b\}$ exists only for certain discrete values, the eigenvalues, of the matrix

$$\partial^2 H(x_0)/\partial x_i^b \partial x_j^b, \quad i, j = 1, 2, \ldots N. \tag{61}$$

General equations

In order to solve equilibrium and buckling (or vibration) problems, one must obtain the vector $\partial H(x_0)/\partial x_i$, $i = 1, 2, \ldots N$ and the matrix $\partial^2 H(x_0)/\partial x_i \partial x_j$, $i, j = 1, 2, \ldots N$. To derive these quantities one starts from eqns (44) to (47), assuming that the displacement state $\{q\}$ is given by $\{q_0 + q^b\}$, $\beta = \beta_0 + \beta^b$, where $\{q^b\}$ and β^b are considered to be small compared to $\{q_0\}$ and β_0, and the superscript b may signify either a correction to the trial solution in the Newton–Raphson iterations or a buckling or vibration modal quantity. One
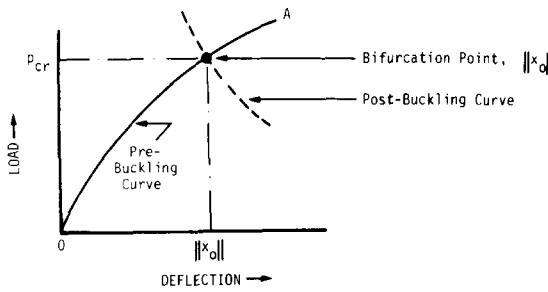
Fig. 14. Bifurcation buckling at p_{cr} from prebuckling equilibrium state determined from nonlinear equations.

inserts

$$\{q\}=\{q_0+q^b\}; \quad \beta=\beta_0+\beta^b \tag{62}$$

into eqns (44)–(47), then differentiates with respect to x_i, which represents one of the components of the vector $\{q\}$. Note that the rotation β is given by

$$\beta=\lfloor \bar{R} \rfloor \{q\} \tag{63}$$

in which $\lfloor \bar{R} \rfloor$ is given by eqn (40).

Dealing with just the first line of eqn (44), assuming that $\{q\}=\{q_0+q^b\}$, and making use of eqn (63) for β, one finds that this first line of eqn (44) contributes the following terms to the first variation of H for the kth finite element:

$$\frac{\partial H(q_0+q^b)}{\partial q_i^b}=\frac{h_k}{2}\left[\left(\lfloor q_0+q^b \rfloor [B]^T\right.\right.$$
$$+\left\lfloor \left(\frac{1}{2}\beta_0^2+\beta_0\beta^b+\frac{1}{2}\beta^{b2}\right),0\right\rfloor\right)[C]$$
$$\times\left(\{B_i\}+\left\{\begin{matrix}\beta_0\bar{R}_i+\beta^b\bar{R}_i\\0\end{matrix}\right\}\right)$$
$$+\left(\lfloor B_i \rfloor+\lfloor \beta_0\bar{R}_i+\beta^b\bar{R}_i,0 \rfloor\right)[C] \tag{64}$$
$$\left.\times\left([B]\{q_0+q^b\}+\left\{\begin{matrix}\left(\frac{1}{2}\beta_0^2+\beta_0\beta^b+\frac{1}{2}\beta^{b2}\right)\\0\end{matrix}\right\}\right)\right].$$

If one now allows $\{q^b\}\to 0$, identifies q_i^b as one of the global displacement degrees of freedom x_i, and includes terms from eqns (45) and (46) in the first variation of H, one obtains

$$\frac{\partial H(q_0)}{\partial q_i^b}=\frac{\partial H(x_0)}{\partial x_i}$$

$$=\left[\left(\lfloor q_0 \rfloor [B]^T+\left\lfloor\frac{1}{2}\beta_0^2,0\right\rfloor\right)[C]\left(\{B_i\}+\left\{\begin{matrix}\beta_0\bar{R}_i\\0\end{matrix}\right\}\right)\right.$$

$$\left.+\lfloor N^T,M^T \rfloor\left(\{B_i\}+\left\{\begin{matrix}\beta_0\bar{R}_i\\0\end{matrix}\right\}\right)\right]h_k \tag{65}$$

$$-\left(\lfloor p_t,p_n,0 \rfloor\{D_i\}h_k+\lfloor H,V,M \rfloor\{[\bar{T}][D]\}_i\delta_L^k\right)$$

$$+\lfloor \lambda_0 \rfloor\{[K_A][\bar{T}][D]\}_i\delta_0^k+\lfloor \lambda_L \rfloor\{[K_B][\bar{T}][D]\}_i\delta_L^k.$$

If x_i is a Lagrange multiplier one obtains the same expression as eqn (65) except the fourth line in eqn (65) is replaced by

$$\lfloor q_0 \rfloor\{[[K_A][\bar{T}][D]]^T\}_i\delta_0^k+\lfloor q_0 \rfloor\{[[K_B][\bar{T}][D]]^T\}_i\delta_L^k. \tag{66}$$

The elements in the generalized stiffness matrix $\partial^2 H(x_0)/\partial x_i\,\partial x_j$ are derived in a similar way. The contribution of the first line of eqn (44) to the second variation of H is obtained by differentiating the r.h.s. of eqn (64) with respect to q_j^b and allowing $\{q^b\}$ to vanish:

$$\frac{\partial^2 H(q_0)}{\partial q_i^b\partial q_j^b}\bigg|_{q=q_0}=\frac{h_k}{2}\left[\left(\lfloor q_0 \rfloor [B]^T+\left\lfloor\frac{1}{2}\beta_0^2,0\right\rfloor\right)[C]\left\{\begin{matrix}\bar{R}_i\bar{R}_j\\0\end{matrix}\right\}\right.$$

$$+(\lfloor B_j \rfloor+\lfloor \beta_0\bar{R}_j,0 \rfloor)[C]\left(\{B\}_i+\left\{\begin{matrix}\beta_0\bar{R}_i\\0\end{matrix}\right\}\right)$$

$$+(\lfloor B_i \rfloor+\lfloor \beta_0\bar{R}_i,0 \rfloor)[C]\left(\{B\}_j+\left\{\begin{matrix}\beta_0\bar{R}_j\\0\end{matrix}\right\}\right)$$

$$\left.+\lfloor \bar{R}_i\bar{R}_j,0 \rfloor[C]\left([B]\{q_0\}+\left\{\begin{matrix}\frac{1}{2}\beta_0^2\\0\end{matrix}\right\}\right)\right]. \tag{67}$$

The r.h.s. of eqn (67) can be simplified by combining lines 1 and 4 and lines 2 and 3. Doing so, adding the kinetic energy term derived from eqn (47), and including the remaining terms from eqns (44) and (46), one obtains for the second variation of H associated with the kth finite element:

$$\frac{\partial^2 H(q_0)}{\partial q_i^b\partial q_j^b}=\frac{\partial^2 H(x_0)}{\partial x_i\,\partial x_j}=\left[\left(\lfloor q_0 \rfloor[B]^T+\left\lfloor\frac{1}{2}\beta_0^2,0\right\rfloor\right)[C]\left\{\begin{matrix}\bar{R}_i\bar{R}_j\\0\end{matrix}\right\}\right.$$

$$+(\lfloor B_i \rfloor+\lfloor \beta_0\bar{R}_i,0 \rfloor)[C]\left(\{B_j\}+\left\{\begin{matrix}\beta_0\bar{R}_j\\0\end{matrix}\right\}\right)$$

$$+\lfloor N^T,M^T \rfloor\left\{\begin{matrix}\bar{R}_i\bar{R}_j\\0\end{matrix}\right\}\bigg]h_k$$

$$+[[K_A][\bar{T}][D]]_{ij}\delta_0^k+[[K_B][\bar{T}][D]]_{ij}\delta_L^k$$

$$+\Omega^2[[D]^T[M][D]]_{ij}h_k. \tag{68}$$

In eqns (65) and (68) subscript and superscript k denotes finite element number and subscripts i and j refer to degree of freedom numbers the range of which includes all degrees of freedom associated with the kth finite element.

The governing equations for linear and nonlinear stress analysis, buckling analysis, and modal vibration analysis can be obtained by insertion of the r.h.s. of eqns (65) and (68) into eqns (56) and (60).

Linear stress analysis

From eqn (56) it is seen that the global equations governing equilibrium are

$$\sum_{j=1}^{N}\frac{\partial^2 H(x_0)}{\partial x_i\partial x_j}\Delta x_j=-\frac{\partial H(x_0)}{\partial x_i} \quad i=1,2,\dots N. \tag{69}$$

For linear systems the initial deformations $\{x_0\}$ or $\{q_0\}$ are zero and $\{\Delta x\}$ is replaced by $\{x\}$, since the Δ denotes "change from a previous known solution $\{x_0\}$".

The (i,j)th term of the local element stiffness matrix for the kth finite element is therefore given from eqn (68) by

$$K_{ij}{}^k = (\lfloor B_i \rfloor [C]\{B_j\} + N^T \bar{R}_i \bar{R}_j) h_k + Q_{ij}{}^A \delta_o{}^k + Q_{ij}{}^B \delta_L{}^k \quad (70)$$

in which the range of i and j covers the nodal degrees of freedom associated with the kth finite element. (See Fig. 11 and eqns (32), (33), (36), and (37), for example.) In eqn (70) $\lfloor B_i \rfloor$ denotes the ith row of $[B]^T$, $\{B_j\}$ the jth column of $[B]$, $Q_{ij}{}^A$ the (i,j)th element of the matrix $[K_A][\bar{T}][D]$, and $Q_{ij}{}^B$ the (i,j)th element of the matrix $[K_B][\bar{T}][D]$.

The ith component of the local force vector corresponding to the kth finite element is given from eqns (65) and (69) by

$$F_i{}^k = (-\lfloor N^T, M^T \rfloor \{B_i\} + \lfloor p_t, p_n, 0 \rfloor \{D_i\}) h_k$$
$$+ \lfloor H, V, M \rfloor \{[\bar{T}][D]\}_i \delta_L{}^k \quad (71)$$

in which the range of i covers the nodal degrees of freedom associated with the kth finite element. The linear stress analysis problem is formulated by assembly of the terms $K_{ij}{}^k$ of the local finite element stiffness matrices into the global stiffness matrix $[K]$ and assembly of the components $F_i{}^k$ of the local force vector into a global force vector $\{F\}$, yielding the global linear equation system

$$[K]\{x\} = \{F\}. \quad (72)$$

Bifurcation buckling and modal vibration analyses

Bifurcation buckling and modal vibration are governed by eqn (60). The matrix of coefficients, $\partial^2 H(x_0)/\partial x_i{}^b \partial x_j{}^b$, $i,j = 1,2,\ldots N$ can be derived from eqn (68).

The terms in eqn (68) have the following physical significance: The first line represents the work done by the prebuckling (or pre-vibration) stress and moment resultants, shown in Fig. 15, during infinitesimal buckling or vibration modal rotation, β^b. These stress and moment resultants are given by

$$\lfloor N_0, M_0 \rfloor = \left(\lfloor q_0 \rfloor [B]^T + \left\lfloor \frac{1}{2}\beta_0{}^2, 0 \right\rfloor \right)[C]. \quad (73)$$

Note that the prebuckling moment resultant M_0 does not enter the buckling equations because the second term in the vector $\lfloor \bar{R}_i \bar{R}_j, 0 \rfloor$ is zero. This follows directly from the linearity of the assumed kinematic relationship (16b) between the change in curvature κ and the displacement components u and w. The second line in eqn (68) represents a contribution to the stiffness matrix of the structure as deformed by the loads. The amount of deformation is given by β_0. The third line represents a contribution to the work done by the thermal stress resultants during buckling or vibration modal rotation β^b. The fourth line represents the constraint conditions. The last line represents a contribution to the mass matrix and the associated modal vibration eigenvalue Ω^2.
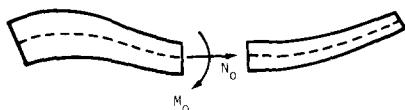

Fig. 15. Prestress resultants at an interior point along the beam reference surface.

Unlike the case for linear stress analysis, described in connection with eqn (70), the case of bifurcation buckling or modal vibration in the presence of prestress involves initial deformations. The expression for the stiffness matrix is therefore somewhat more complicated. The (i,j)th term of the local element stiffness matrix $[K_1]^k$ for the kth finite element is given from eqn (68) by

$$K_{1ij}{}^k = \left[(\lfloor B_i \rfloor + \lfloor \beta_0 \bar{R}_i, 0 \rfloor)[C] \left(\{B_j\} + \left\{ \begin{matrix} \beta_0 \bar{R}_j \\ 0 \end{matrix} \right\} \right) \right.$$
$$\left. + N^T \bar{R}_i \bar{R}_j \right] h_k + Q_{ij}{}^A \delta_o{}^k + Q_{ij}{}^B \delta_L{}^k \quad (74)$$

in which the range of i and j covers the nodal degrees of freedom associated with the kth finite element and the other terms are defined as before in connection with eqn (70). Equation (74) should be compared to the simpler expression (70) for the linear stress analysis.

Bifurcation buckling. The (i,j)th term of the local element "load-geometric" matrix $[K_2]^k$ for the kth finite element arises from the first line of eqn (68):

$$K_{2ij}{}^k = \lfloor N_0, M_0 \rfloor \left\{ \begin{matrix} \bar{R}_i \bar{R}_j \\ 0 \end{matrix} \right\} = N_0 \bar{R}_i \bar{R}_j \quad (74a)$$

where $\lfloor N_0, M_0 \rfloor$ are given by eqn (73). In cases for which the temperature rise is regarded as an eigenvalue, that is one wishes to find buckling temperatures, the term $N^T \bar{R}_i \bar{R}_i$ which in this presentation contributes to the stiffness matrix $[K_1]^k$ would instead appear in the "load geometric" matrix $[K_2]^k$.

The global bifurcation buckling problem is formulated by assembly of the terms K_{1ij}^k of the local finite element stiffness matrices into the global stiffness matrix $[K_1]$ and assembly of the terms K_{2ij}^k of the local finite element load-geometric matrix into the global load-geometric matrix $[K_2]$, yielding the global bifurcation buckling problem

$$[K_1]\{x^b\} + \lambda[K_2]\{x^b\} = 0. \quad (75)$$

In eqn (75) λ is a load factor to be multiplied by whatever the prestress distribution in $[K_2]$ is. This distribution may, of course, vary along the reference surface.

Note that the effect of prebuckling rotation β_0, which usually varies with the loading, has been assembled into the stiffness matrix $[K_1]$ rather than into the load-geometric matrix $[K_2]$. This is not a rigorously correct procedure. If β_0 varies with the buckling load, as is usually the case, the eigenvalue problem assumes the general form

$$[K_1]\{x\} + \lambda[K_2]\{x\} + \lambda^2[K_3]\{x\} = 0. \quad (76)$$

However, experience with difficulties associated with the extraction of eigenvalues of such quadratic systems has led to implementations in computer programs in which the loading is divided into two parts, a fixed part and an "eigenvalue" part. The prebuckling rotations β_0 associated with the fixed part are retained by inclusion of the β_0 in the stiffness matrix as in eqn (74). The prebuckling rotations associated with the part of the loading to be multiplied by the eigenvalue λ are neglected, leading to a load-geometric matrix generated only from prebuckling

stress resultants, as in eqn (75). Bifurcation buckling loads for systems in which prebuckling rotations β_0 are important are calculated through a converging sequence of eigenvalue problems in which the fixed part of the load becomes very large compared to the "eigenvalue" part of the load. An example of this type will be discussed later.

Modal vibrations. The stiffness matrix for the modal vibration of a pre-stressed structure is given by

$$[K_{\text{vib}}]=[K_1]+[K_2] \tag{77}$$

with K_1 and K_2 derived as just described. The mass matrix is derived in a straightforward manner from the last line of eqn (68). The global modal vibration eigenvalue problem takes the form

$$[K_{\text{vib}}]\{x\}+\Omega^2[M_{\text{vib}}]\{x\}=0 \tag{78}$$

with $[K_{\text{vib}}]$ given by eqn (77).

SECTION 3

ANALYSIS OF SHELLS OF REVOLUTION

The importance of this class of structures is attested to by the numerous computer programs that have been written for analysis of stress, buckling and vibration of axisymmetric shells.

COMPUTER PROGRAMS

In Fig. 16 the names of computer programs or their authors are located in a space with coordinates that measure complexity of geometry versus generality of phenomenon. Each name indicates the capability of the corresponding computer program to perform the analysis indicated by the intersection of these coordinates. In this coordinate system increasingly general-purpose computer codes lie increasing distances from both axes.

Other codes, existing just outside of the region depicted, apply to structures that are "almost" shells of revolution, such as shells with cutouts, shells with material properties that vary around the circumference, or panels of shells of revolution.

The region shown in Fig. 16 is divided by a heavy line into two fields: Programs lying within the heavy line are based on numerical methods that are essentially one-dimensional, that is, the dependent variables are separable and only one spatial variable need be discretized; programs lying outside the heavy line are based on numerical methods in which two or more spatial variables are discretized. It is generally true that analysis methods and programs lying outside the heavy line require perhaps an order of magnitude more computer time for a given case with given nodal point density than do those lying inside the line. This distinction arises because the band-widths and ranks of equation systems in two-dimensional numerical analyses are greater than those in one-dimensional numerical analyses. Certain of the areas in Fig. 16 are blank. Those near the origin correspond in general to cases for which closed-form solutions exist and for which slightly more general programs are clearly applicable. The blank areas lying near the outer boundaries of the chart are for the most part covered by more general programs such as NASTRAN, SPAR, STAGS, STRUDL, ASKA, MARC, ANSYS and other general-purpose programs described in Ref. [24].

As of 1980 the most commonly used computer programs for complex shells of revolution are those by Cohen[1], Kalnins[2], Svalbonas[3], and Bushnell[18,25]. A typical summary of the capabilities of such programs is listed in Table 1. In general the shell-of-revolution codes represent implementation of three distinct analyses:

(1) A nonlinear stress analysis for axisymmetric behavior of axisymmetric shell systems (large deflections, elastic or elastic–plastic).

(2) A linear stress analysis for axisymmetric and non-

Table 1. State-of-the-art for computer programs for the stress, buckling, and vibration analysis of complex axisymmetric shells

Type of analysis	Shell geometry	Wall construction	Loading
Nonlinear axisymmetric stress	Multiple-segment shells, each segment with its own wall construction, geometry, and loading	Monocoque, variable or constant thickness	Axisymmetric or non-symmetric thermal and/or mechanical line loads and moments
Linear symmetric or nonsymmetric stress		Skew-stiffened shells	
Stability with linear symmetric or nonsymmetric prestress or with nonlinear symmetric prestress	Cylinder, cone, spherical, ogival, toroidal, ellipsoidal, etc.	Fiber-wound shells	Axisymmetric or non-symmetric thermal and/or mechanical dis-tributed loads
		Layered orthotropic shells	
		Corrugated, with or without skin	
Vibration with non-linear prestress analysis	General meridional shape; point-by-point input	Layered orthotropic with temperature-dependent material properties	Proportional loading
			Non-proportional loading
Variable mesh point spacing within each segment	Axial and radial dis-continuities in shell meridian	Any of above wall types reinforced by stringers and/or rings treated as "smeared out"	
	Arbitrary choice of reference surface		
	General edge conditions	Any of above wall types further rein-forced by rings treated as discrete	
	Branched shells		
	Prismatic shells and composite built-up panels	Wall properties vari-able along meridian	

[a] From Bushnell [18]

	Axisymmetric Linear Stress	Axisymmetric Large-Deflection Stress	Axisymmetric Elastic-Plastic Stress	Axisymmetric Large-Deflection Elastic-Plastic Stress	Nonsymmetric Linear Stress	Eigenvalue Vibration	Eigenvalue Buckling	Dynamic Response, 1-D Nonlinear	Dynamic Response, 2-D Linear	Static 2-D Nonlinear	Dynamic Response, 2-D Nonlinear
Thick-Walled Shells or Solids	MARCAL WILSON WASP				GHOSH						
Branched, Segmented Shells	BOSOR4	BOSOR4 COHEN			BOSOR4 COHEN SABOR5 CAPELLI LESTINGI RADKOWSKI	BOSOR4 COHEN	BOSOR4 COHEN		SABOR5-DRASTIC5		
Segmented Shells	SADISTIC IV SABOR I WASP	BOSOR3 SADAOS SALORS STARS II	SADAOS	GERDEEN	BOSOR3 KALNINS SABOR3 STARS II SALORS	BOSOR3 KALNINS VALOR	BOSOR3 KALNINS BALOR STARS II	SADAOS	SABOR5-DRASTIC		
Thin-Walled Simple Shells		BOSOR2 WILSON-JONES	KHOJASTEH-BAKHT SHARIFI	MARCAL LEVINE EPSOR YAGMAI	SCHAEFFER MARGOLIAS	BOSOR2 ADELMAN MARGOLIAS	BOSOR2 HSEUH MARGOLIAS	GIRLS II	SABOR5-DRASTIC	BALL SNASOR GREENBAUM MARTIN	BALL SHORE DYNASOR II
Stiffened Cylinders							SCAR				
Monocoque Cylinders										NULACS	CYLINDER GRIVET SMERSH SPECTRE
Rings or Infinite Cylinders								UNIVALVE II GIRLS I PUFF			

INCREASING GENERALITY OF ANALYSIS OR PHENOMENUN ⟶

INCREASING GENERALITY OF STRUCTURE ⟶

Fig. 16. Computer programs for shells and solids in revolution (from Bushnell[18]).

symmetric behavior of axisymmetric shell systems submitted to axisymmetric and nonsymmetric loads.

(3) An eigenvalue analysis in which the eigenvalues represent buckling loads or vibration frequencies of axisymmetric shell systems submitted to axisymmetric loads. (Eigenvectors may correspond to axisymmetric or nonsymmetric modes.)

Some of the codes [1, 18] have an additional branch corresponding to buckling of nonsymmetrically loaded shells of revolution. In the BOSOR4 program [18] this branch is really a combination of the second and third analyses just listed.

Advantage of axisymmetric geometry: separation of variables

The great advantage of the computer programs cited above is their efficiency. This efficiency derives from the fact that for the three types of analysis just listed the independent variables can be separated and an analytically two-dimensional problem thus reduced to a numerically one-dimensional model. Such a model leads to compact, narrowly banded stiffness, load-geometric, and mass matrices, as we have seen from the beam analysis of the previous section. The reduction of these matrices for solving equilibrium and eigenvalue problems is performed speedily on the computer.

For example, the independent variables of the BOSOR4 analysis[18] are the arc length s measured along the shell reference surface and the circumferential coordinate θ. The dependent variables are the displacement components u, v and w of the shell wall reference surface. For the three types of analyses listed above it is possible to eliminate the circumferential coordinate θ by separation of variables: in the nonlinear stress analysis θ is not present; in the linear stress analysis the nonsymmetric load system is expressed as a sum or harmonically varying quantities, the shell response to each harmonic being calculated separately; and in the eigenvalue analysis the eigenvectors vary harmonically around the circumference. Buckling under non-symmetric loads is handled by calculation of the nonsymmetric prestress distribution from the linear theory and establishment of an eigenvalue problem in which the prestress distribution along a given meridian, presumably the meridian with the most destabilizing prestress, is assumed to be axisymmetric. Thus, the θ-dependence, where applicable, is eliminated by the assumption that displacements $u(s, \theta)$, $v(s, \theta)$, $w(s, \theta)$ are given by $u_n(s)\sin n\theta$, $v_n(s)\cos n\theta$, $w_n(s)\sin n\theta$, or by $u_n(s)\cos n\theta$, $v_n(s)\sin n\theta$, $w_n(s)\cos n\theta$.

The advantages of being able to eliminate one of the independent variables cannot be overemphasized. The number of calculations performed by the computer for a given nodal point spacing along the arc length s is greatly reduced, leading to significant reductions in computer time. Because the numerical analysis is "one-dimensional" a rather elaborate composite shell structure can be analyzed in a single "pass" through the computer. The disadvantage is, of course, the restriction to axisymmetric structures.

ENERGY FORMULATION—A SUMMARY

The following analysis of a segmented, ring-stiffened shell of revolution is similar to that for the beam given in the previous section. It is based on energy minimization with constraint conditions. The total energy of the system involves (1) strain energy of the shell segments U_s, (2) strain energy of the discrete rings U_r, (3) potential energy of the applied line loads and pressures U_p, (4) kinetic energy of the shell segments T_s, and (5) kinetic energy of the discrete rings T_r. In addition the total energy functional includes constraint conditions U_c arising from (1) displacement conditions at the ends of the composite shell, and (2) compatibility conditions between adjacent segments of the composite shell.

These components of energy and the constraint conditions are initially integrodifferential forms. They are then written in terms of the shell reference surface nodal point displacement components u_i, v_i and w_i and Lagrange multipliers λ_i. The integration along the reference surface meridian is performed numerically. Now an algebraic form, the energy is minimized with respect to the discrete dependent variables, u_i, v_i, w_i and λ_i.

In the nonlinear stress analysis the energy expression has terms linear, quadratic, cubic, and quartic in the dependent variables. The cubic and quartic terms arise from the "rotation-squared" terms which appear in the constraint conditions and in the kinematic expressions for reference surface strains e_1, e_2, and e_{12}. Nonlinear material properties (plasticity) are not included here. For details on plastic buckling the reader should consult Ref. [26]. Energy minimization leads to a set of nonlinear algebraic equations which are solved by the Newton–Raphson method. Stress and moment resultants are calculated in a straightforward manner from the mesh point displacement components through the constitutive equations (stress–strain law) and kinematic (strain-displacement) relations.

The results from the nonlinear axisymmetric stress analysis are used in the eigenvalue analyses for buckling and vibration. The "prebuckling" or "prestress" meridional and circumferential stress resultants N_{10} and N_{20} and the meridional rotation β_0 appear as known variable coefficients in the energy expression which governs bifurcation buckling and modal vibration. This bifurcation buckling or modal vibration energy expression is a homogenous quadratic form. The values of a parameter (load or frequency) which render the quadratic form stationary with respect to infinitesimal variations of the dependent variables represent buckling loads or natural frequencies. These "eigenvalues" are calculated from a set of linear, homogeneous equations.

Similar linear equations, with a "right-hand-side" vector added, are used for the linear stress analysis of axisymmetrically and nonsymmetrically loaded shells. The "right-hand-side" vector represents load terms and terms due to thermal stress. The variable coefficients N_{10}, N_{20} and β_0 mentioned above are zero, of course, since there is no nonlinear "prestress" phase in the linear nonsymmetric equilibrium analysis.

BASIC ASSUMPTIONS

The assumptions upon which the following analysis is based are:

(1) The wall material is elastic and behaves linearly.

(2) Thin-shell theory holds; i.e. normals to the undeformed surface remain normal and undeformed. Transverse shear deformation is neglected.

(3) The structure is axisymmetric, and in vibration analysis and nonlinear stress analysis the loads and prebuckling or prestress deformations are axisymmetric.

(4) The axisymmetric prebuckling deflections in the nonlinear theory, while considered finite, are moderate;

i.e. the square of the meridional rotation can be neglected compared with unity.

(5) In the calculation of displacement and stresses in nonsymmetrically loaded shells, linear theory is used. This analysis is based on standard small-deflection analysis.

(6) A typical cross-section dimension of a discrete ring stiffener is small compared with the radius of the ring.

(7) The cross-sections of the discrete rings remain undeformed as the structure deforms, and the rotation about the ring centroid is equal to the rotation of the shell meridian at the attachment point of the ring.

(8) The discrete ring centroids coincide with their shear centers.

(9) If meridional stiffeners are present, they are numerous enough to include in the analysis by an averaging or 'smearing' of their properties over any parallel circle of the shell structure.

(10) The shell is thin enough to neglect terms of order t/R compared to unity, where t is a typical thickness and R a typical radius of curvature.

(11) Prebuckling in-plane shear resultants are neglected in the stability analysis.

(12) The integrated constitutive law is restricted to the form given in eqn (84). For example, any coupling between normal stress resultants and shearing and twisting motions is neglected.

In eqns (79) and (80) subscript 1 refers to the meridional coordinate direction and subscript 2 refers to the circumferential coordinate direction. As with the beam analysis, T is the temperature rise above the zero stress state. The coordinate z along the normal to the reference surface is measured outward from an arbitrary reference, not necessarily from the middle surface.

If "normals remain normal" and undeformed (a classical thin shell theory approximation), the strains as functions of the thickness $\epsilon_1(z)$, $\epsilon_2(z)$, and $\epsilon_{12}(z)$ can be expressed in terms of reference surface strains e_1, e_2, and e_{12} and changes in curvature κ_1, κ_2, and κ_{12}, thus

$$\epsilon_1 = e_1 - z\kappa_1, \quad \epsilon_2 = e_2 - z\kappa_2, \quad \epsilon_{12} = e_{12} + 2z\kappa_{12}. \quad (82)$$

It is convenient to perform the z integration in eqn (79) at this point. The following definitions of stress and moment resultants are required:

$$N_1 = \int \sigma_1 \, dz \quad N_2 = \int \sigma_2 \, dz \quad N_{12} = \int \tau_{12} \, dz$$

$$(83)$$

$$M_1 = -\int \sigma_1 z \, dz \quad M_2 = -\int \sigma_2 z \, dz \quad M_{12} = \int \tau_{12} z \, dz.$$

These stress and moment resultants are shown in Fig. 17. Substitution of eqns (80) with eqns (83) yields

$$\begin{Bmatrix} N_1 \\ N_2 \\ N_{12} \\ M_1 \\ M_2 \\ M_{12} \end{Bmatrix} = \begin{bmatrix} C_{11} & C_{12} & 0 & C_{14} & C_{15} & 0 \\ C_{12} & C_{22} & 0 & C_{24} & C_{25} & 0 \\ 0 & 0 & C_{33} & 0 & 0 & C_{36} \\ C_{14} & C_{24} & 0 & C_{44} & C_{45} & 0 \\ C_{15} & C_{25} & 0 & C_{45} & C_{55} & 0 \\ 0 & 0 & C_{36} & 0 & 0 & C_{66} \end{bmatrix} \begin{Bmatrix} e_1 \\ e_2 \\ e_{12} \\ \kappa_1 \\ \kappa_2 \\ 2\kappa_{12} \end{Bmatrix} + \begin{Bmatrix} N_1{}^T \\ N_2{}^T \\ 0 \\ M_1{}^T \\ M_2{}^T \\ 0 \end{Bmatrix} \quad (84)$$

ENERGY COMPONENTS AND CONSTRAINT CONDITIONS

The various components of the energy (U_s, U_r, U_p, T_s, T_r) and the constraint conditions U_c are derived in this section. The energy is derived for a typical discrete ring. The total energy is obtained by summation over all shell segments and all discrete rings.

Shell strain energy

A shell element is shown in Fig. 17. The strain energy in the shell wall is

$$U_s = \frac{1}{2} \int_s \int_\theta \int_z \{\sigma_1(\epsilon_1 - \alpha_1 T) + \sigma_2(\epsilon_2$$

$$- \alpha_2 T) + \tau_{12}\epsilon_{12}\} \, r \, dz \, d\theta \, ds \quad (79)$$

which is analogous to eqns (13) for the beam.

For an orthotropic wall material

$$\begin{Bmatrix} \sigma_1 \\ \sigma_2 \\ \tau_{12} \end{Bmatrix} = \begin{bmatrix} E_{11} & E_{12} & 0 \\ E_{12} & E_{22} & 0 \\ 0 & 0 & G \end{bmatrix} \begin{Bmatrix} \epsilon_1 - \alpha_1 T \\ \epsilon_2 - \alpha_2 T \\ \epsilon_{12} \end{Bmatrix} \quad (80)$$

in which

$$E_{11} = E_1/(1 - \nu_{12}\nu_{21}); \quad E_{22} = E_2/(1 - \nu_{12}\nu_{21})$$

$$(81)$$

$$E_{12} = \nu_{12}E_{22}.$$

in which the C_{ij} are given by

$$C_{11} = \int E_{11} \, dz \quad C_{12} = \int E_{12} \, dz \quad C_{14} = -\int E_{11} z \, dz$$

$$C_{15} = -\int E_{12} z \, dz \quad C_{22} = \int E_{22} \, dz \quad C_{24} = -\int E_{12} z \, dz$$

$$C_{25} = -\int E_{22} z \, dz \quad C_{33} = \int G \, dz \quad C_{36} = \int Gz \, dz$$

$$C_{66} = \int Gz^2 \, dz \quad C_{44} = \int E_{11} z^2 \, dz \quad C_{45} = \int E_{12} z^2 \, dz$$

$$C_{55} = \int E_{22} z^2 \, dz \quad (85)$$

and the thermal resultants $N_1{}^T$, $N_2{}^T$, $M_1{}^T$, $M_2{}^T$ are given by

$$N_1{}^T = -\int (E_{11}\alpha_1 T + E_{12}\alpha_2 T) \, dz$$

$$N_2{}^T = -\int (E_{12}\alpha_1 T + E_{22}\alpha_2 T) \, dz$$

$$(86)$$

$$M_1{}^T = \int (E_{11}\alpha_1 T + E_{12}\alpha_2 T) \, dz$$

$$M_2{}^T = \int (E_{12}\alpha_1 T + E_{22}\alpha_2 T) \, dz.$$

The thickness coordinate z is measured from the arbitrary reference surface outward. The integrations through the thickness in eqns (85) and (86) can be performed explicitly for layered shells with material properties constant through the thickness of each layer, or numerical integration can be performed (e.g. Simpson's rule) for layered shells with temperature-dependent material properties. Equations appropriate for laminated composite wall construction are given later.

Equations (80) and (82) are analogous to eqns (18) and (15), respectively, for the beam analysis. The C_{ij} and N_1^T, N_2^T, M_1^T, M_2^T in eqns (84)–(86) are analogous to similar quantities in eqns (20) and (21).

Using eqns (82), (83) and (86), one can write the shell strain energy in eqn (79) in the form

$$U_s = \frac{1}{2}\int_s \int_\theta [\lfloor S\rfloor\{e\} + \lfloor N^T\rfloor\{e\} + C(T)]r\, d\theta\, ds \quad (87)$$

in which

$$\lfloor S\rfloor \equiv \lfloor N_1, N_2, N_{12}, M_1, M_2, M_{12}\rfloor$$

$$\{e\} = e^T \equiv \lfloor e_1, e_2, e_{12}, \kappa_1, \kappa_2, 2\kappa_{12}\rfloor^T$$

$$N^T \equiv \lfloor N_1^T, N_2^T, 0, M_1^T, M_2^T, 0\rfloor$$

and $C(T)$ is a function of the shell parameters and temperature rise only. Therefore it can be dropped. Since

$$\lfloor S\rfloor = \{S\}^T = [[C]\{e\} + \{N^T\}]^T$$

$$= \lfloor e\rfloor [C]^T + \lfloor N^T\rfloor \quad (88)$$

$$= \lfloor e\rfloor [C] + \lfloor N^T\rfloor$$

substitution of eqn (88) for $\lfloor S\rfloor$ and the dropping of $C(T)$ in eqn (87) leads to

$$U_s = \frac{1}{2}\int_s \int_\theta \left(\lfloor e\rfloor \overset{6\times6}{[C]}\{e\} + 2\overset{6\times1}{\lfloor N^T\rfloor}\{e\}\right)r\, d\theta\, ds \quad (89)$$

which is analogous to eqn (20) for the beam.

Strain-displacement and curvature-displacement relations valid for moderately large relations are

$$\{e\} = \begin{Bmatrix} e_1 \\ e_2 \\ e_{12} \\ \kappa_1 \\ \kappa_2 \\ 2\kappa_{12} \end{Bmatrix} = \begin{Bmatrix} u' + w/R_1 + \frac{1}{2}(\beta^2 + \gamma^2) \\ \dot{v}/r + ur'/r + w/R_2 + \frac{1}{2}(\psi^2 + \gamma^2) \\ \dot{u}/r + r(v/r)' + \beta\psi \\ \beta' \\ \dot{\psi}/r + r'\beta/r \\ 2(-\dot{\beta}/r + r'\psi/r + v'/R_2) \end{Bmatrix} \quad (90)$$

in which

$$\beta = w' - u/R_1, \quad \psi = \dot{w}/r - v/R_2$$

$$\gamma = \frac{1}{2}(\dot{u}/r - v' - r'v/r). \quad (91)$$

Dots indicate differentiation with respect to the circumferential coordinate θ; primes indicate differentiation with respect to the meridional coordinate s. Positive values of u, v, w, β, ψ and γ are shown in Fig. 17. The
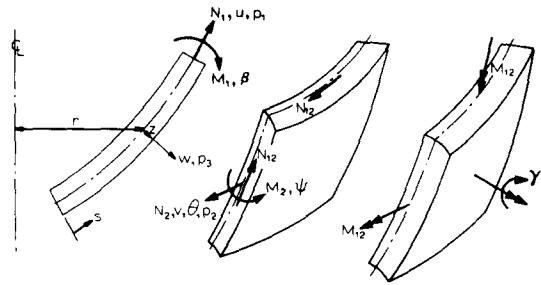

Fig. 17. Shell element with displacements, rotations, forces (from Bushnell[27]).

quantities R_1 and R_2 are the meridional and normal circumferential radii of curvature. Equations (90) and (91) are of the Novoshilov–Sanders type [10, 11]; they are analogous to eqns (16) and (17) for the curved beam. The same equations form the theoretical basis for Cohen's computer program[1].

Discrete ring strain energy

Figure 18 shows a ring cross section with displacements u_c, v_c, w_c, β of the centroid and applied loads V, S, H, M. The ring cross-sectional area A is greatly exaggerated relative to its centroidal radius r_c. The centroid and the shear center are assumed to coincide and plane normal sections are assumed to remain plane and normal during deformations. In the absence of warping, the ring strain energy is given by

$$U_r = (r_c/2)\int_\theta \int_A \sigma_r(\epsilon_r - \alpha_r T)\, dA\, d\theta$$

$$+ \frac{1}{2}(GJ/r_c)\int_\theta (\dot{\beta} + \dot{u}_c/r_c)^2\, d\theta \quad (92)$$

in which A is the ring cross-section area and GJ is the torsional rigidity.

The ring hoop stress is given by

$$\sigma_r = E_r(\epsilon_r - \alpha_r T). \quad (93)$$

The hoop strain ϵ_r can be expressed as a function of strain of the centroidal axis plus terms due to in-plane and out-of-plane curvature changes κ_x and κ_y, respectively:

$$\epsilon_r = e_r - x\kappa_x + y\kappa_y. \quad (94)$$

Substitution of eqns (94) and (93) into eqn (92), integration over the ring area, and the dropping of the term which contains only ring parameters and temperature, leads to the following expression for the ring energy:

$$U_r = (r_c/2)\int_\theta (e_r^2 E_r A + \kappa_x^2 E_r I_y + \kappa_y^2 E_r I_x - 2\kappa_x \kappa_y E_r I_{xy}$$

$$+ (GJ/r_c^2)(\dot{\beta} + \dot{u}_c/r_c)^2 + 2[e_r N_r^T + \kappa_x M_y^T + \kappa_y M_x^T])\, d\theta \quad (95)$$

in which

$$N_r^T = -\int E_r \alpha_r T\, dA$$

$$M_y^T = +\int E_r \alpha_r Tx\, dA \quad M_x^T = -\int E_r \alpha_r Ty\, dA. \quad (96)$$
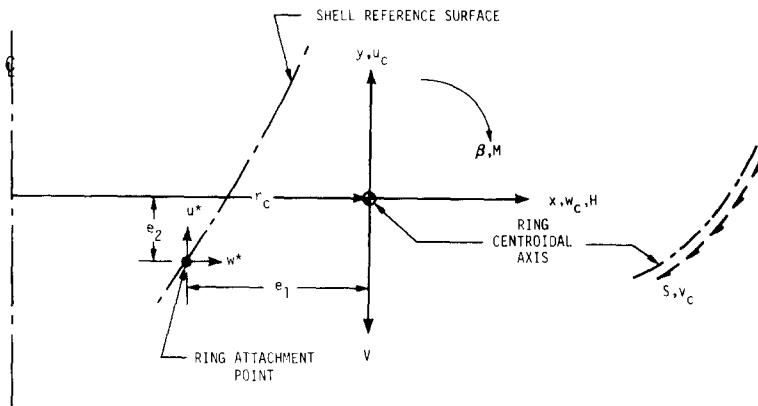
Fig. 18. Discrete ring with centroidal displacements, forces (from Bushnell[27]).

The ring kinematic relations are

$$e_r = \dot{v}_c/r_c + w_c/r_c + \frac{1}{2}(\psi_c^2 + \gamma_c^2)$$

$$\kappa_z = \dot{\psi}_c/r_c$$

$$\kappa_y = -\dot{\gamma}_c/r_c + \beta/r_c \qquad (97)$$

$$\psi_c = (\dot{w}_c - v_c)/r_c$$

$$\gamma_c = \dot{u}_c/r_c.$$

Equations (92)–(97) are analogous to eqns (79)–(91) for the shell.

Potential energy of mechanical loads

Two types of loads are permitted in the analysis: line loads and moments V, S, H, and M, which act at ring centroids and at shell segment boundaries, and surface tractions p_1, p_2 and pressure p_3. These loads are shown in Figs. 17 and 18. The potential energy associated with constant-directional line loads at a given ring station is

$$U_{p1} = -\int_\theta (-Vu_c + Sv_c + Hw_c + M\beta)r_c \, d\theta. \qquad (98)$$

The potential energy associated with constant directional surface tractions p_1 and p_2 and pressure p_3 is

$$U_{p2} = -\int_s \int_\theta (p_1 u + p_2 v + p_3 w)r \, d\theta \, ds. \qquad (99)$$

These equations are analogous to eqn (22) for the beam. Additional terms required to account for following or "live" loads are introduced later.

Kinetic energy of shell segment

The kinetic energy of the shell segment is given by

$$T_s = \frac{1}{2}\int_s \int_\theta m(u_{,t}^2 + v_{,t}^2 + w_{,t}^2)r \, d\theta \, ds. \qquad (100)$$

in which $(\ )_{,t}$ denotes differentiation with respect to time. The shell rotatory inertia in neglected.

Kinetic energy of discrete ring

The kinetic energy of a discrete ring stiffener is given by

$$T_r = \rho_r(r_c/2)\int_\theta [A(u_{c,t}^2 + v_{c,t}^2 + w_{c,t}^2) + I_p\beta_{,t}^2 + I_s\psi_{c,t}^2 + I_n\gamma_{c,t}^2$$
$$+ 2I_{sn}\psi_{c,t}\gamma_{c,t}] \, d\theta \qquad (101)$$

in which I_p, I_s, I_n, I_{sn} are cross-sectional area moments of inertia relative to axes normal and tangential to the shell meridian at the ring attachment point. In the case of harmonic oscillations, the differentiations with respect to time are replaced by a factor Ω, which is a frequency parameter. Equations (100) and (101) are analogous to eqn (28) for the beam.

Constraint conditions

Figure 19 shows a meridional discontinuity (+, −) between two adjacent shell segment reference surfaces and discontinuities at shell edge support points "A" and "B". The compatibility conditions for the junction are

$$u^{*+} = u^{*-} + \Delta u^* \qquad v^{*+} = v^{*-} + \Delta v^*$$
$$w^{*+} = w^{*-} + \Delta w^* \qquad \beta^+ = \beta^- \qquad (102)$$

in which

$$\Delta u^* = -(d_1\beta + d_2\beta^2/2)$$

$$\Delta v^* = -(d_1 + \Delta w^*)(\dot{w}^{*-} - v^{*-})/r^- - (d_2 + \Delta u^*)\dot{u}^{*-}/r^- \qquad (103)$$

$$\Delta w^* = d_2\beta - d_1\beta^2/2.$$

The constraint conditions (102) arise from the requirement that the motion of the point (+) relative to the point (−) involves no deformation of a line joining the meridional gap (+, −) and compatibility of meridional rotation β across this (+, −) gap is enforced.

At a support point the terms u^{*+}, v^{*+}, and w^{*+} in eqns (102) are constrained to be zero if the appropriate boundary condition integers K_{A1}, K_{A2}, etc. and K_{B1}, K_{B2}, etc (see below), are equal to unity. The constraint conditions (102) are incorporated into the total system energy by the introduction of four Lagrange multipliers λ_1, λ_2, λ_3, and λ_4 for each edge support and each segment junction. Thus, the "energy of constraint" corresponding to each

junction has the form

$$U_c = \lfloor \lambda_1, \lambda_2, \lambda_3, \lambda_4 \rfloor \begin{Bmatrix} u^{*+} - u^{*-} - \Delta u^* \\ v^{*+} - v^{*-} - \Delta v^* \\ w^{*+} - w^{*-} - \Delta w^* \\ \beta^+ - \beta^- \end{Bmatrix}. \quad (104)$$

At the shell ends the constraint conditions have the following forms: at end point "A"

$$U_c = \lfloor K_{A1}{}^* \lambda_1, K_{A2}{}^* \lambda_2, K_{A3}{}^* \lambda_3, K_{A4}{}^* \lambda_4 \rfloor \begin{Bmatrix} -u^{*-} - \Delta u^* \\ -v^{*-} - \Delta v^* \\ -w^{*-} - \Delta w^* \\ -\beta^- \end{Bmatrix}$$

$$(105a)$$

at end point "B"

$$U_c = \lfloor K_{B1}{}^* \lambda_1, K_{B2}{}^* \lambda_2, K_{B3}{}^* \lambda_3, K_{B4}{}^* \lambda_4 \rfloor \begin{Bmatrix} -u^{*-} - \Delta u^* \\ -v^{*-} - \Delta v^* \\ -w^{*-} - \Delta w^* \\ -\beta^- \end{Bmatrix}.$$

$$(105b)$$

These equations are analogous to eqns (26) for the beam.

Variable transformations

The components of energy of the system are represented by the shell strain energy U_s (eqn 89), the strain energy of a discrete ring U_r (eqn 95), the potential energy of line loads U_{p1} and surface tractions U_{p2} (eqns 98 and 99), the shell kinetic energy T_s (eqn 100), and the discrete ring kinetic energy T_r (eqn 101). The constraint conditions U_c are given by eqns (104) and (105).

It is desired to express all energy components in terms of the shell reference surface displacements u, v, and w. The displacements u_c, v_c, and w_c of the ring centroid (Fig. 18), which appear in eqns (95), (97), 98, and (101), are given by

$$u_c = u^* + \Delta u^* \quad v_c = v^* + \Delta v^* \quad w_c = w^* + \Delta w^*. \quad (106)$$

The quantities Δu^*, Δv^*, and Δw^* are given by eqns (103) with d_1 and d_2 replaced by e_1 and e_2, the ring eccentricity components (Fig. 18), and u^{*-}, v^{*-}, w^{*-}, r^- replaced by the displacement components and radius u^*, v^*, w^*, r which correspond to the ring attachment joint. The axial, circumferential, and radial displacement components u^*, v^*, and w^*, which appear in eqns (102)–(106), are given by

$$u^* = ur/R_2 - wr' \quad v^* = v \quad w^* = ur' + wr/R_2 \quad (107)$$

which is analogous to eqn (42) for the beam.

Equations (106) and (107) can be used to eliminate u_c, v_c, w_c and u^*, v^*, and w^* from the energy components and constraint conditions. The dependent variables are then u, v, w and the Lagrange multipliers λ_1, λ_2, λ_3, and λ_4.

The total energy in the system is obtained by summing over all shell segments, discrete ring stiffeners, junctions and boundaries.

Separation of variables

The dependent variables u, v, and w are functions of arc length s and circumferential coordinate θ. The θ

dependence can be eliminated from the analysis by the assumption that

$$u(s, \theta) = u_0(s) + \sum_{n=n_{min}}^{n_{max}} u_{n1}(s) \sin n\theta + \sum_{n_{min}}^{n_{max}} u_{n2}(s) \cos n\theta$$

$$v(s, \theta) = \sum_n v_{n1}(s) \cos n\theta + \sum_n v_{n2}(s) \sin |n|\theta \quad (108)$$

$$w(s, \theta) = w_0(s) + \sum_n w_{n1}(s) \sin n\theta + \sum_n w_{n2}(s) \cos n\theta.$$

The temperature distribution, surface tractions and pressures, and thermal and mechanical line loads have similar expansions, which are given explicitly later.

If the expressions (108) were inserted into the energy components just derived, all the harmonics would couple in the analysis, since the kinematic relations (90), (97) and (103) are nonlinear.

In the analysis, large deflections are permitted in the *axisymmetric* components, but the *nonsymmetric* harmonics are considered to be small. The various harmonics do not couple, and a solution for each $u_n(s)$, $v_n(s)$, and $w_n(s)$ can be obtained with the circumferential wave number n appearing as a parameter in the analysis. The θ integration indicated in eqns (89), (95) and (98)–(101) is replaced by a factor of π for $n \neq 0$ and 2π for $n = 0$. In a linear stress analysis for nonsymmetrically loaded shells, the static response of a shell to arbitrary varying loads is obtained by superposition. (In this case, even the axisymmetric components are assumed to be small.) In buckling and vibration analyses the "small" deflections $u_{n1}, v_{n1}, w_{n1}, u_{n2}, v_{n2}, w_{n2}$ are considered to be kinematically admissible variations from the "pre-buckled" or "prestressed" axisymmetric state represented by the large deflections $u_0(s)$ and $w_0(s)$ in eqns (108). The $u_0(s)$ and $w_0(s)$ are determined in the nonlinear stress phase of the analysis by Newton–Raphson iterations, as described in the discussion associated with eqn (56).
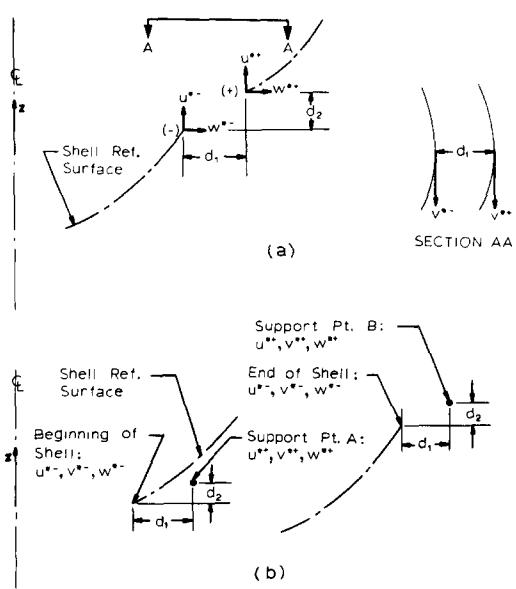

Fig. 19. Geometry for constraint conditions: (a) shell reference surface discontinuity; (b) support points (from Bushnell[27]).

In the linear analysis for nonsymmetric behavior and in the buckling and vibration analyses, the second summations in eqns (108) can be represented by zero or negative values of the circumferential wave number, n.

DISCRETIZATION

The θ dependence has been replaced with a parameter n, so that only one independent variable remains—the arc length s. Figure 20(a) shows a shell meridian of two segments, and Fig. 20(b) shows a discretized model. The continuous variables $u(s)$, $v(s)$, and $w(s)$ are replaced by discrete variables u_i, v_i, and w_i. The u_i and v_i occur at stations midway between the w_i in a manner analogous to the discretized beam model shown in Fig. 11. With constant nodal point spacing within each shell segment, as shown in Fig. 20(b), the energy is evaluated at the mesh points where the w_i are located. The displacements and the s derivatives required in the energy are

$$u = (u_i + u_{i-1})/2, \quad v = (v_i + v_{i-1})/2$$

$$u' = (u_i - u_{i-1})/h, \quad v' = (v_i - v_{i-1})/h$$

$$w = w_i, \quad w' = (w_{i+1} - w_{i-1})/2h, \tag{109}$$

$$w'' = (w_{i+1} - 2w_i + w_{i-1})/h^2$$

in which h is the mesh point spacing. These expressions are analogous to eqns (32) for the beam.

If the nodal point spacing varies within a shell segment, the expressions for u, v, u', and v' remain as given in eqns (109), but the three-point formulas for w, w', and w'' become

$$\begin{Bmatrix} w \\ w' \\ w'' \end{Bmatrix} = \begin{bmatrix} a_{11} & a_{12} & a_{13} \\ a_{21} & a_{22} & a_{23} \\ a_{31} & a_{32} & a_{33} \end{bmatrix} \begin{Bmatrix} w_{i-1} \\ w_i \\ w_{i+1} \end{Bmatrix} \tag{110}$$

in which

$$a_{11} = (h-k)(3k+h)/[16(h^2+hk)]$$

$$a_{12} = (h+3k)(3h+k)/(16hk)$$

$$a_{13} = (k-h)(3h+k)/[16(k^2+hk)]$$

$$a_{21} = -1/2h \quad a_{22} = (1/2h - 1/2k) \quad a_{23} = 1/2k \tag{111}$$

$$a_{31} = 2/[h(h+k)]$$

$$a_{32} = -2/(hk)$$

$$a_{33} = 2/[k(h+k)].$$

The quantities h and k are defined in Fig. 21.

Finite-difference energy method vs finite element method

The discretization technique just described has been called the "finite difference energy method". This method is described in detail and compared to the finite element method in Ref. [19]. Figure 21 shows a typical shell segment meridian with variable nodal point spacing. As in the case of constant nodal point spacing shown in Fig. 20, the 'u' and 'v' points are located halfway between adjacent 'w' points. The energy contains up to first derivatives in u and v and up to second derivatives in w. Hence, the shell energy density evaluated at the point
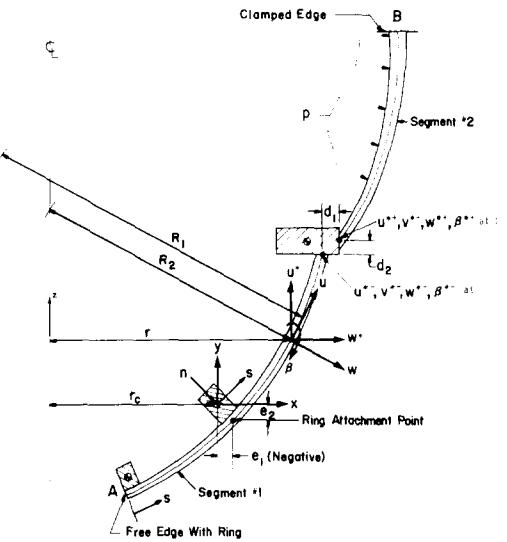

Fig. 20(a). Two-segment shell meridian with discrete rings, discontinuity, and various quantities identified (from Bushnell[27]).

labeled E (center of the length l) involves the seven points w_{i-1} through w_{i+1}. The energy per unit circumferential length is simply the energy per unit area multiplied by the length l of the finite-difference element, which is the arc length of the reference surface between two adjacent u or v points. This formulation yields a 7×7 local element stiffness matrix corresponding to a constant-strain, constant-curvature-change finite element that is incompatible in normal displacement and rotation at its boundaries but that in general gives very rapidly convergent results with increasing density of nodal points. Note that two of the w-points lie outside of the element. If the mesh spacing is constant, the algebraic equations obtained by minimization of the energy with respect to nodal degrees-of-freedom can be shown to be equivalent to the Euler equations of the variational problem in finite form[19]. Further description and proofs are given later and in Ref.[19].

Figures 2 and 22 show rates of convergence with increasing nodal point density for a poorly conditioned problem—a stress analysis of a thin, non-symmetrically loaded hemisphere with a free edge. The u and w displacement components at $\theta = 0$ are plotted in Fig. 1. The finite-element results indicated in Fig. 2 were obtained by programming various kinds of finite elements into the BOSOR4 program[18]. The computer times for computation of the stiffness matrices K_1 are shown in Fig. 22. A much smaller time for computation of the finite-difference K_1 is required than for the finite element K_1 because there are fewer calculations for each "Gaussian" integration point and because there is only one "Gaussian" point per finite-difference element. Other comparisons of rate of convergence with the two methods used in BOSOR4 are shown for buckling and vibration problems in Ref. [19].

Energy functional converted to algebraic form

With the substitution of eqns (108) in the various energy components and constraint conditions, the replacement of s derivatives by eqns (109) or (110), the replacement of time derivatives by a frequency parameter $i\Omega$, and the numerical integration over s and
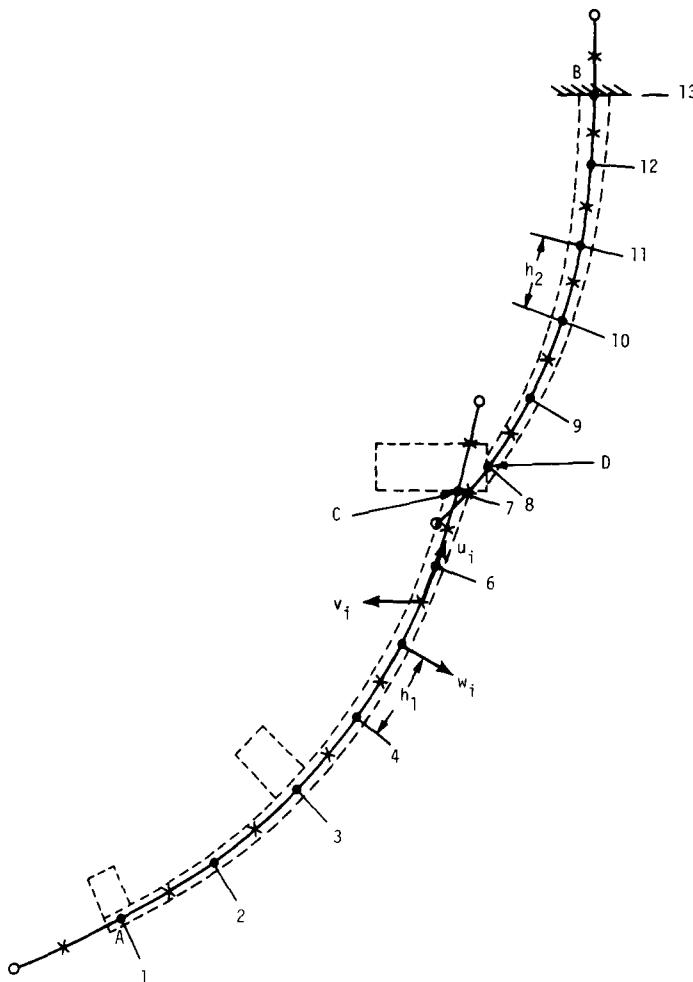
Fig. 20(b). Shell meridian with discretized model (from Bushnell[27]).

exact integration over θ, the system energy and constraint conditions are now represented by an algebraic form which contains as dependent variables u_i, v_i, and w_i and the Lagrange multipliers λ_1, λ_2, λ_3, and λ_4 (for each junction and boundary). The algebraic form also contains as parameters the shell and ring properties, the loads and temperature, and the frequency parameter Ω.

STRESS, BUCKLING, AND VIBRATION ANALYSIS—A SUMMARY

Nonlinear stress analysis

In the nonlinear stress analysis only the axisymmetric components of the load are considered and only $u_0(s)$ and $w_0(s)$ in eqns (108) are nonzero. Terms linear through quartic appear in the algebraic form for the total energy, as with eqn (44) in the beam analysis. The simultaneous nonlinear algebraic equations obtained by energy minimization with respect to the nodal point displacement components u_{0i} and w_{0i} and Lagrange multipliers λ_i are solved by the Newton-Raphson method, as described in the discussion associated with eqn (56). The coefficient matrix for each iteration is symmetric and is strongly banded about the main diagonal. Such narrowly banded systems can be solved in a matter of seconds of computer time. For example, a BOSOR4 case with about 200 degrees of freedom requires somewhat less than about 2 seconds per itera-

tion with double precision on the UNIVAC 1108 computer. The number of iterations required depends on how nonlinear the problem is. Generally, less than about five iterations are needed for convergence at a given load level.
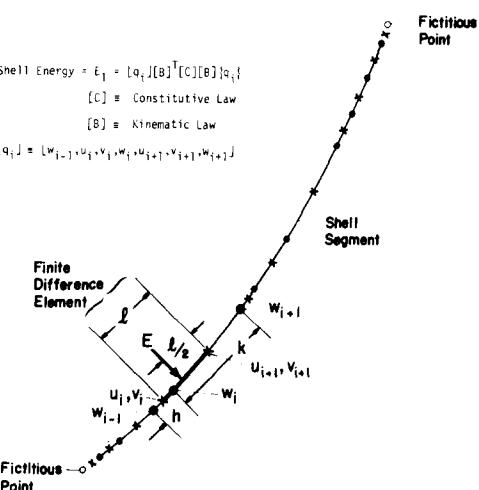
Fig. 21. Nodal displacement degrees of freedom for variable nodal point spacing.
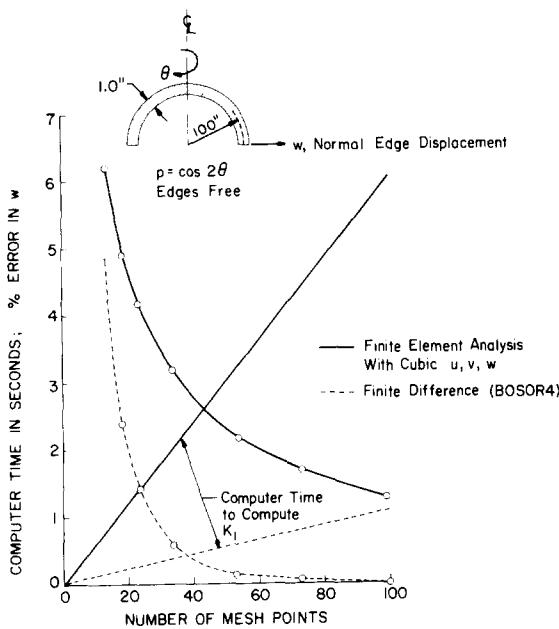
Fig. 22. Computer times to form stiffness matrix K_1 and rates of convergence of normal edge displacement for free hemisphere with nonuniform pressure $p(s,\theta) = p_0 \cos 2\theta$ (from Bushnell[18]).

A reasonable convergence criterion for the nonlinear prebuckling solution at each load step is that successive values of all u_{i0}, w_{i0} greater than a tenth of the largest displacement be different by less than 0.1% of their absolute values. The starting vector for the first iteration at the first load value is zero, which means that the first solution represents the linear theory solution. The starting vectors for the first iterations at subsequent load values are the converged solutions obtained at the loads immediately preceding the current load. Once the displacements u_{i0} and w_{i0} have been calculated, the reference surface strains and stress resultants are obtained in a straightforward manner by means of eqns (84) and (90).

Bifurcation buckling and modal vibration

In the buckling and vibration analyses the symmetric and nonsymmetric displacement components contained in the summations indicated in eqn (108) are considered to be infinitesimal, kinematically admissible variations of the displacements from the "prebuckled" or "prestressed" state obtained in the nonlinear stress analysis described above. Since the "buckling" displacements u_n, v_n, and w_n are infinitesimal, one need only retain linear terms in u_n, v_n, and w_n in the kinematic relations and constraint conditions. However, it must be remembered that the displacements and relations in eqns (90)–(106) represent the total displacements from the undeformed state. Hence, cross-product terms such as $w'_0 w'_n$ obtained by insertion of eqns (108) (with the use of eqns 91 and 109) into eqns (90), for example, must be retained. The energy minimization in the buckling and vibration analyses is performed with respect to u_n, v_n, w_n and the Lagrange multipliers.

The buckling and vibration analysis is described in detail below. Here it is sufficient to point out that the energy expression on which the numerical analysis is

based is a homogeneous quadratic form. The form is stationary with respect to the dependent variables u_n, v_n, w_n and the Lagrange multipliers λ for certain discrete values of a parameter—the so-called eigenvalues. The eigenvalue parameter can be a load or load ratio, a temperature, or a frequency.

Linear equilibrium for nonaxisymmetric loading

The linear stress analysis is based on the same equations as the stability and vibration analysis, except that the "prestress" terms which appear in the stability and vibration quadratic form are not present, and the gradient of the energy functional is not homogeneous, since a "right-hand-side" vector is nonzero. This vector arises from the thermal terms in eqns (89) and (95) and the load terms in eqns (98) and (99).

Corresponding to the nonsymmetric portions of $u(s,\theta)$, $v(s,\theta)$, and $w(s,\theta)$ given in eqns (108), the temperature rise distribution T, surface tractions p_1, p_2, and pressure p_3, mechanical line loads V, S, H, M and thermal line loads N_r^T, M_y^T, M_x^T have the following expansions:

$$T(s,\theta) = \sum_n T_{n1}(s) \sin n\theta + \sum_n T_{n2}(s) \cos n\theta$$

$$p_1(s,\theta) = \sum_n p_{1n1}(s) \sin n\theta + \sum_n p_{1n2}(s) \cos n\theta$$

$$p_2(s,\theta) = \sum_n p_{2n1}(s) \cos n\theta + \sum_n p_{2n2}(s) \sin n\theta$$

$$p_3(s,\theta) = \sum_n p_{3n1}(s) \sin n\theta + \sum_n p_{3n2}(s) \cos n\theta$$

$$V(\theta) = \sum_n V_{n1} \sin n\theta + \sum_n V_{n2} \cos n\theta$$

$$S(\theta) = \sum_n S_{n1} \cos n\theta + \sum_n S_{n2} \sin n\theta \qquad (112)$$

$$H(\theta) = \sum_n H_{n1} \sin n\theta + \sum_n H_{n2} \cos n\theta$$

$$M(\theta) = \sum_n M_{n1} \sin n\theta + \sum_n M_{n2} \cos n\theta$$

$$N_r^T(\theta) = \sum_n N_{rn1}^T \sin n\theta + \sum_n N_{rn2}^T \cos n\theta$$

$$M_y^T(\theta) = \sum_n M_{yn1}^T \sin n\theta + \sum_n M_{yn2}^T \cos n\theta$$

$$M_x^T(\theta) = \sum_n M_{xn1}^T \sin n\theta + \sum_n M_{xn2}^T \cos n\theta$$

in which N_r^T, M_y^T, and M_x^T are given by eqns (96). As with eqns (108), the first summations on the left-hand-side correspond to positive or zero n and the second summations to negative or zero n.

ENERGY IN TERMS OF NODAL DEGREES OF FREEDOM

Strain energy of shell segment

For constant nodal point spacing the shell reference surface displacement components u, v, w can be written

in terms of the nodal displacements in the form

$$\begin{Bmatrix} u \\ v \\ w \end{Bmatrix} \overset{3\times 7}{=} [D]\{q\} \tag{113}$$

in which

$$\overset{3\div 7}{[D]} = \begin{bmatrix} 0 & 1/2 & 0 & 0 & 1/2 & 0 & 0 \\ 0 & 0 & 1/2 & 0 & 0 & 1/2 & 0 \\ 0 & 0 & 0 & 1 & 0 & 0 & 0 \end{bmatrix} \tag{114}$$

and

$$\lfloor q \rfloor = \{q\}^T \equiv \lfloor w_{i-1},\ u_{i-1},\ v_{i-1},\ w_i,\ u_i,\ v_i,\ w_{i+1} \rfloor. \tag{115}$$

The reference surface strain, change in curvature, and twist are given, from eqns (90) and (109) by

$$\{\epsilon\} \equiv \begin{Bmatrix} \epsilon_1 \\ \epsilon_2 \\ \epsilon_{12} \\ \kappa_1 \\ \kappa_2 \\ 2\kappa_{12} \end{Bmatrix} \overset{6\times 7}{=} [B_1]\{q\} + \begin{Bmatrix} \frac{1}{2}(\beta^2 + \gamma^2) \\ \frac{1}{2}(\beta^2 + \gamma^2) \\ \beta\psi \\ 0 \\ 0 \\ 0 \end{Bmatrix} \tag{116}$$

in which

and for $n = 0$

$$u(s,\theta) = u(s); \quad v(s,\theta) = v(s); \quad w(s,\theta) = w(s). \tag{119}$$

The rotation-displacement relations (91) can be written in the form

$$\begin{Bmatrix} \beta \\ \psi \\ \gamma \end{Bmatrix} \equiv \{\omega\} \overset{3\times 7}{=} [R]\{q\} \tag{120}$$

where

$$\overset{3\times 7}{[R]} = \begin{bmatrix} -1/2h & -1/2R_1 & 0 & 0 & -1/2R_1 & 0 & 1/2h \\ 0 & 0 & -1/2R_2 & n/r & 0 & -1/2R_2 & 0 \\ 0 & n/4r & (1/2h - r'/4r) & 0 & n/4r & (-1/2h - r'/4r) & 0 \end{bmatrix} \tag{121}$$

Equations (113)–(117) are analogous to eqns (34)–(38) for the curved beam. Equations (120) and (121) are analogous to eqns (63) and (40), respectively. Insertion of eqn (116) into eqn (89) yields an expression for the strain energy of the shell which is analogous to eqn (44) for the beam. The only differences are the dimensions of the vectors and matrices and the fact that the shell energy must be integrated over θ as well as over s.

The nonlinear axisymmetric "prebuckling" (or in a modal vibration calculation, "prestress") analysis is carried out after specializing eqns (116) and (117) to axisymmetric displacements, that is, after setting e_{12}, κ_{12}, γ, ψ and n equal to zero.

Other components of the energy

A similar procedure is followed for the strain energy of the discrete rings. (Remember the smeared rings and stringers are included by appropriate modification of the

$$[B_1] \equiv \begin{bmatrix} 0 & -1/h & 0 & 1/R_1 \\ 0 & r'/2r & -n/2r & 1/R_2 \\ 0 & n/2r & \left(-\dfrac{1}{h} - \dfrac{r'}{2r}\right) & 0 \\ \dfrac{1}{h^2} & \left[\dfrac{1}{hR_1} - \dfrac{(1/R_1)'}{2}\right] & 0 & -\dfrac{2}{h^2} \\ -r'/2rh & -r'/2rR_1 & n/2rR_2 & -n^2/r^2 \\ \dfrac{n}{rh} & \dfrac{n}{rR_1} & \left(-\dfrac{r'}{rR_2} - \dfrac{2}{hR_2}\right) & 2\dfrac{nr'}{r^2} \end{bmatrix}$$

$$\begin{bmatrix} 1/h & 0 & 0 \\ r'/2r & & \\ n/2r & \left(\dfrac{1}{h} - \dfrac{r'}{2r}\right) & 0 \\ \left[-\dfrac{1}{hR_1} - \dfrac{(1/R_1)'}{2}\right] & 0 & 0 \\ -r'/2rR_1 & n/2rR_2 & r'/2rh \\ \dfrac{n}{rR_1} & \left(-\dfrac{r'}{rR_2} + \dfrac{2}{hR_2}\right) & -\dfrac{n}{rh} \end{bmatrix}. \tag{117}$$

Equation (117) is based on the assumption that for $n > 0$

$$u(s,\theta) = u_n(s)\sin n\theta, \quad v(s,\theta) = v_n(s)\cos n\theta;$$
$$= w_n(s)\sin n\theta \tag{118}$$

6×6 integrated constitutive law $[C]$!) The potential energy of the applied loads, the kinetic energies of the shell and of the discrete rings, and the junction and boundary conditions are handled in an analogous way.

BIFURCATION BUCKLING ANALYSIS

Two sets of loads

The bifurcation buckling problem represents perhaps the most difficult of the three types of analyses performed by shell-of-revolution computer programs. Therefore, details of the formulation are given here.

It is practical to consider bifurcation buckling of complex, ring-stiffened shell structures under various systems of loads, some of which are considered to be known and constant, or "fixed" during a computer run and others of which are considered to be unknown eigenvalue parameters, or "variable".

The notion of "fixed" and "variable" systems of loads not only permits the analysis of structures submitted to nonproportionally varying loads, but also helps in the formulation of a sequence of simple or "classical" eigenvalue problems of the form of eqn (75) for the solution of problems governed by "nonclassical" eigenvalue problems of the form of eqn (76). An example is a shallow spherical cap under external pressure, such as shown in Fig. 23. Very shallow caps fail by nonlinear collapse, or snap-through buckling, not by bifurcation buckling. Deep spherical caps fail by bifurcation buckling in which nonlinearities and edge effects in the prebuckling phase are not particularly important. There is a range of cap geometries for which bifurcation buckling is the mode of failure and for which the critical pressures are somewhat sensitive to predictable nonlinearities and nonuniform deformations in prebuckling behavior. The analysis of this intermediate class of spherical caps is simplified by the concept of "fixed" and "variable" pressure.

Figure 23 shows the load-deflection curve of a shallow cap in this intermediate range. Nonlinear axisymmetric collapse (p_{n1}), linear bifurcation (p_{1b}), and nonlinear bifurcation (p_{nb}) loads are shown. The purpose of the analysis in this section is to determine the pressure p_{nb}. It is useful to consider the pressure p_{nb} as composed of two parts

$$p_{nb} = p^f + \lambda \Delta p \qquad (122)$$

in which p^f denotes a known or "fixed" quantity, λ is an eigenvalue, and Δp is a known load increment. The fixed
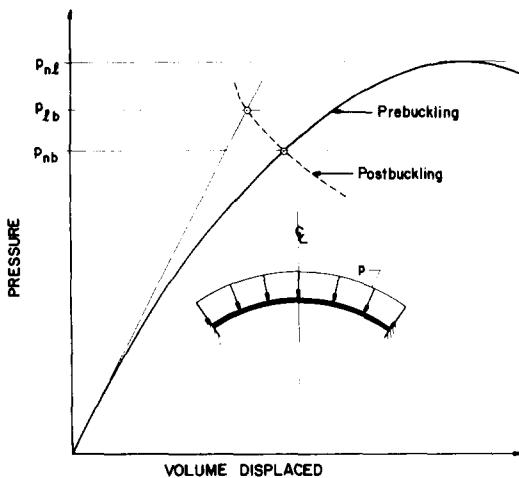
portion p^f is an initial guess or represents the results of a previous iteration. It is clear from Fig. 23 that if p^f is fairly close to p_{nb}, the behavior in the range $p = p^f \pm \lambda \Delta p$ is reasonably linear. Thus, the bifurcation point p_{nb} can be calculated by means of a sequence of eigenvalue problems of the form

$$[K_1(p_{(m)}^f)]\{x\} + \lambda[K_2(\Delta p_{(m)})]\{x\} = 0 \qquad (123)$$

through which, for increasing iteration index (m), ever and ever smaller values of $\lambda \Delta p_{(m)}$ are determined and added to the known results $p_{(m)}^f$ from the previous iterations. The initial guess $p_{(0)}^f$ need not be close to the solution p_{nb}.

The matrix K_1 is the stiffness matrix including the effects of the "fixed" loads $p_{(m)}^f$. The matrix K_2 is the "load-geometric" matrix and is proportional to the stress resultant increments due to the known load increment Δp. The derivation of these matrices follows.

As in the case of the beam analysis, it is known that an axisymmetric equilibrium state $\{x_0^f\} = \{(u_0^f, v_0^f, w_0^f)\}$ exists corresponding to the "fixed" load $p = p^f$. The object of the bifurcation buckling analysis is to determine whether $\{x_0^f + x^b\}$, where $\{x^b\}$ is an infinitesimal, nontrivial, kinematically admissible buckling mode, also represents an equilibrium state at $p = p^f$.

First a prebuckling solution $\{x_0^f + \Delta x_0\}$ is obtained at a neighboring load $p = p^f + \Delta p$. (Note that $\{\Delta x_0\}$ is a *finite* quantity, not infinitesimal as is the buckling mode $\{x^b\}$.) The total displacement $\{x\} = \{u\}, \{v\}, \{w\}$ is given by

$$\{u\} = \{u_0^f + \Delta u_0 + u^b\}; \quad \{v\} = \{v_0^f + \Delta v_0 + v^b\};$$
$$\{w\} = \{w_0^f + \Delta w_0 + w^b\}. \qquad (124)$$

Shell strain energy

When the r.h.s. of eqns (124) are inserted into eqns (90), the total reference surface strain and curvature-change vector can be expressed in the form

$$\{e\} = \{e^{(0)}\} + \{e^{(1)}\} + \{e^{(2)}\} \qquad (125)$$

in which $\{e^{(0)}\}$ represents the contribution of the displacements $\{x_0^f + \Delta x_0\}$; $\{e^{(1)}\}$ represents the contribution of the terms that are linear in the infinitesimal modal displacements $\{x^b\}$; and $\{e^{(2)}\}$ represents the contribution of the terms that are quadratic in $\{x^b\}$. The strain energy U_s in eqn (89) can be arranged such that terms of similar power in $\{x^b\}$ are collected

$$U_s = U^{(0)} + U^{(1)} + U^{(2)} + \dots \qquad (126)$$

The zero-th order terms in eqn (126) can be dropped because they are independent of the dependent variables $\{x^b\}$. The first order terms, when combined with the other components of the total energy functional H, cancel because $\{x_0^f + \Delta x_0\}$ is an equilibrium state. Terms of higher order than second in $\{x^b\}$ are vanishingly small compared to $U^{(2)}$. Hence, the expression for $U^{(2)}$ governs bifurcation buckling. From eqn (89) one can write

$$U^{(2)} = \frac{1}{2} \int_s \int_\theta (\lfloor e^{(1)} \rfloor [C] \{e^{(1)}\}$$
$$+ 2(\lfloor e^{(0)} \rfloor [C] + \lfloor N^T \rfloor)\{e^{(2)}\}) r \, d\theta \, ds. \qquad (127)$$

Analogous expressions can be written for the discrete

Fig. 23. Load-deflection curves for shallow spherical cap, showing bifurcation points from linear prebuckling curve (p_{1b}) and nonlinear prebuckling curve (p_{nb}) (from Bushnell[18]).

ring strain energy (eqn 95) and the junction and boundary conditions, eqns (104) and (105).

If the prebuckling state $\{x_0{}^f + \Delta x_0\}$ is axisymmetric and torsionless, the first order strain and curvature-change vector $\{\epsilon^{(1)}\}$ calculated from eqns (90) is given by

$$\{\epsilon^{(1)}\} = \begin{Bmatrix} u^{b\prime} + w^b/R_1 + (\beta_0{}^f + \Delta\beta_0)\beta^b \\ \dot{v}^b/r + u^b r'/r + w^b/R_2 \\ \dot{u}^b/r + r(v^b/r)' + (\beta_0{}^f + \Delta\beta_0)\psi^b \\ \beta^{b\prime} \\ \dot{\psi}^b/r + r'\beta^b/r \\ 2(-\dot{\beta}^b/r + r'\psi^b/r + v^{b\prime}/R_2) \end{Bmatrix} \quad (128)$$

The second order terms $\{\epsilon^{(2)}\}$ are given by

$$\{\epsilon^{(2)}\} = \begin{Bmatrix} \frac{1}{2}(\beta^b)^2 + \frac{1}{2}(\gamma^b)^2 \\ \frac{1}{2}(\psi^b)^2 + \frac{1}{2}(\gamma^b)^2 \\ \beta^b\psi^b \\ 0 \\ 0 \\ 0 \end{Bmatrix} \quad (129)$$

From eqn (84), the quantity $(\lfloor\epsilon^{(0)}\rfloor[C] + \lfloor N^T\rfloor)$ in eqn (127) can be written as $\lfloor S_0\rfloor$, where

$$\lfloor S_0\rfloor = \lfloor S_0{}^f\rfloor + \lfloor \Delta S_0\rfloor$$

$$= \lfloor N_{10}{}^f, N_{20}{}^f, 0, M_{10}{}^f, M_{20}{}^f, 0\rfloor \quad (130)$$

$$+ \lfloor \Delta N_{10}, \Delta N_{20}, 0, \Delta M_{10}, \Delta M_{20}, 0\rfloor.$$

It can easily be verified that the second product in eqn (127) can be transformed as follows

$$2\lfloor S_0\rfloor\{e^{(2)}\} = \lfloor \omega^b\rfloor[N_0{}^f + \Delta N_0]\{\omega^b\} \quad (131)$$

in which

$$\lfloor \omega^b\rfloor \equiv \lfloor \beta^b, \psi^b, \gamma^b\rfloor \quad (132)$$

$$[N_0{}^f + \Delta N_0] = \begin{bmatrix} N_{10}{}^f & 0 & 0 \\ 0 & N_{20}{}^f & 0 \\ 0 & 0 & (N_{10}{}^f + N_{20}{}^f) \end{bmatrix} + \begin{bmatrix} \Delta N_{10} & 0 & 0 \\ 0 & \Delta N_{20} & 0 \\ 0 & 0 & (\Delta N_{10} + \Delta N_{20}) \end{bmatrix} \quad (133)$$

The $\Delta\beta_0$ should be neglected in eqn (128) because these terms contribute to the stiffness matrix $[K_1(p_{(m)}]$, which is to be evaluated at $p_{(m)}{}^f$, not at $p_{(m)}{}^f + \Delta p_{(m)}$. The vector $\{\epsilon^{(1)}\}$ can be written in terms of the nodal point degrees of freedom $\lfloor q^b\rfloor$:

$$\{\epsilon^{(1)}\} = \left[\overset{6\times 7}{[B_1]} + \beta_0{}^f\overset{6\times 7}{[B_2]}\right]\{q^b\} \quad (134)$$

in which $[B_1]$ is given by eqn (117), $[B_2]$ is given by

$$[B_2] \equiv \begin{bmatrix} -1/2h & -1/2R_1 & 0 & 0 & -1/2R_1 & 0 & 1/2h \\ 0 & 0 & 0 & 0 & 0 & 0 & 0 \\ 0 & 0 & -1/2R_2 & n/r & 0 & -1/2R_2 & 0 \\ 0 & 0 & 0 & 0 & 0 & 0 & 0 \\ 0 & 0 & 0 & 0 & 0 & 0 & 0 \\ 0 & 0 & 0 & 0 & 0 & 0 & 0 \end{bmatrix} \quad (135)$$

and $\{q^b\}$ is given by eqn (115) with superscript "b" added. The rotation vector $\lfloor\omega\rfloor$ is expressed in terms of the nodal point degrees of freedom in eqn (120) and (121).

Using eqns (120), (131) and (134); integrating over θ (multiply by 2π if $n = 0$, π if $n \neq 0$); and integrating over s (multiply by h), one can transform the shell strain energy expression (127) into the form

$$U^{(2)} = \frac{(\pi \text{ or } 2\pi)}{2} hr_k\Big(\overset{1\times 7}{\lfloor q^b\rfloor}\Big[\overset{7\times 6}{[B_1 + \beta_0{}^f B_2]^T}\overset{6\times 6}{[C]}\overset{6\times 7}{[B_1 + \beta_0{}^f B_2]}$$

$$+ \overset{7\times 3}{[\bar{R}]^T}\overset{3\times 3}{[N_0{}^f]}\overset{3\times 7}{[\bar{R}]}\Big]\{q^b\} \quad (136)$$

$$+ \lfloor q^b\rfloor\overset{7\times 3}{[\bar{R}]^T}\overset{3\times 3}{[\Delta N_0]}\overset{3\times 7}{[\bar{R}]}\{q^b\}\Big)$$

in which r_k is the radius r (Fig. 20a) evaluated at the midlength of the kth finite element. For the kth finite element the local stiffness mass matrix $[K_1(p_{(m)})]^k_{\text{shell}}$ of the shell as loaded by the "fixed" loads $p_{(m)}{}^f$ is given by hr_k times the first set of terms in eqn (136) that are premultiplied by $\lfloor q^b\rfloor$ and postmultiplied by $\{q^b\}$. The local load-geometric matrix $[K_2(\Delta p_{(m)})]^k_{\text{shell}}$ is given by hr_k times the second set, that is

$$[K_2(\Delta p_{(m)})]^k_{\text{shell}} = hr_k[\bar{R}]^T[\Delta N_0][\bar{R}]. \quad (137)$$

The $K_1{}^k$ and $K_2{}^k$ just described are analogous to the local stiffness and load-geometric matrices for the curved beam, given in eqns (74) and (74a), respectively. These local matrices are assembled into the global matrices of eqn (123) in the same way as described in connection with the discussion associated with Figs. 12 and 13 for the curved beam. Figure 24 shows the format of the global stiffness matrix $[K_1]$ corresponding to the two-segment discretized model in Fig. 20(b).

Strain energy of a discrete ring stiffener

The strain energy U_r of a discrete ring, given by eqn (95), can be expanded in the same manner as that of the shell,

$$U_r = U_r^{(0)} + U_r^{(1)} + U_r^{(2)} + \dots \quad (138)$$

Again, it is $U_r^{(2)}$ that governs bifurcation buckling

$$U_r^{(2)} = \frac{1}{2}\int_\theta (\lfloor\epsilon_r^{(1)}\rfloor\overset{4\times 4}{[\bar{G}]}\{\epsilon_r^{(1)}\}$$

$$+ 2(\lfloor\epsilon_r^{(0)}\rfloor[\bar{G}] + \lfloor\bar{N}_r{}^T\rfloor)\{\epsilon_r^{(2)}\})r_c\, d\theta \quad (139)$$

in which, from eqns (95) and (97)

$$\{\epsilon_r^{(1)}\} = \begin{Bmatrix} \epsilon_r \\ \kappa_x \\ \kappa_y \\ \kappa_{xy} \end{Bmatrix} = \begin{Bmatrix} \dot{v}_c^b/r_c + w_c^b/r_c \\ \dot{\psi}_c^b/r_c \\ -\dot{\gamma}_c^b/r_c + \beta^b/r_c \\ \dot{\beta}^b/r_c + \dot{u}_c^b/r_c^2 \end{Bmatrix} \quad (140)$$

$$\{\epsilon_r^{(2)}\} = \begin{Bmatrix} \frac{1}{2}\psi_c^2 + \frac{1}{2}\gamma_c^2 \\ 0 \\ 0 \\ 0 \end{Bmatrix} \quad (141)$$

$$[\overset{4\times4}{\bar{G}}] = \begin{bmatrix} E_rA & 0 & 0 & 0 \\ 0 & E_rI_y & -E_rI_{xy} & 0 \\ 0 & -E_rI_{xy} & E_rI_x & 0 \\ 0 & 0 & 0 & GJ \end{bmatrix} \quad (142)$$

and

$$\lfloor \bar{N}_r^T \rfloor = \lfloor N_r^T, M_y^T, M_x^T \rfloor \quad (143)$$

with N_r^T, M_y^T, M_x^T given by eqns (96). As with the shell strain energy, the term $(\lfloor \epsilon_r^{(0)} \rfloor [\bar{G}] + \lfloor \bar{N}_r^T \rfloor)$ in eqn (139) represents an axisymmetric prebuckling force and

moment $\lfloor S_{ro} \rfloor$ in the ring. $\lfloor S_{ro} \rfloor$ can be written in the form

$$\lfloor S_{ro} \rfloor = \lfloor S_{ro}^f \rfloor + \lfloor \Delta S_{ro} \rfloor$$
$$= \lfloor N_{ro}^f, 0, M_{ro}^f, 0 \rfloor + \lfloor \Delta N_{ro}, 0, \Delta M_{ro}, 0 \rfloor. \quad (144)$$

The second product in eqn (139) can be expressed in the form

$$2\lfloor S_{ro} \rfloor \{\epsilon_r^{(2)}\} = \lfloor \omega_c^b \rfloor [\bar{N}_{ro}^f + \Delta \bar{N}_{ro}]\{\omega_c^b\} \quad (145)$$

in which

$$\lfloor \omega_c^b \rfloor \quad \lfloor \psi_c^b, \gamma_c^b \rfloor \quad (146)$$

$$[\bar{N}_{ro}^f + \Delta \bar{N}_{ro}] \equiv \begin{bmatrix} N_{ro}^f & 0 \\ 0 & N_{ro}^f \end{bmatrix} + \begin{bmatrix} \Delta N_{ro} & 0 \\ 0 & \Delta N_{ro} \end{bmatrix}. \quad (147)$$

The quantities N_{ro}^f and ΔN_{ro} represent the prebuckling ring hoop force due to the "fixed" load $p_{(m)}^f$ and change in load $\Delta p_{(m)}$, respectively. The prebuckling ring moment does not appear in eqn (147) because the ring curvature-change expressions are linear.

It is necessary to express the discrete ring strain energy $U_r^{(2)}$ in terms of the shell reference surface nodal point degrees of freedom $\lfloor q^b \rfloor$. First eqn (140) can be
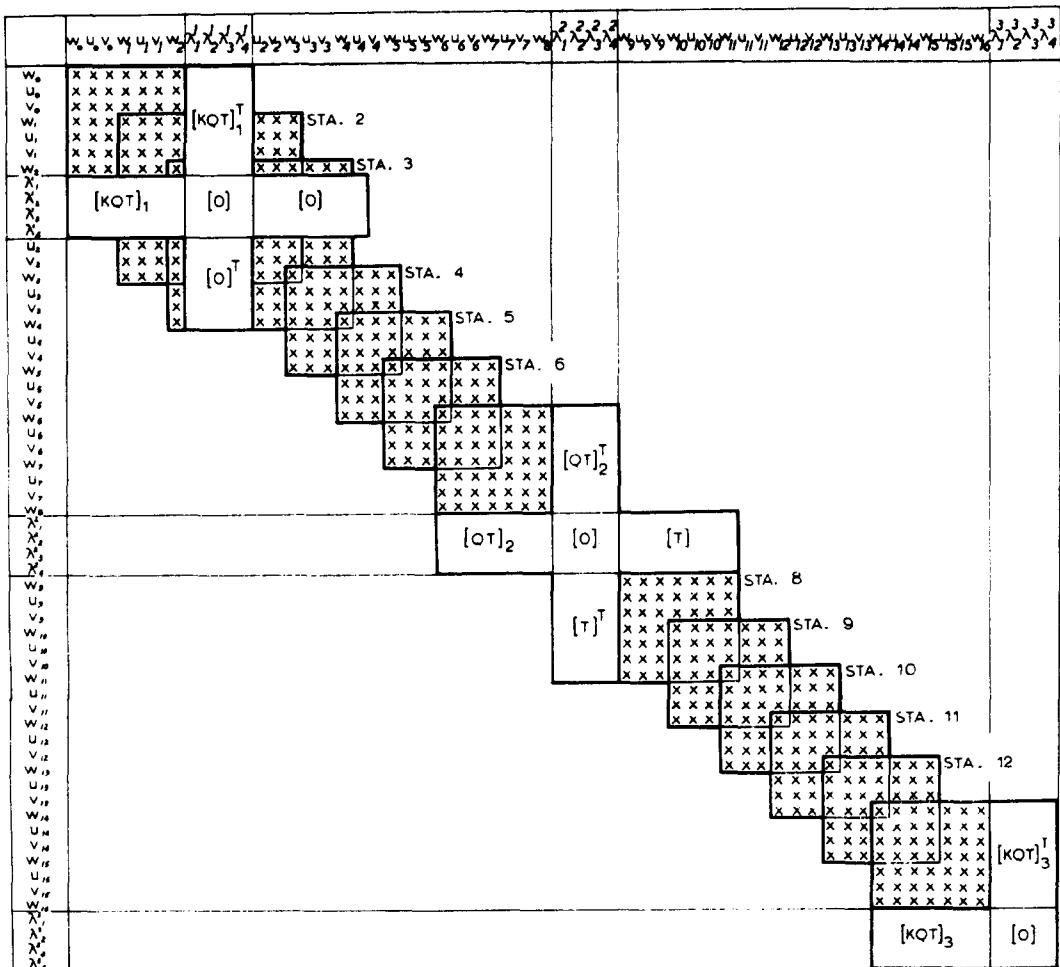

Fig. 24. Form of global stiffness matrix $[K_1]$ including constraint conditions. This matrix corresponds to the discretized model in Fig. 20(b) (from Bushnell[30]).

written in the form

$$\{\epsilon_r^{(1)}\} = [B_r] \overset{4\times4}{\begin{Bmatrix} u_c^{b} \\ v_c^{b} \\ w_c \\ \beta^{b} \end{Bmatrix}} \tag{148}$$

where

$$\overset{4\times4}{[B_r]} = \begin{bmatrix} 0 & -n/r_c & 1/r_c & 0 \\ 0 & n/r_c^2 & -n^2/r_c^2 & 0 \\ n^2/r_c^2 & 0 & 0 & 1/r_c \\ n/r_c^2 & 0 & 0 & n/r_c \end{bmatrix} \tag{149}$$

Equations (97d) and (97e) for the rotation components ψ_c and γ_c were used in the derivation of eqn (149). Similarly,

$$\{\omega_c^{b}\} = \begin{Bmatrix} \psi_c^{b} \\ \gamma_c^{b} \end{Bmatrix} = \overset{2\times4}{[B_\omega]} \begin{Bmatrix} u_c^{b} \\ v_c^{b} \\ w_c^{b} \\ \beta^{b} \end{Bmatrix} \tag{150}$$

in which

$$[B_\omega] = \begin{bmatrix} 0 & -1/r_c & n/r_c & 0 \\ n/r_c & 0 & 0 & 0 \end{bmatrix}. \tag{151}$$

Next, it is necessary to express the vector $\lfloor u_c^{b}, v_c^{b}, w_c^{b}, \beta^{b} \rfloor$ in terms of displacement components $\lfloor u^{*b}, v^{*b}, w^{*b}, \beta^{b} \rfloor$ of the shell reference surface at the line of attachment of the ring to the shell. (The displacement components u^* and w^* are shown in Fig. 18. The circumferential component $v^* = v$.) This transformation has the form

$$\begin{Bmatrix} u_c^{b} \\ v_c^{b} \\ w_c^{b} \\ \beta^{b} \end{Bmatrix} = [\bar{E}_1 + \beta_0^{f} \bar{E}_2] \overset{4\times4}{} \begin{Bmatrix} u^{*b} \\ v^{*b} \\ w^{*b} \\ \beta^{b} \end{Bmatrix} \tag{152}$$

where β_0^{f} is the prebuckling meridional rotation associated with the "fixed" loads. Consistent with eqns (106) and (103) and Fig. 18, it can be shown that

$$\overset{4\times4}{[\bar{E}_1]} = \begin{bmatrix} 1 & 0 & 0 & -e_1 \\ -e_2 n/r & (1+e_1/r) & -e_1 n/r & 0 \\ 0 & 0 & 1 & e_2 \\ 0 & 0 & 0 & 1 \end{bmatrix} \tag{153}$$

$$\overset{4\times4}{[\bar{E}_2]} = \begin{bmatrix} 0 & 0 & 0 & -e_2 \\ e_1 n/r & e_2/r & -e_2 n/r & 0 \\ 0 & 0 & 0 & -e_1 \\ 0 & 0 & 0 & 0 \end{bmatrix}. \tag{154}$$

Finally, the vector $\lfloor u^{*b}, v^{*b}, w^{*b}, \beta^{b} \rfloor$ must be expressed, with the help of eqns (107), in terms of the nodal point degrees of freedom

$$\begin{Bmatrix} u^{*b} \\ v^{*b} \\ w^{*b} \\ \beta^{b} \end{Bmatrix} = \overset{4\times7}{[\bar{T}]} \{q^{b}\} \tag{155}$$

in which

$$\overset{4\times7}{[\bar{T}]} = \begin{bmatrix} 0 & r/2R_2 & 0 & -r' & r/2R_2 & 0 & 0 \\ 0 & 0 & 1/2 & 0 & 0 & 1/2 & 0 \\ 0 & r'/2 & 0 & r/R_2 & r'/2 & 0 & 0 \\ -1/2h & -1/2R_1 & 0 & 0 & -1/2R_1 & 0 & 1/2h \end{bmatrix}. \tag{156}$$

Using eqns (148), (150), (152) and (155) and integrating over θ, one can express the ring strain energy expression (139) in the form

$$U_r^{(2)} = \frac{(\pi \text{ or } 2\pi)}{2} r_c \Big(\overset{1\times7}{\lfloor q^{b} \rfloor} \overset{7\times4}{[\bar{T}]^T} [\bar{E}_1 + \beta_0^{f} \bar{E}_2]^T \overset{4\times4}{} \Big[\overset{4\times4}{[B_r]^T} \overset{4\times4}{[\bar{G}]} \overset{4\times4}{[B_r]}$$
$$+ \overset{4\times2}{[B_\omega]^T} (\overset{2\times2}{[\bar{N}_{r0}^{f}]} + \overset{2\times2}{[\Delta\bar{N}_{r0}]}) \overset{2\times4}{[B_\omega]} \Big] [\bar{E}_1 + \beta_0^{f} \bar{E}_2] \overset{4\times7}{[\bar{T}]} \{q^{b}\} \Big). \tag{157}$$

All of the terms in eqn (157) except those involving $[\Delta\bar{N}_{r0}]$ contribute to the stiffness matrix $[K_1(p_{(m)})]$. The terms involving $[\Delta\bar{N}_{r0}]$ contribute to the load-geometric matrix $[K_2(\Delta p_{(m)})]$. The contributions of each discrete ring to the total strain energy of the axisymmetric structure are added to the local stiffness and load-geometric matrices of the shell finite element which contains the attachment point of that ring.

Constraint conditions

The junction conditions (104) and boundary conditions (105a,b) contribute only to the stiffness matrix $[K_1(p_{(m)}^{f})]$ of the structure as loaded by the "fixed" loads $p_{(m)}^{f}$.

The mth constraint condition U_c^{m} can be written in the form

$$U_c^{m} = \lfloor \lambda_1^{m}, \lambda_2^{m}, \lambda_3^{m}, \lambda_4^{m} \rfloor$$
$$\times [I] \begin{Bmatrix} u^{*+} \\ v^{*+} \\ w^{*+} \\ \beta^{+} \end{Bmatrix}_l + [Q_1^{m} + \beta_{0l}^{f} Q_2^{m}] \begin{Bmatrix} u^{*-} \\ v^{*-} \\ w^{*-} \\ \beta^{-} \end{Bmatrix}_l \tag{158}$$

in which the superscript "b" has been dropped for convenience, subscript l refers to the meridional station corresponding to the mth junction between segments, and $[Q_1^{m}]$ and $[Q_2^{m}]$ are analogous to the negatives of $[\bar{E}_1]$ and $[\bar{E}_2]$:

$$[Q_1^{m}] = \begin{bmatrix} -1 & 0 & 0 & d_1 \\ nd_2/r & -(1+d_1/r) & nd_1/r & 0 \\ 0 & 0 & -1 & -d_2 \\ 0 & 0 & 0 & -1 \end{bmatrix} \tag{159}$$

$$[Q_2^{m}] = \begin{bmatrix} 0 & 0 & 0 & d_2 \\ -nd_1/r & -d_2/r & nd_2/r & 0 \\ 0 & 0 & 0 & d_1 \\ 0 & 0 & 0 & 0. \end{bmatrix} \tag{160}$$

In eqns (159) and (160) superscript m has been omitted for convenience from the arrays. The $\lambda_1^{m}, \lambda_2^{m}, \lambda_3^{m}$, and λ_4^{m} are the mth set of Lagrange multipliers associated with the lth station at which constraints are imposed on the quantities u^*, v^*, w^* and β. For example, the con-

straint conditions between Segments 1 and 2 in Fig. 20(b) ($m = 2, l = 7$) arise from the requirement that the motion during buckling or vibration of point D relative to point C involves no deformation, only rigid body translation and rotation of the ring cross-section. The quantity $\lambda_1{}^m$ corresponds to compatibility of axial displacements u^{*-} and u^{*+}; $\lambda_2{}^m$ corresponds to compatibility of circumferential displacements v^{*-} and v^{*+}; $\lambda_3{}^m$ to compatibility of radial displacements w^{*-} and w^{*+}; and $\lambda_4{}^m$ to compatibility of meridional rotations β^- and β^+.

Displacement boundary conditions applied at the A and B ends of the meridian (see Fig. 20) take the form

$$U_c{}^m = \lfloor \lambda_1{}^m, \lambda_2{}^m, \lambda_3{}^m, \lambda_4{}^m \rfloor \ [K^m] \ [Q_1{}^m + \beta_{01} Q_2{}^m] \begin{Bmatrix} u^* \\ v^* \\ w^* \\ \beta \end{Bmatrix}$$

(161)

Corresponding to the end A of the meridian ($m = 1$):

$$[K^m] = \begin{bmatrix} K_{A1} & 0 & 0 & 0 \\ 0 & K_{A2} & 0 & 0 \\ 0 & 0 & K_{A3} & 0 \\ 0 & 0 & 0 & K_{A4} \end{bmatrix}.$$

(162)

Corresponding to the end B of the meridian ($m = 3$):

$$\begin{bmatrix} K_{B1} & 0 & 0 & 0 \\ 0 & K_{B2} & 0 & 0 \\ 0 & 0 & K_{B3} & 0 \\ 0 & 0 & 0 & K_{B4} \end{bmatrix}$$

(163)

Equations (162) and (163) are analogous to eqns (27a,b) in the curved beam analysis. The quantities K_{A1}, K_{A2}, etc. and K_{B1}, K_{B2}, etc. are assigned values, either unity if the corresponding displacement component is zero or zero if the corresponding force component is zero. The displacement conditions correspond to a shell which is supported at distances $d_1{}^m$ and $d_2{}^m$ from the reference surface. For the shell in Fig. 20(a) the K_{A1}, K_{A2}, etc. would all be zero and the K_{B1}, K_{B2}, etc. would all be unity. The constraint conditions (158) and (161) can be written in terms of the vectors $[q^+]$ and $[q^-]$ by use of eqn (155). The compatibility condition (158) can be written as a symmetric quadratic form in the following way:

$$U_c{}^m = \lfloor q^-, \lambda, q^+ \rfloor [F] \begin{Bmatrix} q^- \\ \lambda \\ q^+ \end{Bmatrix}$$

(164)

with

$$\lambda \equiv \lfloor \lambda_1{}^m, \lambda_2{}^m, \lambda_3{}^m, \lambda_4{}^m \rfloor$$

(165)

$$[F] = \begin{bmatrix} \overset{7\times7}{[0]} & \overset{7\times7}{[QT]^T} & \overset{7\times7}{[0]} \\ \overset{4\times7}{[QT]} & \overset{4\times4}{[0]} & \overset{4\times7}{[T]} \\ \overset{7\times7}{[0]} & \overset{7\times4}{[T]^T} & \overset{7\times7}{[0]} \end{bmatrix}$$

(166)

$$Q \equiv [Q_1{}^m + \beta_{01} Q_2{}^m].$$

(167)

The boundary conditions (161) take a similar form:

$$U_c{}^m = \lfloor q^-, \lambda, q^+ \rfloor \begin{bmatrix} [0] & [KQT]^T & [0] \\ [KQT] & [0] & [0] \\ [0] & [0] & [0] \end{bmatrix} \begin{Bmatrix} q^- \\ \lambda \\ q^+ \end{Bmatrix}$$

(168)

The contributions of the junction conditions (164) and boundary conditions (168) to the global stiffness matrix of the structure shown in Fig. 20 appear in Fig. 24. The boundary conditions at A contribute the elements $[KQT]_1$ and $[KQT]_1{}^T$; the compatibility conditions for conformity of displacements and rotation at the junction between Segment 1 and Segment 2 contribute the elements $[QT]_2$, $[QT]_2{}^T$, $[T]$, and $[T]^T$; and the boundary conditions at B contribute the elements $[KQT]_3$ and $[KQT]_3{}^T$.

Live load effects

The expressions (98) and (99) for the potential energy of the applied loads are valid for constant-directional loads. Cohen[29] gives the conditions of conservativeness for a load that rotates with structural deformations, such as a pressure acting normal to a continuously deforming shell. The potential energy expression, including pressure-rotation or "live" load effects, is given by Cohen[29] for a shell of revolution as follows:

$$U_{p2} = -\int_s \int_\theta \left[(p_1 u + p_2 v + p_3 w) - \frac{1}{2} p_3 \left(\frac{1}{R_1} + \frac{1}{R_2} \right) w^2 \right.$$
$$\left. + \frac{1}{2} p_3 \left(\frac{u^2}{R_1} + \frac{v^2}{R_2} \right) + u w p_3' \right] r \, d\theta \, ds.$$

(169)

The quadratic terms in eqn (169) contribute to the stiffness matrix $[K_1(p_{(m)}')]$ and to the load-geometric matrix $[K_2(\Delta p_{(m)})]$. The contribution to $[K_1(p'_{(m)})]$ arises from

$$\frac{(\pi \text{ or } 2\pi)}{2} h r_k (\lfloor q^b \rfloor \overset{7\times3}{[D]^T} \overset{3\times3}{[\bar{P}']} \overset{3\times7}{[D]} \{q^b\}$$

(170)

and the contribution to $[K_2(\Delta p_{(m)})]$ arises from

$$\frac{(\pi \text{ or } 2\pi)}{2} h r_k (\lfloor q^b \rfloor \overset{7\times3}{[D]^T} \overset{3\times3}{[\Delta \bar{P}]} \overset{3\times7}{[D]} \{q^b\})$$

(171)

in which r_k is the radius r evaluated at the midlength of the kth finite element, $[D]$ is given by eqn (114), and $[\bar{P}']$ is

$$\overset{3\times3}{[\bar{P}']} = \begin{bmatrix} -p_3{}^f/R_1 & 0 & -p_3' \\ 0 & -p_3{}^f/R_2 & 0 \\ -p_3' & 0 & p_3{}^f(1/R_1 + 1/R_2) \end{bmatrix}$$

(172)

The matrix $[\Delta \bar{P}]$ is given by eqn (172) with $p_3{}^f$ replaced by Δp_3.

There is an analogous contribution from the horizontal line load H (Fig. 18) acting normal to the deformed centroidal axis of the discrete ring. The contribution of the line load-rotation effect to $[K_1(p_{(m)}')]$ arises from

$$\frac{(\pi \text{ or } 2\pi)}{2} r_c \left(\lfloor q^b \rfloor \overset{7\times4}{[\bar{T}]^T} [\bar{E}_1 + \overset{4\times4}{\beta_0{}^f \bar{E}_2}]^T \overset{4\times4}{[\bar{H}^f]} \right.$$
$$\left. \times [\bar{E}_1 + \overset{4\times4}{\beta_0{}^f \bar{E}_2}] \overset{4\times7}{[\bar{T}]} \{q^b\} \right)$$

(173)

in which

$$[\overset{4\times4}{H^f}] = \begin{bmatrix} 0 & 0 & 0 & 0 \\ 0 & -H^f/r_c & 0 & 0 \\ 0 & 0 & H^f/r_c & 0 \\ 0 & 0 & 0 & 0 \end{bmatrix} \quad (174)$$

The contribution to $[K_2(\Delta p_{(m)})]$ arises from the same expressions with $\bar{H}^f$ replaced by $\Delta \bar{H}$ and H^f by ΔH.

Summary of bifurcation buckling matrices

The eigenvalue problem for bifurcation buckling is expressed in eqn (123). The contributions of the three energy components U_s, U_r, U_p, to the kth finite element local stiffness matrix $[K_1(p_{(m)}{}^f)]^k$ and load-geometric matrix $[K_2(\Delta p_{(m)})]^k$ can be combined from eqns (136), (157), (170), (171) and (173). These local finite element matrices, divided by a common factor, π or 2π (depending on n), are given by

$$[K_1(p_{(m)}{}^f)]^k = hr_k [\overset{\text{①}}{[[B_1 + \beta_0{}^f B_2]^T [C][B_1 + \beta_0{}^f B_2]}$$

$$+ \overset{\text{②}}{[\bar{R}]^T [N_0{}^f][\bar{R}]} + \overset{\text{③}}{[D]^T [\bar{P}^f][D]]_k}$$

$$+ \overset{\text{④}}{\delta_j{}^k r_{cj} [[\bar{T}]^T [\bar{E}_1 + \beta_0{}^f \bar{E}_2]^T ([B_r]^T [\bar{G}][B_r]}$$

$$\overset{\text{⑤}}{+ [B_\omega]^T [\bar{N}_{r0}{}^f][B_\omega]}$$

$$\overset{\text{⑥}}{+ [\bar{H}^f])[\bar{E}_1 + \beta_0{}^f \bar{E}_2][\bar{T}]]_j} \quad (175)$$

$$[K_2(\Delta p_{(m)})]^k = hr_k [\overset{\text{⑦}}{[\bar{R}]^T [\Delta N_0][\bar{R}]} + \overset{\text{⑧}}{[D]^T [\Delta \bar{P}][D]]_k}$$

$$+ \overset{\text{⑨}}{\delta_j{}^k r_{cj} [[\bar{T}]^T [\bar{E}_1 + \beta_0{}^f \bar{E}_2]^T ([B_\omega]^T [\Delta \bar{N}_{r0}][B_\omega]}$$

$$\overset{\text{⑩}}{+ [\Delta \bar{H}])[\bar{E}_1 + \beta_0{}^f \bar{E}_2][\bar{T}]]_j} \quad (176)$$

in which k indicates "kth finite element", $\delta_j{}^k$ are Kronecker deltas, and j indicates a station to which is attached a discrete ring.

Figure 24 shows how the local stiffness matrices $[K_1]^k$ are assembled or accumulated into the global stiffness matrix $[K_1]$ for the two-segment structure shown in Fig. 20(a), discretized as indicated in Fig. 20(b). Each of the thirteen 7×7 subarrays $[K_1]^k$ is centered on the main diagonal of $[K_1]$ and overlaps its neighbors as shown. The constraint condition arrays given by eqns (166) and (168) are assembled into $[K_1]$ right after assembly of the local stiffness matrix corresponding to the station at which the constraint is applied. Assemblage of $[K_2]^k$ into $[K_2]$ is similar, the only difference being that there are no contributions from the constraint conditions.

Table 2 summarizes where the various terms in eqns (175) and (176) come from and their physical meanings.

Computational strategy for calculation of critical bifurcation load

The stiffness matrix $[K_1]$, load-geometric matrix $[K_2]$, and eigenvalue λ in eqns (123) depend on the number of circumferential waves n in the buckling mode $\{x^b\}$.

Hence, the bifurcation buckling eigenvalue problem might be better posed as

$$[K_1(p_{(m)}{}^f, n)]\{x^b\} + \lambda_n [K_2(\Delta p_{(m)}, n)]\{x^b\} = 0. \quad (177)$$

Figure 25 shows a sequence of critical load estimates $p_{cr}(n)$ that might result, for example, from an analysis of a spherical cap under uniform external pressure, such as is depicted in Fig. 23. The computer program user provides a range of n, $n_{min} \leq n \leq n_{max}$, which is to be explored during a search for the minimum $p_{cr}(n)$. The user also provides as input initial values for $n, p_{(0)}{}^f$, and $\Delta p_{(0)}$. Usually, he will choose n in the middle of the range n_{min} to n_{max}, $p_{(0)}{}^f = 0$, and $\Delta p_0 = $ unity. Such a choice yields eigenvalues λ_n which are numerically equal to the bifurcation load $p_{cr}(n)$. Figure 25 indicates an initial choice of $n = 8$ and $p_{(0)}{}^f = 10.0$. Suppose that initially $\Delta p_{(0)} = 1.0$. The first eigenvalue problem to be posed and solved is

$$[K_1(p_{(0)}{}^f = 10, n = 8)]\{x^b\} + \lambda_8 [K_2(\Delta p_{(0)} = 1, n = 8)]\{x^b\}$$
$$= 0. \quad (178)$$

The point on the dashed curve labeled "1" indicates the first computed bifurcation buckling load estimate, which is calculated from

$$p_{cr}(8) = p_{(0)}{}^f + \lambda_8 * \Delta p_{(0)} \approx 70. \quad (179)$$

From the scale shown in Fig. 25 and the initial conditions $p_{(0)}{}^f = 10.0$, $\Delta p_{(0)} = 1.0$, it is seen that the first eigenvalue λ_8 calculated by the program would have been about 60.

With $p_{(0)}{}^f$ fixed at 10.0 and $\Delta p_{(0)}$ fixed at 1.0, an eigenvalue is next calculated for $n = 9$. The result,

$$p_{cr}(9) = 10.0 + \lambda_9 * 1.0 \approx 60 \quad (180)$$

is labeled "2" on the dashed curve and corresponds to a smaller eigenvalue than that for $n = 8$. Hence, n is further increased by the computer program until a minimum $p_{cr}(n)$ is perceived. The loads $p_{(0)}{}^f$ and $\Delta p_{(0)}$ are held fixed during this phase of the calculations, so that the
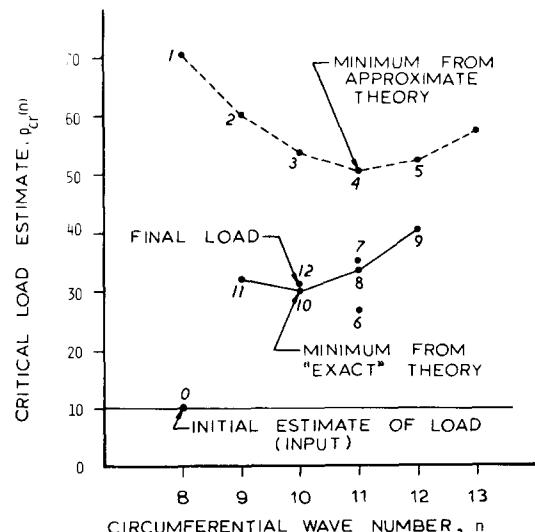

Fig. 25. Strategy for calculation of critical buckling load p_{nb}.

Table 2. Physical explanations of terms in local stiffness and load-geometric matrices eqns (175) and (176)

	Term Number	Derived From Equation Number	Physical Explanation of the Term
Local Stiffness Matrix $[(K_1)(p^f_{(m)})]$	①	136	Stiffness matrix for shell as deformed by the 'fixed' load $p^f_{(m)}$ (Smeared stiffeners included here.)
	②	136	Modification of shell stiffness due to 'fixed' membrane prestress in shell wall
	③	170	Pressure-rotation (live load) effect from 'fixed' load $p^f_{(m)}$
	④	157	Contribution to stiffness of discrete ring as deformed by 'fixed' load.
	⑤	157	Modification of discrete ring stiffness due to pre-buckling hoop force from 'fixed' load
	⑥	173	Line load-rotation (live load) effect from 'fixed' load $p^f_{(m)}$.
Local Load Geometric Matrix $[K_2(\Delta p_{(m)})]^k$	⑦	136	Work done by prebuckling shell wall stress resultant increments due to load increment $\Delta p_{(m)}$ during buckling modal shell wall rotations.
	⑧	171	Pressure rotation (live load) effect from load increment $\Delta p_{(m)}$.
	⑨	157	Work done by prebuckling discrete ring hoop force increment due to load increment $\Delta p_{(m)}$ during buckling modal ring rotations.
	⑩	173	Line load-rotation (live load) effect from load increment $\Delta p_{(m)}$.

nonlinear prebuckling analysis is not repeated for $n = 9$, 10, 11, or 12.

The program "perceives" that the estimated critical load $p_{cr}(11)$ is a minimum in the range of n provided. At this point new values of the "fixed" load and load increment are established

$$p_{(1)}^f = p_{(0)}^f + \lambda(11) * \Delta p_{(0)}, \quad (181)$$

$$\Delta p_{(1)} = p_{(1)}^f / 1000. \quad (182)$$

The load increment $\Delta p_{(1)}$ is set very small compared to "fixed" component $p_{(1)}^f$ to minimize the difficulty of finding a nonlinear prebuckling solution at the load $p_{(1)}^f + \Delta p_{(1)}$. Also, the small increment added to a relatively large fixed load yields an accurate approximation of the rate of change of prebuckling stress resultants in the neighborhood of $p_{(1)}^f$. New prebuckling solutions are obtained for loads $p_{(1)}^f$ and $p_{(1)}^f + \Delta p_{(1)}$. A new eigenvalue problem

$$[K_1(p_{(1)}^f, n = 11)]\{x^b\} + \lambda_{11}[K_2(\Delta p_{(1)}, n = 11)]\{x^b\} = 0 \quad (183)$$

is set up and solved, leading to the result labeled "6" in Fig. 25:

$$p_{cr}^{(6)}(11) = p_{(1)}^f + \lambda_{11}^{(6)} * \Delta p_{(1)} \approx 28. \quad (184)$$

From Fig. 25 it is seen that $p_{cr}^{(6)}(11)$ is considerably less than $p_{cr}^{(4)}(11)$, so that $\lambda_{11}^{(6)}$ must have been negative.

For the next two critical load estimates, $p_{cr}^{(7)}$ and $p_{cr}^{(8)}$, the number of circumferential waves n is held constant at 11 and new values of $p_{(m)}^f$ and $\Delta p_{(m)}$ established until $|\lambda * \Delta p_{(m)}|$ is smaller than $|p_{(m)}^f / 1000|$. First, new nonlinear prebuckling solutions are obtained corresponding to

$$p_{(2)}^f = p_{cr}^{(6)}(11); \quad \Delta p_{(2)} = p_{(2)}^f / 1000 \quad (185)$$

and a new eigenvalue problem

$$[K_1(p_{(2)}^f, n = 11)]\{x^b\} + \lambda_{11}^{(7)}[K_2(\Delta p_{(2)}, n = 11)]\{x^b\} = 0 \quad (186)$$

is solved, leading to the result labeled "7" in Fig. 25:

$$p_{cr}^{(7)}(11) = p_{(3)}^f = p_{(2)}^f + \lambda_{11}^{(7)} * \Delta p_{(2)} \approx 36. \quad (187)$$

This process is repeated once more before convergence at

$$p_{cr}^{(8)}(11) = p_{(4)}^f = p_{(3)}^f + \lambda_{11}^{(8)} * \Delta p_{(3)}. \quad (188)$$

At this point the circumferential wave number is again varied with $p_{(4)}^f = p_{cr}^{(8)}(11)$ and $\Delta p_{(4)} = p_{(4)}^f / 1000$ held constant. A new minimum critical load is perceived at

$n = 10$. Once more the procedure described in connection with eqns (181)–(188) is followed. The final critical load estimate is $p_{cr}^{(12)}$ and the corresponding critical circumferential wave number is $n = 10$. This is the load denoted p_{nb} in Fig. 23.

Pitfalls

The strategy just described works well if the collapse load p_{nl} corresponding to axisymmetric snap-through is higher than any of the estimates $p_{(m)}{}^f$ and if the eigenvalues $\lambda_n^{(j)}$ always correspond to the lowest bifurcation point. The strategy must be modified if the situations depicted in Figs. 26 or 27 exist.

If the program user sets $p_{(0)}{}^f = 0$ and $\Delta p_{(0)}$ equal to a very small fraction of p_{nl}, the dashed curve in Fig. 25 will correspond closely to a linear bifurcation buckling analysis. If the minimum $p_{cr}^{(4)}(n = 11)$ corresponds to p_{lb} in Fig. 26, that is, if it is higher than the axisymmetric collapse load p_{nl}, the program will be unable to determine nonlinear prebuckling solutions for $p_{(1)}{}^f$ or $p_{(1)}{}^f + \Delta p_{(1)}$.

Note that the result labeled "6" in Fig. 25 implies the calculation of a negative eigenvalue $\lambda_{11}^{(6)}$, as discussed immediately following eqn (184). If the situation shown in Fig. 27 exists, conventional subroutines for the extraction of eigenvalues will yield the second bifurcation point, $\lambda_{11}^{(2)}$, rather than the first, $\lambda_{11}^{(1)}$, for $n = 11$ circumferential waves.

Modifications of strategy to avoid pitfalls

The pitfalls illustrated in Figs. 26 and 27 can almost always be avoided by the following approach. The program user first selects an initial number of circumferential waves n_0 which he feels corresponds to the minimum bifurcation load. For this wave number n_0 the stability determinant $|[K_1(p_{(m)}{}^f, n_0)]|$ is calculated for a sequence of load increments $\Delta p_{(0)}$ as shown in Fig. 28(a). The initial load $p_{(0)}{}^f$ and load increment are chosen to be fairly small compared to the expected critical load, say about $p_{cr}/10$.

For each load increment the nonlinear prebuckling equilibrium state is determined and the stability determinant is calculated for $n = n_0$. The load $p_{(m)}{}^f$ is in-


Fig. 26. Situation in which the strategy corresponding to eqns (178)–(188) fails because the axisymmetric collapse load p_{nl} is lower than the critical load estimate $p_{cr}^{(4)}(n = 11)$.
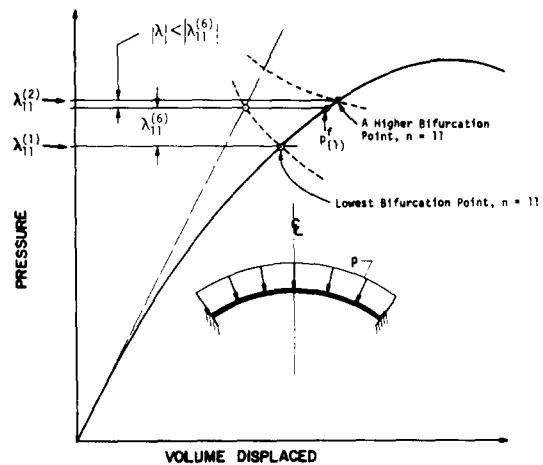

Fig. 27. Situation in which the strategy corresponding to eqns (178)–(188) fails because $\lambda_{11}^{(6)}$ in eqn (184) is not the smallest eigenvalue in absolute value.

creased until one or more eigenvalues are detected between two sequential load steps (e.g. stability determinant changes sign in Fig. 28(a)) or until the maximum allowable user specified load has been reached.

At this point in the calculations a series of eigenvalue problems of the form

$$[K_1(p_{(m-1)}^f, n)]\{x^b\} + \lambda_n[K_2(\Delta p_{(0)}, n)]\{x^b\} = 0 \quad (189)$$

is set up and solved, where $[K_1(p_{(m-1)}^f, n)]$ = the stiffness matrix corresponding to n circumferential waves, of the structure as loaded by $L_1 = p_{(m-1)}^f$; $[K_2(\Delta p_{(0)}, n)]$ = the load-geometric matrix corresponding to the prestress increment resulting from the load increment $L_2 - L_1 = \Delta p_{(0)}$; $p_{(m-1)}^f = L_1$ = the load state just before the sign change of the stability determinant, or the second-to-last load; $p_{(m-1)}^f + \Delta p_{(0)} = L_2$ = the load state just after the sign change of the stability determinant, or the last load; λ_n = the eigenvalue; x^b = the eigenvector; and n = the number of circumferential waves; n lies in a range $n_{min} \leq n \leq n_{max}$, with n_{min} and n_{max} provided by the program user. Note that the initial guess n_0 also lies in the range $n_{min} \leq n_0 \leq n_{max}$. Also note that the increment in n need not be unity, but may be a suitable fairly small percentage of the average of n_{min} and n_{max}, say $\Delta n = 0.05$ $(n_{min} + n_{max})$. From this point on the strategy is the same as already described in connection with eqns (178)–(188). If Fig. 28(b) is used as a reference, the program next calculates eigenvalues corresponding to $\lambda_{n_0}^{(1)}, \lambda_{n_0+1}^{(2)}, \lambda_{n_0-1}^{(3)}, \lambda_{n_0-2}^{(4)}$, and $\lambda_{n_0-3}^{(5)}$.

New prebuckling solutions are then obtained for the loads

$$p_{(m+1)}^f = p_{(m-1)}^f + \lambda_{n_{crit}}^{(4)} * \Delta p_{(0)} \quad (190)$$

and $p_{(m+1)}^f + \Delta p_{(1)}$, where $\Delta p_{(1)} = p_{(m+1)}^f / 1000$. A series of new eigenvalue problems of the type in eqn (189) would then be set up with n held constant at $n = n_{crit}$ until $|\lambda \Delta p_{(m)}|$ becomes smaller than $|p_{(m)}^f / 1000|$, as described earlier in connection with eqns (187) and (188). If some of the eigenvalues $\lambda_n^{(j)}$ corresponding to the problem given in eqn (189) take on negative values, such as shown in Fig. 28(c), the pitfall illustrated in Fig. 27 might still prevent a finding of the true lowest eigenvalue. The
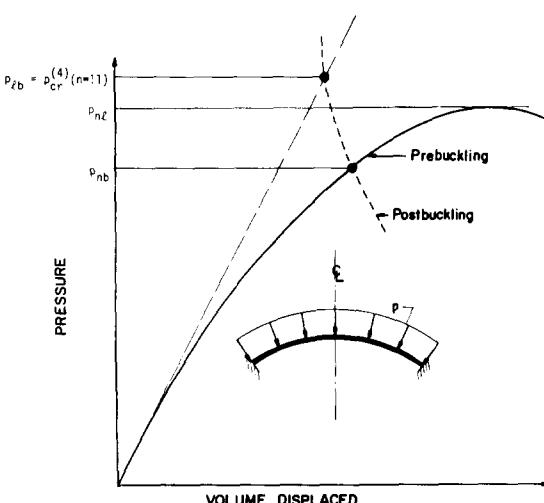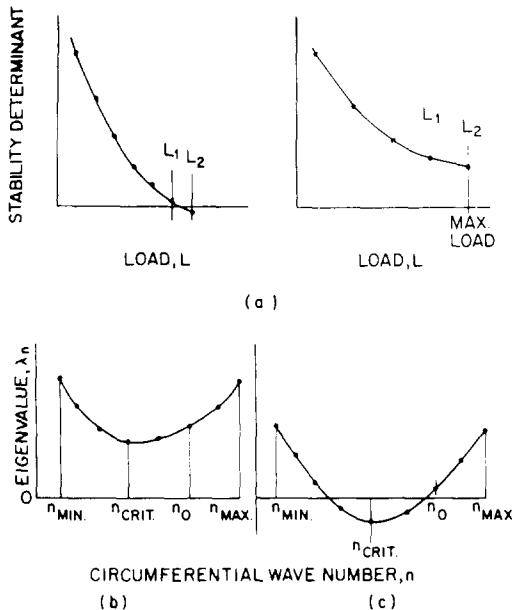
Fig. 28. (a) Stability determinant at $n = n_0$ as function of load L, (b), (c) eigenvalues as function of number of circumferential waves, n.

Fig. 29. Buckling of axially compressed cylinder (from Bushnell[18]).

following example illustrates such a case and presents a remedy.

Example—buckling of a very thin cylinder under axial compression

This example is included here because it is a difficult case from a numerical point of view, since eigenvalues are close together and close to the axisymmetric collapse load, and the case demonstrates some of the internal checks and automatic internal control in one of the computer programs for buckling of shells of revolution[18]. Because of these properties and because the geometry is simple, this is a good test case for computer programs that perform buckling analysis including nonlinear prebuckling behavior and nonuniform prebuckling stress and displacement.

Figure 29 shows the model of a cylinder with radius $R = 500$ in., thickness $t = 1$ in., length $L = 2000$ in., Young's modulus $E = 10^7$ psi and Poisson's ratio $\nu = 0.3$. The cylinder is treated as being symmetric about the midlength, and the 1000-inch half-cylinder thus analyzed is divided into two segments: a 200-inch-long edge zone segment with 83 nodal points, and an 800-inch-long interior segment with 99 nodal points. The axisymmetric prestress model contains 379 degrees-of-freedom, and the stability model 566 degrees-of-freedom. Simple support conditions are applied at the edge, and symmetry conditions at the midlength. Also shown in Fig. 29 are the prebuckling displacement distribution at the predicted critical load of 10,274 lb/in. and the critical buckling mode corresponding to $n = 18$ circumferential waves.

Figure 30 shows the sequence of wave numbers and loads automatically explored by the computer program[18] to obtain the final result $L_6 = N_{cr} = 10,274$ lb/in. With an initial base or "fixed" load $p_{(0)}{}^f = 0$ and a load increment $\Delta p_{(0)} = 1.0$ lb/in., eigenvalues labeled (1)–(4) are calculated. The base or "fixed" load is then set equal to the local minimum or 12,008 lb/in. and the load increment is set equal to 12,008/1000 lb/in.
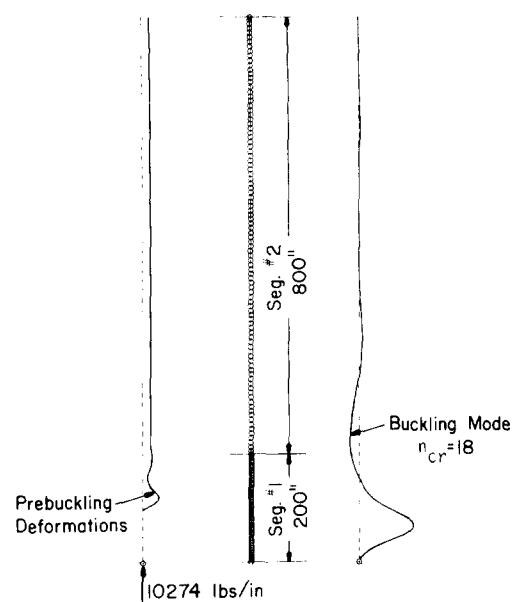
In this case, it is discovered from a count of the negative terms on the main diagonal of the factored stiffness matrix $[K_1(p_{(1)}{}^f = 12008, \ n = 12)]_{(factored)}$ that for $n = 12$ circumferential waves, three eigenvalues exist below the "fixed" load $p_{(1)}{}^f = L_2 = 12,008$ lb/in. Hence the load is automatically reduced by a factor of 0.7, to $L_3 = 8414$ lb/in. After the eigenvalues corresponding to points 5–9 in Fig. 30 have been determined, the new base load $p_{(2)}{}^f = L_3 = 10,819$ lb/in. is established corresponding to $n = 18$ waves. It is also determined that at $n = 18$ one eigenvalue exists below this new "fixed" or base
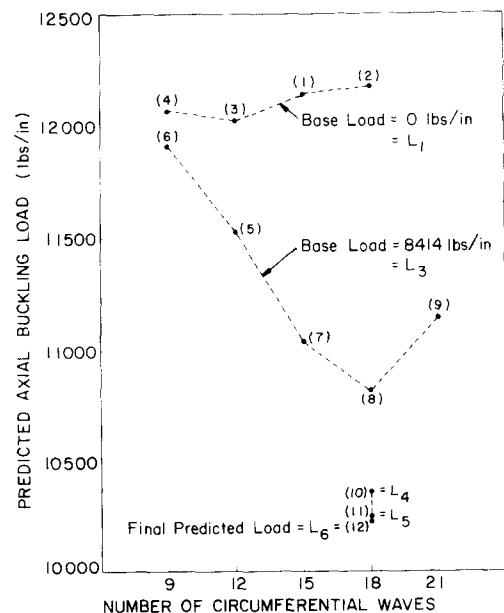
Fig. 30. Sequence of axial load and circumferential wave number estimates during calculation of buckling of cylinder with nonlinear prebuckling effects included (from Bushnell[18]).

load. However, the new base load need not be reduced by some factor because initial inverse power iterations for the eigenvalue nearest to $L_3 = 10,819$ indicate that subsequent critical load estimates will further reduce the base loads L_4, L_5, etc. to the lowest eigenvalue rather than increase them toward the second eigenvalue. Had the opposite trend developed, the program would have caused the base load to be reduced to $0.9*10,819$. Figure 30 shows the final three load estimates, L_4, L_5, and L_6.

Figure 31 gives the prebuckling load deflection curve for this cylinder. The abscissa represents the difference between the actual end shortening and the linear end shortening that would exist if there were no prebuckling rotation. Eigenvalues computed with $\Delta p = 1.0$ and $p_{(m)}{}^f = N_0 = 0, 5000, 10000, 11000, 11500$, and 11900 lb/in. and $n = 18$ circumferential waves are indicated as crosses. Several runs were made in order to obtain these

results, each run corresponding to a different "fixed" load $p^f = N_0$. The open circles in the load-end shortening curve correspond to the various loads, $N_0 = 5000, 10000,\ldots11900$. The large dots represent the "fixed" loads used in the sequence shown in Fig. 30. Two to four eigenvalues are calculated corresponding to each open-circle fixed load. These eigenvalues are indicated by crosses on the same vertical lines as the open circles. The eigenvectors are shown in Fig. 32. Notice that for "fixed" load $L_1 = p_{(0)}{}^f = 0$, the lowest four eigenvalues are very close and are all approximately equal to the "classical" load $0.605 \, Et^2/R$. The lowest eigenvalues are also close for $n_0 = 15$, the starting circumferential wave number in the search for the minimum critical load $p_{(cr)}(n = n_{crit})$. Therefore, several inverse power iterations and spectral shifts are required to obtain the lowest eigenvalue at that wave number. For $N_0 = 5000$ lb/in. the
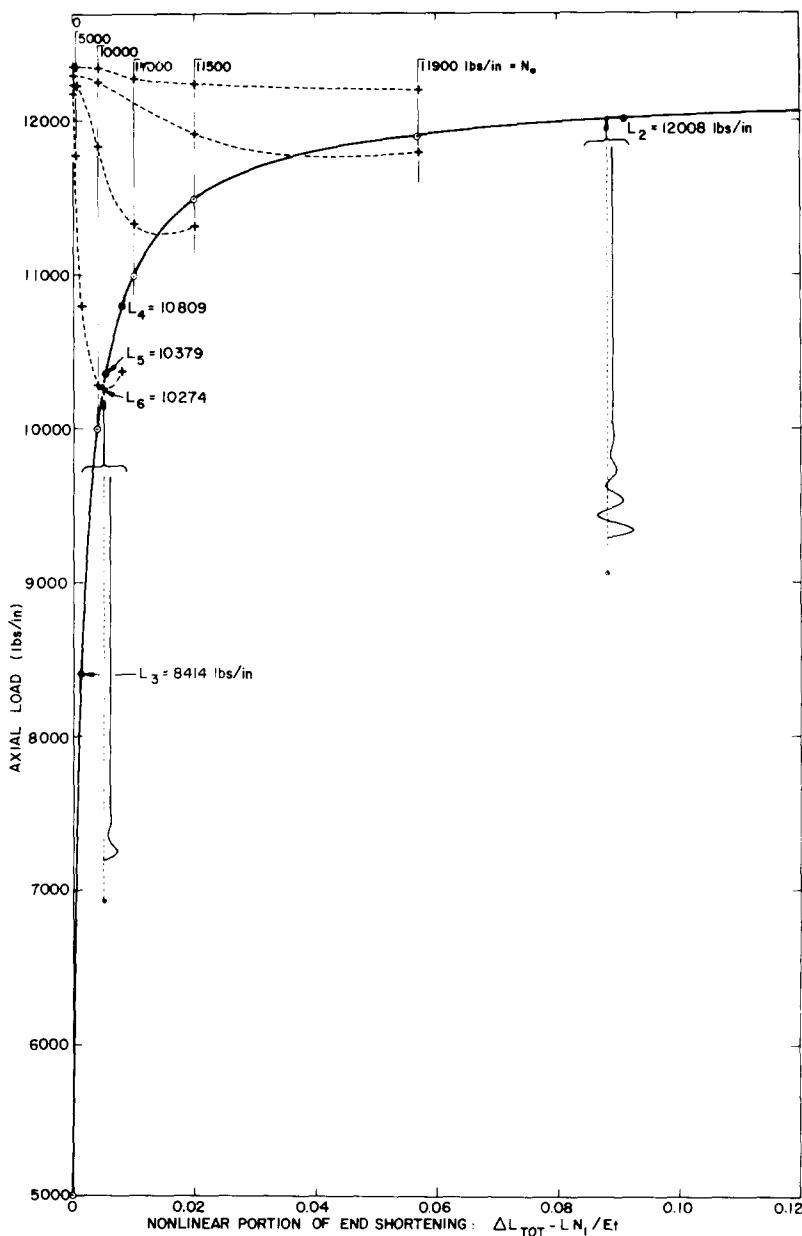
Fig. 31. Eigenvalue "separation" for axially compressed cylinder (from Bushnell[18]).
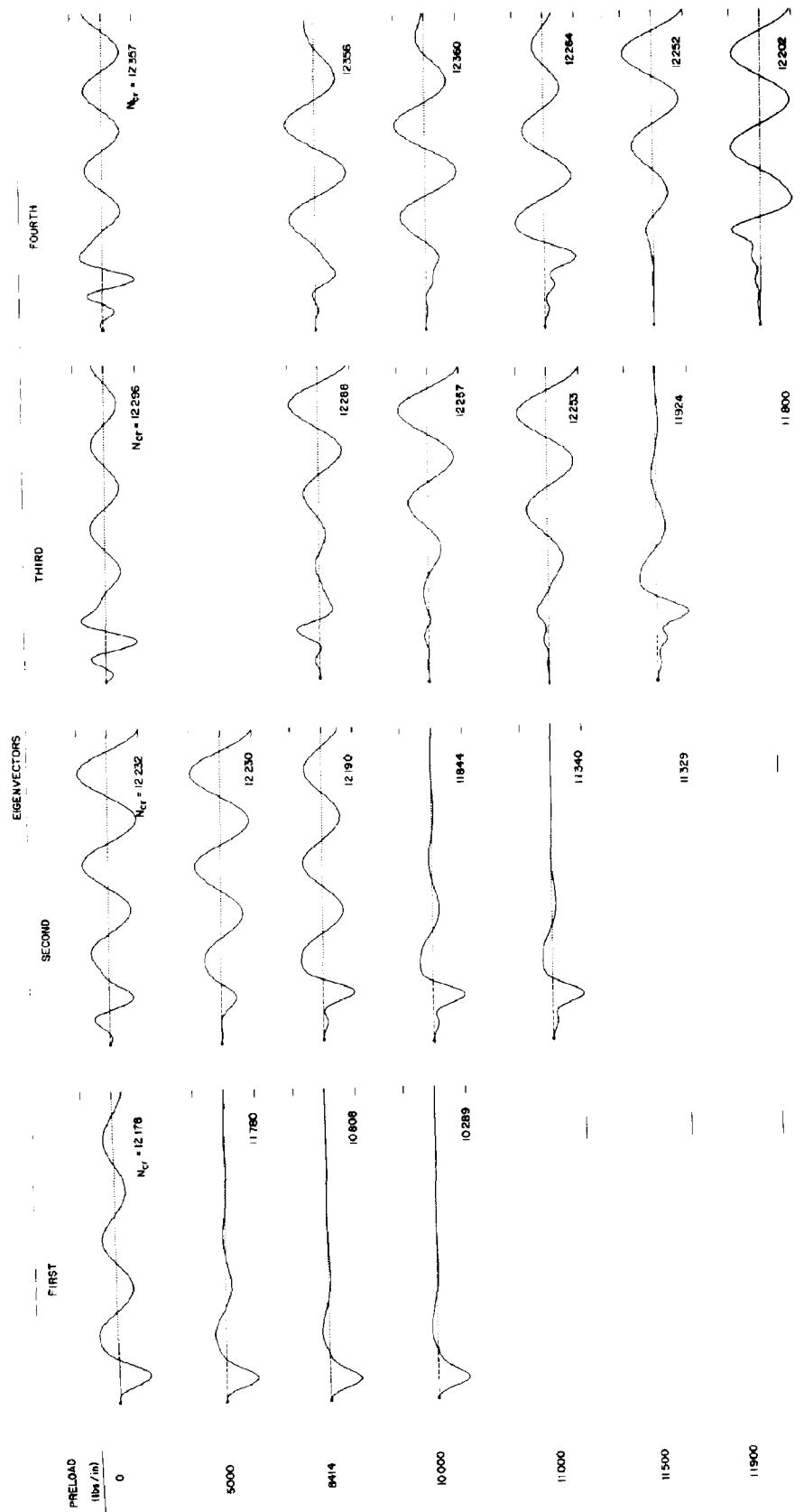
Fig. 32. Eigenvectors and eigenvalues for axially compressed cylinder with various base loads (from Bushnell[18]).

lowest eigenvalue "separates" from the others, and the localized nature of the corresponding eigenvector is strongly developed (Fig. 32). Because of this separation of the lowest eigenvalue, fewer inverse power iterations and spectral shifts are required for convergence. Thus, the user may save computer time by choosing a base or "fixed" load to be some reasonable percentage of the estimated final buckling load. This is particularly true if many values of the wave number n are to be explored and if the predicted n corresponding to the minimum $p_{cr}(n)$ is likely to depend strongly on the fixed portion of the load, as is the case for axially compressed very thin cylinders.

Another pitfall—failure to find the global minimum $p_{cr}(n)$

In all of the examples shown in Figs. 25, 28 and 30 the curve of critical load or eigenvalue vs circumferential wave number n has a single minimum and corresponding n_{crit}, given $p_{(m)}{}^f$. However, the curve of $p_{cr}(n)$ vs n for optimally designed stiffened shell structures often has several minima, all of them at approximately the same load, as shown in Fig. 33. This is because the minimum weight design often yields a configuration in which general and local instability occur at almost the same load. In Fig. 33 the general instability mode and local modes corresponding to primary failure in the first, second, and third bays of the conical shell are shown as insets in a plot of $p_{cr}(n)$ vs n. In addition the rings might cripple at still higher values of n. It is generally up to the computer program user to provide a wide enough range of n or to make several runs with different ranges of n in order to cover all possible failure modes.

Physical intuition is invaluable as a guide for finding the absolute minimum load. One may idealize each bay of a ring stiffened shell by assuming that the bay is simply supported, calculate corresponding "panel" buckling loads with certain appropriate ranges of n, and then use the critical loads and values of n as starting points in an investigation of the assembled structure.

It is not necessary always to increase the circumferential wave number n by one. In the search for the minimum buckling load, for example, one may only be certain that the n corresponding to the minimum buckling load, n_{crit}, lies in the range $2 \leqslant n \leqslant 100$. One might, therefore, choose $\Delta n = 10$ and "zero in" on a more accurate value in a subsequent run.

Experimental evidence is of course very useful in determining a good choice of initial number of circumferential waves n_0 and range limits n_{min} and n_{max}. If none is available the user is advised to try the following formulas:

(1) *"Square" buckles for short cylindrical or conical shells or panel buckling*

$n = \pi r/L$, where L is the shell meridional arc length corresponding to the half-wavelength.

(2) *For monocoque deep shells, axial compression*
n proportional to [(Nominal circumferential radius of curvature)/t]$^{1/2}$.

(3) *For shallow spherical caps supported rigidly at their edges; external pressure:*

$n = 1.8 * \alpha_2 * (R/t)^{1/2} - 5$ ($\alpha_2 =$ angle in radians from the axis of revolution to the edge).
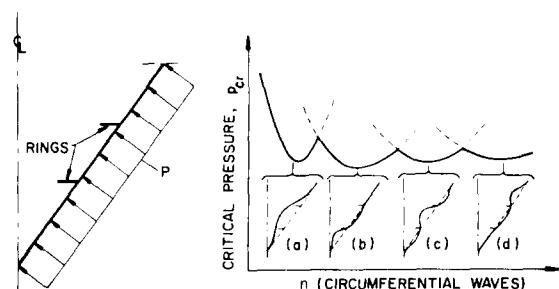
Fig. 33. Ring-stiffened conical shell with simultaneous local and general instability modes (from Bushnell[34]).

(4) *For axially compressed conical shells and frustrums:*
Use formula 2 where the circumferential radius of curvature, R, is the average of the radii at the ends.

(5) *Spherical segments of any depth under axial tension*

$$n = 1.8 * (R/t)^{1/2} \sin[\alpha_1 + 4.2(t/R)^{1/2}]$$

where α_1 and α_2 are the meridional angles measured from the axis of revolution to the segment beginning and end, respectively ($\alpha_1 < \alpha_2$).
The above list of formulas is by no means complete. However, notice that $(R/t)^{1/2}$ is a significant parameter. If n is known for a shell of a given geometry loaded in a certain way, a new value can be predicted for a new R/t through the knowledge that n often seems to vary as $(R/t)^{1/2}$. (R is the normal circumferential radius of curvature.)

MODAL VIBRATION ANALYSIS FOR PRESTRESSED SHELLS

For modal vibration analysis the stiffness matrix $[K_1(p^f, n)]$ of the shell as loaded by p^f is the same as that appearing in the eigenvalue problem for bifurcation buckling. The eigenvalue problem for modal vibration analysis is

$$[K_1(p^f, n)]\{x^b\} + \Omega^2[M(n)]\{x^b\} = 0 \qquad (191)$$

in which $[M(n)]$ is the global mass matrix corresponding to n circumferential waves.

Starting from eqn (100) for the shell and eqn (101) for the discrete ring, and assuming that the displacement as a function of time is

$$\{x\} = \{x^b\} e^{i\Omega t} \qquad (192)$$

one can derive the local mass matrix for the kth finite element:

$$[M]^k = hr_k m_k [\overset{7\times3}{[D]}^T \overset{3\times3}{[I]} \overset{3\times7}{[D]}]_k$$

$$+ \delta_j{}^k r_{cj} \rho_j [A[\bar{T}]^T [\bar{E}_1 + \beta_0{}^f \bar{E}_2]^T \overset{4\times4}{[T_A]} [\bar{E}_1 + \beta_0{}^f \bar{E}_2][\bar{T}]$$

$$+ [\bar{R}]^T \overset{3\times3}{[T_B]}[\bar{R}]]_j \qquad (193)$$

in which m_k is the shell wall mass/area, $[I]$ is the identity matrix, ρ_j is the jth ring material mass density, A is the

discrete ring cross section area, and

$$T_A = \begin{bmatrix} 1 & 0 & 0 & 0 \\ 0 & 1 & 0 & 0 \\ 0 & 0 & 1 & 0 \\ 0 & 0 & 0 & I_p^k/A^k \end{bmatrix} \qquad (194)$$

$$T_B = \begin{bmatrix} 0 & 0 & 0 \\ 0 & I_s & -I_{sn} \\ 0 & -I_{sn} & I_n \end{bmatrix}. \qquad (195)$$

The matrices $[D]$, $[\bar{T}]$, $[\bar{E}_1 + \beta_0{}^f\bar{E}_2]$, and $[\bar{R}]$ are the same as those used in the derivation of $[K_1]^k$ and $[K_2]^k$, appearing in eqns (175) and (176). The I_s, I_{sn}, I_n are components of the moment of inertia of the discrete ring with respect to the (s,n) axis system, which is shown in Fig. 20(a).

LINEAR STRESS ANALYSIS

Arbitrary loads $p(s,\theta)$, acting on the shell reference surface and $L(\theta)$, acting along discrete ring centroidal axes, are decomposed into Fourier harmonics, as listed in eqns (112). For each Fourier harmonic, the stiffness matrix $[K_1(p^f = 0, n)]$ and "right-hand-side" vector $\{f(n)\}$ are formed. A solution $\{x(n)\}$ to the linear system

$$[K_1(p^f = 0, n)]\{x(n)\} = \{F(n)\} \qquad (196)$$

is obtained and added to solutions obtained for previous values of n. The stiffness matrix $[K_1]$ is the same as that used in the buckling and vibration analyses with the "fixed" load $p_{(m)}{}^f$ now set equal to zero. The right-hand-side vector $F(n)$ is formed from assembly or accumulation of the local right-hand-side vectors for each finite element into the global vector. The local vectors are generated from the first variation of the total energy evaluated for the undeformed structure. Contributions to these local vectors arise from the second term in the integrand in eqn (89) (thermal loads in the shell), the last three terms in eqn (95) (thermal loads in the discrete rings), and all of the terms in eqn (98) (line loads on the discrete ring centroidal axes) and eqn (99) (distributed loads on the shell reference surface). The total shell and ring energy components corresponding to these linear terms in q are:

$$U_{\text{shell}}(\text{linear in } q) = \frac{1}{2}\int_s \int_\theta 2\lfloor N^T\rfloor\{\epsilon^{(1)}\}r\, d\theta\, ds$$

$$- \int_s \int_\theta (p_1 u + p_2 v + p_3 w)r\, d\theta\, ds \qquad (197)$$

$$U_{\text{ring}}(\text{linear in } q) = \frac{1}{2}\int_\theta 2\lfloor \bar{N}_r{}^T\rfloor\{\epsilon_r{}^{(1)}\}r_c\, d\theta$$

$$- \int_\theta (-Vu_c + Sv_c + Hw_c + M\beta)r\, d\theta \qquad (198)$$

in which $\lfloor N^T\rfloor$ is defined in eqns (84) and (86); $\{\epsilon^{(1)}\}$ is defined in eqn (128) (Remember $\beta_0{}^f = 0$ in this analysis); $\lfloor \bar{N}_r{}^T\rfloor$ is defined in eqns (143) and (96); and $\{\epsilon_r{}^{(1)}\}$ is defined in eqn (140). Using principles and equations introduced in the discussions and derivations leading to eqns (136) and (157), one can express eqns (197) and (198) in the forms

$$U_{\text{shell}}(\text{linear in } q) = (\pi \text{ or } 2\pi)\, hr_k \lfloor N^T\rfloor [B_1]$$

$$- \lfloor p\rfloor [D]\rfloor\{q\} \qquad (199)$$

$$U_{\text{ring}}(\text{linear in } q) = (\pi \text{ or } 2\pi)r_c \lfloor \bar{N}_r{}^T\rfloor [B_r][\bar{E}_1][\bar{T}]$$

$$- \lfloor L\rfloor [\bar{E}_1][\bar{T}]\rfloor\{q\} \qquad (200)$$

in which the transformations involving $[B_1]$, $[D]$, $[B_r]$, $[\bar{E}_1]$, and $[\bar{T}]$ appear in eqns (134), (113), (148), (152) and (155), respectively, and

$$\lfloor p\rfloor \equiv \lfloor p_1, p_2, p_3\rfloor$$

$$\lfloor L\rfloor \equiv \lfloor -V, S, H, M\rfloor. \qquad (201)$$

Corresponding to the kth finite element, the local force vector, divided by the common factor π or 2π (depending on n), is given by the negatives of the r.h.s. of eqns (199) and (200) without the $\{q\}$:

$$\{F\}^k = -hr_k \lfloor \overset{\text{①}}{\lfloor N^T\rfloor [B_1]} - \overset{\text{②}}{\lfloor p\rfloor [D]}\rfloor_k$$

$$- \delta_j{}^k r_{cj} \lfloor \overset{\text{③}}{\lfloor \bar{N}_r{}^T\rfloor [B_r][\bar{E}_1][\bar{T}]} - \overset{\text{④}}{\lfloor L\rfloor [\bar{E}_1][\bar{T}]}\rfloor_j. \qquad (202)$$

The local "right-hand-side" or force vectors $\{F\}^k$ are assembled into the global force vector $\{F\}$ as described in the discussion following eqns (175) and (176) regarding the local stiffness and load-geometric matrices. Table 3 lists the equations that give rise to the various terms in eqn (202) and identifies the physical significance of these terms.

VARIOUS DISCRETIZATION METHODS

In the preceding development the discretizations shown in Figs. 11 and 21 have been given the appellation "Finite-Difference Energy method". However, as emphasized in Ref. [19], the categorization of discretization methods into "Finite Element" and "Finite-Difference Energy" is somewhat artificial. In both the finite-element and finite-difference energy methods the unknowns of the problem are certain generalized displacement components located at discrete nodes in the domain. Between these nodes the variations of the generalized displacements are expressed as power series in s. Integration can then be performed analytically or numerically. The differing choice of generalized displacement components and locations of the nodes are the only characteristics of the two solution techniques which justify giving them different names. Once the nodes and the appropriate generalized displacement components have been selected, the solution procedure is identical for both methods.

Figure 34 shows five types of discretization. The nodes are denoted by large dots or crosses. The "element" is defined as the solid horizontal line bounded by dots or crosses. Nodal point variables u_i, v_i, w_i, χ_i, etc. are shown next to the nodes with which they are associated. The first three models fall into the category "finite element method", the last two into the category "finite difference method".

The three models ①, ② and ③ represent standard finite elements such as described in Kotanchik et al.[30], Mebane and Stricklin[31], and Adelman et al.[32]. A curved element ② with extra internal degrees of freedom (dof) $\bar{u}_1$, $\bar{v}_1$, $\bar{u}_2$, and $\bar{v}_2$ permits rigid body motion without excessive storage of energy. The internal degrees of freedom represent corrections to the linear function. Elements of this type are described in [31]. An alternate way of obtaining higher-order displacement

functions is to define more degrees of freedom at the nodes [32]. Element ③ is of this type. The displacements within each of these elements are given by the polynomials shown in the figure. Integration of the energy functional can be performed analytically or numerically. Gaussian quadrature seems to be the most accurate and economical method of integration.

Figure 35 shows schematically a structure consisting of five elements. The displacement function w and its first derivative are continuous throughout the domain. The displacement function for u and v corresponds to model ①. Of course, the elements need not be flat. However, if the element is curved, higher-order displacement functions than linear in u and v are required for representation of rigid body motions.

Model ④ represents the discretization method described here in previous sections. As has already been mentioned, in this finite-difference energy discretization, the integrand of the energy functional H (eqn 12) is evaluated at only one point within each element, and the total element energy is obtained by multiplication of the energy per meridional arc length by the element length l. The finite-difference formulas for variable mesh spacing, given in eqns (110) and (111), are obtained by Taylor series expansions of the displacements about the centroid of each element. Since first and second derivatives of w and only first derivatives of u and v occur in the integrand of eqn (12), the appropriate polynomials for the lowest-order difference formulas in each case are shown in Fig. 34(d–e). As in the case of the finite-element method, the α_1 can easily be expressed in terms of the nodal point variables. The finite-difference energy discretization model ④ has been used in computer programs by Stein[33], Bushnell[18], and Brogan and Almroth[22].

Figure 36 shows the finite-difference discretization of the same five-element structure depicted in Fig. 35. In Fig. 36 the element boundaries are at u and v nodal points (crosses). The quadratic w expansions pass through three adjacent w nodes, spanning a longer arc

Standard lowest order finite element

$$u = \alpha_1 + \alpha_2 s$$

$$v = \alpha_3 + \alpha_4 s$$

$$w = \alpha_5 + \alpha_6 s + \alpha_7 s^2 + \alpha_8 s^3$$

(a)

Energy evaluated at Gaussian integration points.

Finite element with extra internal d.o.f.

$$u = \alpha_1 + \alpha_2 s + \alpha_3 s^2 + \alpha_4 s^3$$

$$v = \alpha_5 + \alpha_6 s + \alpha_7 s^2 + \alpha_8 s^3$$

$$w = \alpha_9 + \alpha_{10} s + \alpha_{11} s^2 + \alpha_{12} s^3$$

(b)

Energy evaluated at Gaussian integration points.
Static reduction used to get local [K].

Finite element with extra nodal d.o.f.

$$u = \alpha_1 + \alpha_2 s + \alpha_3 s^2 + \alpha_4 s^3$$

$$v = \alpha_5 + \alpha_6 + \alpha_7 s^2 + \alpha_8 s^3$$

$$w = \alpha_9 + \alpha_{10} s + \alpha_{11} s^2 + \alpha_{12} s^3$$

(c)

Energy evaluated at Gaussian integration points

Finite difference with (u_i, v_i) on half-stations

$$u = \alpha_1 + \alpha_2 s$$

$$v = \alpha_3 + \alpha_4 s$$

$$w = \alpha_5 + \alpha_6 s + \alpha_7 s^2$$

(d)

Energy evaluated at $s = l/2$.

Finite difference with (w_i) on half-stations

$$u = \alpha_1 + \alpha_2 s$$

$$v = \alpha_3 + \alpha_4 s$$

$$w = \alpha_5 + \alpha_6 s + \alpha_7 s^2$$

(e)

Energy evaluated at $s = l/2$.

Fig. 34. Various discrete models for energy methods (from Bushnell[19]).

Table 3. Physical explanations of terms in local force vector and where they came from

Term Number	Derived From Equations	Physical Explanation of Term
①	(89), (134)	Thermal Loading on shell wall.
②	(99), (113), (201)	Surface tractions and pressure acting on shell reference surface.
③	(95), (148), (152), (155)	Thermal loading on discrete ring.
④	(98), (152), (155), (201)	Line loading along discrete ring centroidal axis.

length than the element. However, the integration, or "lumping" corresponds only to the lengths between adjacent crosses. The in-plane displacements u and v are continuous everywhere. Notice that at element boundaries the normal displacements and derivatives are discontinuous. It can be shown that the displacement discontinuity Δw_i is of maximum order

$$|\Delta w_i| = \frac{h_i h_{i+1}}{8}(h_{i-1} + 2h_i + 2h_{i+1} + h_{i+2}) \qquad (203)$$

and the slope discontinuity is of maximum order

$$|\Delta \beta_i| = \left|\frac{h_i - h_{i+1}}{2}\right|(h_{i-1} + 2h_i + 2h_{i+1} + h_{i+2}). \qquad (204)$$

The finite-difference discretizations ④ and ⑤ are similar to replacement of the actual structure by a structure consisting of elements linked as shown in Fig. 37. The normal displacement w is continuous at the pinned joints and u and v are continuous at the stations where the projections stick into the rounded holes.

At first glance it would seem that this structure is far too flexible to represent the behavior of a continuous shell. However, notice in Fig. 36 that u and v must be continuous at the stations where w is discontinuous. Since the circumferential strain, for example, involves at least both w and v, the Δw at the element boundaries must remain small enough to keep this membrane strain component, and hence the energy, at a reasonable level. In other words, the minimum energy state will involve small discontinuities in w at the element boundaries.

In Fig. 22 are given the computer times required to form the global stiffness matrix $[K_l]$ corresponding to the problem shown in Figs. 1 and 2. The curve labeled "Finite Element Analysis" corresponds to Model ② in Fig. 34. As seen from Fig. 2, a high order element of this type (cubic in u and v) is required for convergence to a reasonably accurate answer with a reasonable number of elements.

Figure 38 illustrates why the computer time for the
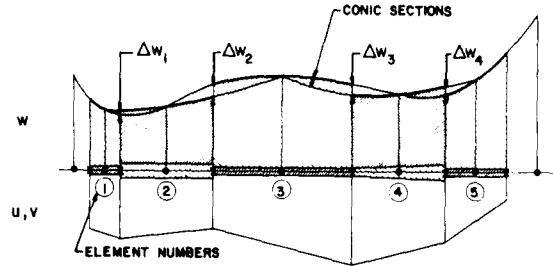
Fig. 36. Displacement functions for finite difference model ⑤ (from Bushnell[19]).

formation of $[K_l]$ is much higher for Model ② than for Models ④ or ⑤:

(1) There is an extra loop over the number of Gaussian integration points per element.

(2) There is more algebra required for formation of the kinematic matrix B and more products required in the formation of $B^T C B$ (B has more columns).
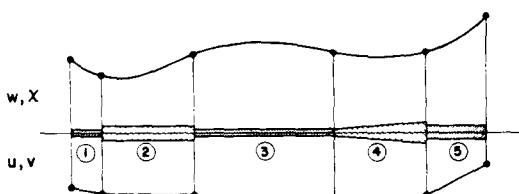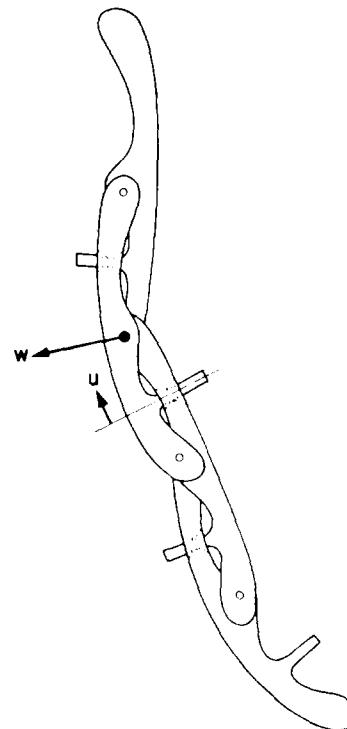
Fig. 35. Displacement functions for finite difference model ① (from Bushnell[19].

Fig. 37. Structural equivalent of finite difference model ④ or ⑤ (courtesy Carlos Felippa) (from Bushnell[19]).

(3) An extra step is required outside of the Gaussian integration loop in order to condense out the internal degrees of freedom in each element.

In spite of the higher order of the finite element ②, the convergence of edge displacement w with increasing nodal point density is far more rapid with the finite difference element ④. For an accuracy of 2.0% in w about 20 finite difference elements would be required, with

about 0.25 sec. needed to form the global stiffness matrix $[K_1]$. For the same accuracy, about 60 finite elements of the type ② would be required, with about 3.5 sec. needed to form $[K_1]$. The difference in the rate of convergence for the two discretization methods probably results from the following:

(1) The lower order (stiffer) approximation for u, v, and w in the finite difference element is compensated by
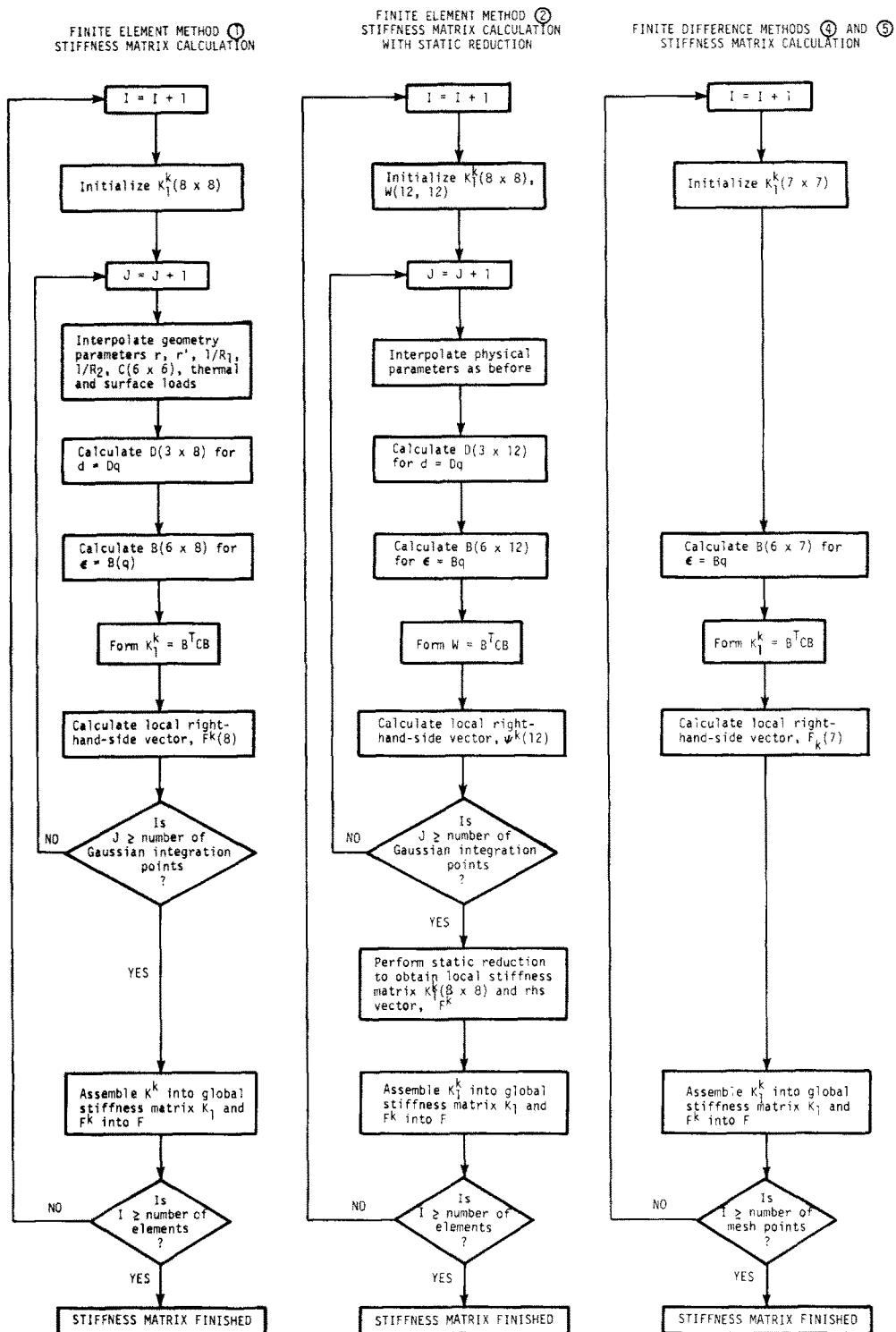
Fig. 38. Flow charts for the calculation of stiffness matrix K_1 with finite element models ① and ② and finite difference models ④ or ⑤ (see Fig. 34).

discontinuities in w and β at finite difference element boundaries.

(2) The fact that the curved finite difference element energy is evaluated at only one station per element results in a more energy-free representation of rigid body motion than of the curved finite element with cubic u, v, and w, in which the energy is evaluated at more than one Gaussian integration point.

CONSTITUTIVE LAW [C] FOR COMPOSITE SHELL WALLS

Here the phrase "composite shell wall" is taken in a broad sense. It may mean laminated as described by Jones et al. in Ref. [6–8]. It may also mean a shell wall modified by stiffeners that are to be smeared out in the computerized model.

Equations (80) and (84) are based on an assumption that the principal axes of orthotropy of the shell wall material are aligned with the orthogonal coordinate lines on the shell reference surface. Thus, they are valid for a stringer and ring stiffened shell wall such as shown in Fig. 39, in which the stringers follow meridians (s-coordinate) and the rings follow parallel circles (θ-coordinate). If the analyst wishes to set up a model in which both sets of stiffeners are smeared or averaged over the entire surface, he can treat the shell wall as if it consisted of four orthotropic layers with properties G, E_1, E_2, ν_{12}, m, α_1, and α_2 assigned as listed in Fig. 39. If the stiffeners do not follow coordinate lines, the more general model described in Ref. [6] is required.

On p. 154 of Ref. [6] Jones writes the equivalent of

$$\begin{Bmatrix} N_1 \\ N_2 \\ N_{12} \\ \hline M_1 \\ M_2 \\ M_{12} \end{Bmatrix} = \left[\begin{array}{ccc|ccc} A_{11} & A_{12} & A_{16} & B_{11} & B_{12} & B_{16} \\ A_{12} & A_{22} & A_{26} & B_{12} & B_{22} & B_{26} \\ A_{16} & A_{26} & A_{66} & B_{16} & B_{26} & B_{66} \\ \hline B_{11} & B_{12} & B_{16} & D_{11} & D_{12} & D_{16} \\ B_{12} & B_{22} & B_{26} & D_{12} & D_{22} & D_{26} \\ B_{16} & B_{26} & B_{66} & D_{16} & D_{26} & D_{66} \end{array} \right] \begin{Bmatrix} e_1 \\ e_2 \\ e_{12} \\ \hline \kappa_1 \\ \kappa_2 \\ 2\kappa_{12} \end{Bmatrix}$$

$$(205)$$

in which the stress and moment resultants are defined as in Fig. 17 and the reference surface strains and changes in curvature are defined as in eqns (90). The A_{ij}, B_{ij}, and D_{ij} in eqn (205) are, of course, equivalent to the corresponding C_{ij} in eqn (84). For the laminate Jones gives

$$A_{ij} = \sum_{k=1}^{N} (\bar{Q}_{ij})_k (z_k - z_{k-1})$$

$$B_{ij} = \frac{1}{2} \sum_{k=1}^{N} (\bar{Q}_{ij})_k (z_k^2 - z_{k-1}^2) \qquad (206)$$

$$D_{ij} = \frac{1}{3} \sum_{k=1}^{N} (\bar{Q}_{ij})_k (z_k^3 - z_{k-1}^3)$$

in which the z_k are measured from an arbitrary reference surface, as shown in Fig. 40. (Jones[6] uses the middle surface, but this is not a necessary restriction.) The $\bar{Q}_{ij}$ for each lamina are given by Jones on p. 51 of Ref. [6]:

$$\bar{Q}_{11} = E_{11}c^4 + 2(E_{12} + 2G)s^2c^2 + E_{22}s^4$$

$$\bar{Q}_{12} = (E_{11} + E_{22} - 4G)s^2c^2 + G(s^4 + c^4)$$

$$\bar{Q}_{22} = E_{11}s^4 + 2(E_{12} + 2G)s^2c^2 + E_{22}c^4$$

$$\bar{Q}_{16} = (E_{11} - E_{12} - 2G)sc^3 + (E_{12} - E_{22} + 2G)s^3c$$

$$\bar{Q}_{26} = (E_{11} - E_{12} - 2G)s^3c + (E_{12} - E_{22} + 2G)sc^3$$

$$\bar{Q}_{66} = (E_{11} + E_{22} - 2E_{12} - 2G)s^2c^2 + G(s^4 + c^4) \qquad (207)$$

in which E_{11}, E_{12}, E_{22} are defined in eqns (81),

$$s \equiv \sin\gamma \qquad c \equiv \cos\gamma \qquad (208)$$

and γ is the angle from the meridional direction to the "1" axis of the lamina (direction in which E_1 is measured).

Note that use of the full matrix in eqn (205) in the analysis of shells of revolution would prevent the separation of variables according to eqns (108). Hence, in most one-dimensionally discretized analyses of stress, buckling, and vibration of composite, laminated shells of revolution, the C_{ij} in eqn (84) are derived as in eqns (205)–(208) and the terms A_{16}, A_{26}, B_{16}, B_{26}, D_{16}, D_{26} are subsequently ignored.

SECTION 4

HYBRID BODIES OF REVOLUTION

INTRODUCTION

By "hybrid" is meant a body of revolution with both one-dimensionally and two-dimensionally discretized regions, such as shown in Fig. 41. The stresses and strains for distances equal approximately to one wall thickness from the junction shown in Fig. 41 cannot adequately be predicted with thin shell theory. Therefore, a small region is defined in which the domain is discretized in two dimensions. Figure 42 shows other examples in which such a hybrid model might be used for accurate prediction of local stresses and strains near structural junctions.

The existence of a special-purpose hybrid body-of-revolution computer program for stress, buckling and vibration analysis is justified because there exist many practical problems in which the geometry is axisymmetric or essentially so.

The user of such a computer program can obtain solutions involving fairly complex configurations with reasonable computer times. A hybrid program of this type should be used primarily for cases in which most of the structure can be modeled with use of thin shell elements, only very localized areas being modeled with use of two-dimensional solids of revolution. If the two-dimensional finite elements are introduced sparingly, the bandwidths of the stiffness, mass amd load-geometric matrices are generally narrow. Such matrices can be stored very compactly with a minimum amount of indexing. Thus, the computer time to decompose the stiffness matrix is small, and input from and output to auxiliary mass storage devices is kept to a minimum. Since most of the structure is modeled with very simple thin shell elements, the program user is able to simulate the behavior of an entire complex structure in one model while retaining reasonable nodal point density and two-dimensional discretization in critical areas.

There are in existence several general purpose computer programs [24] which can yield solutions to problems of the type just described. In fact, the idea of analyzing hybrid bodies of revolution, consisting of thin and thick segments is not new. Strickland et al.[36] created a computer program, WASP, for the axisymmetric linear static analysis of such bodies. Zudans and

ACTUAL MATERIAL PROPERTIES

	Elastic Moduli	Mass Density	Thermal Exp. Coefficients
Shell Wall	E,G	m	a
Stringers	E_s	m_s	a_s
Rings	E_r	m_r	a_r

EQUIVALENT LAYERED ORTHOTROPIC SHELL WALL

Shell Wall Layer	Thick- ness	G	Orthotropic Material Properties					
			E_1	E_2	ν_{12}	m	α_1	α_2
1	h_s	0	$E_s t_s/d_1$	0	0	$m_s t_s/d_1$	a_s	0
2	t	G	E	E	ν	m	a	a
3	L_1	0	0	$E_r t_1/d_2$	0	$m_r t_1/d_2$	0	a_r
4	t_2	0	0	$E_r L_2/d_2$	0	$m_r L_2/d_2$	0	a_r
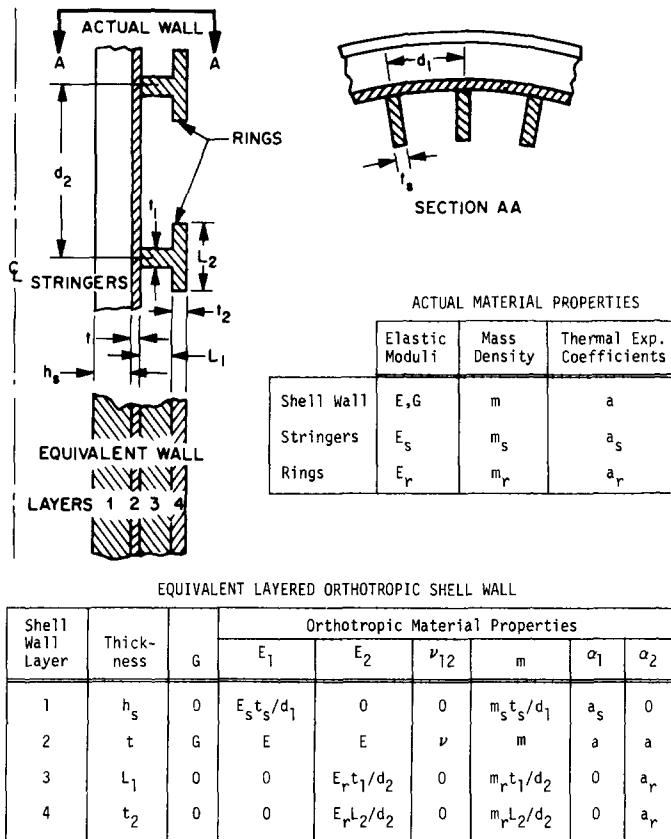
Fig. 39. How to model a shell wall with smeared stringers and rings. Stiffeners and parts of stiffeners are treated as if they were orthotropic layers or lamina (from Bushnell[34]).

Chow[37] wrote a hybrid program, BOXSHL, which permits nonsymmetric linear treatment by means of Fourier Series expansion in the circumferential direction.

Many authors have written computer codes which can handle solids of revolution by means of axisymmetric finite elements. Displacement functions and integration schemes in these elements can be modified such that they are adequate for the analysis of thin shells. Thus, Wilson[16] introduces incompatible modes in order to create correct bending behavior, Ergatoudis et al.[38] derive higher order isoparametric solid elements with one or two midside nodes, and Ahmad et al.[39] and Pawsey[40] specialize these isoparametric elements by taking advantage of certain characteristics of the behavior of thin shells. Isoparametric solid elements are also used for shell analysis by Larsen and Popov[41], by Bathe et al.[42] in NONSAP, by Dunham and Becker[43] in TEXGAP and by Sharifi[44] in NEPSAP. Ferguson[45] extended the capabilities of FARSS[46] to handle stress, buckling and vibration of thin and thick shells and bodies.

These and other investigators favor using solid isoparametric two-dimensional or three-dimensional finite elements for large deflection analysis of shells because the kinematic relations are well known and the rigid body behavior is represented exactly. Other work on thick shells or solids in conjunction with thin shells is presented in[47–50].

CHOICE OF FINITE ELEMENT FOR THE TWO-DIMENSIONAL REGIONS

The guiding principle in the selection of an appropriate element for analysis of the two-dimensionally discretized "solid" or "thick shell" regions is that the element should be capable of reproducing thin shell behavior as

Fig. 40. Geometry of an N-layered laminate (adapted from Jones[6]).
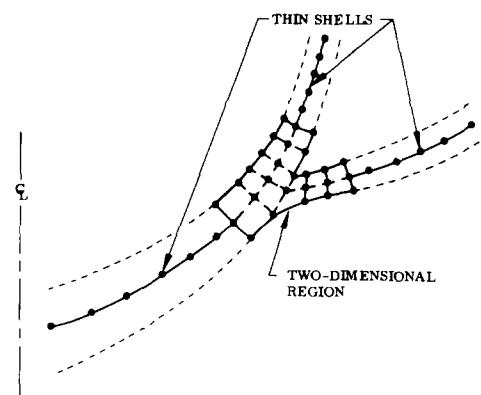
Fig. 41. Hybrid body of revolution: discretization in one and two dimensions (from Bushnell[35]).
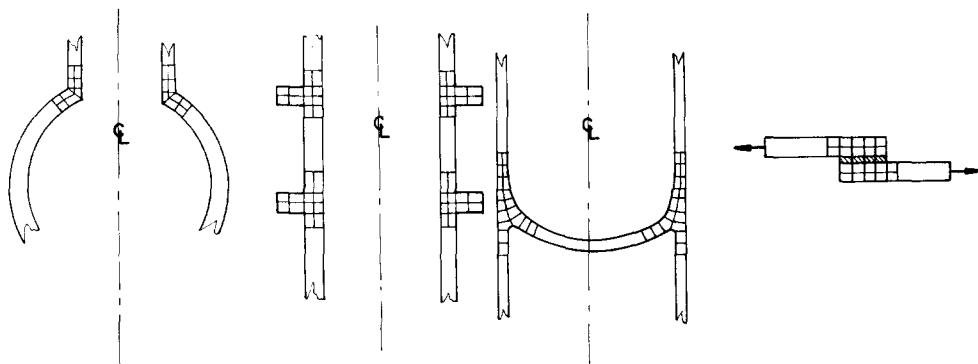
Fig. 42. Problems for which a hybrid program is useful (from Bushnell[35]).

well as general three-dimensional behavior. If this were not the case, large spurious stresses and artificial constraints would be introduced at every junction between "thick" (two-dimensionally discretized) and "thin" (one-dimensionally discretized) regions.

The pressurized flat circular plate (Fig. 43) is a good example to use in a discussion of what properties a "solid" element must have in order to lead to accurate predictions of "thin shell" behavior. Suppose that the plate shown in Fig. 43 is loaded well into the plastic range. Then at the axis of revolution, for example, the topmost fibers are compressed and the bottom-most fibers are stretched plastically. Since the plastic flow is assumed to be associated with zero volume change, the axial strain (normal to the surface) must be extensional at the topmost fiber and compressive at the bottom-most. The simplest assumption is that the axial *strain* varies *linearly* through the plate thickness. It follows that the axial *displacement* must vary *quadratically* through the plate thickness. Thus, at least three nodes are required through the plate thickness if the nodal point unknowns are the displacement components. If only two nodes are used through the plate thickness, the axial strain can only be constant. Such a gross simplification leads to the prediction of very large stresses normal to the surface of

the plate at its extreme fibers, a result that naturally generates serious errors, especially in analyses in which plasticity or creep are included.

It is easy to see that at least three nodes are required in the radial direction in each element in order that bending be possible. Wilson's[16] incompatible element permits bending but still suffers from the insufficiency just discussed relative to normal stress and strains.

The requirement of at least three modes in each direction immediately suggests use of an isoparametric 8-node element. Such elements were first introduced by Irons in 1966[51] and subsequently popularized by Zienkiewicz[52]. These elements can, as seen from the results listed in Table 4, reproduce thin shell behavior. If the programming is done in double precision, the "aspect ratio" is essentially unlimited. In another analysis of a flat plate, use of elements with a radial length-to-thickness ratio of 1000 still led to good prediction of the deformed state.

BASIC EQUATIONS

In this section the possibility of plastic flow and creep will be allowed. Therefore, the equations governing equilibrium and bifurcation buckling will be derived from the principle of virtual work, rather than from minimiza-

Table 4. Comparison of solutions and computer times for uniformly pressurized ($P = 3.0$ psi) flat circular plate with 10 elements (see Fig. 43)

| Item	Type of model	
	8-Node, 2-Dimensional isoparametric finite elements (10 elements)	Thin shell theory: finite difference energy method (10 elements)
(1) Maximum displacement (in.)		
(a) Linear elastic	1.9356	1.9491
(b) Nonlinear elastic	0.38357	0.38043
(c) Nonlinear elastic–plastic	0.58089	0.57221
(2) Number of unknowns	109	31
(3) Maximum matrix bandwidth	19	8
(4) Total Newton iterations req'd for entire case	37	34
(5) Computer time spent in the Newton–Loop (sec)	66.439	2.343
(6) Number of "trials" (times that material properties must be updated)	10	10
(7) Computer time spent in updating material properties (sec)	21.874	4.589
(8) Total run time (sec)	88.313	6.932
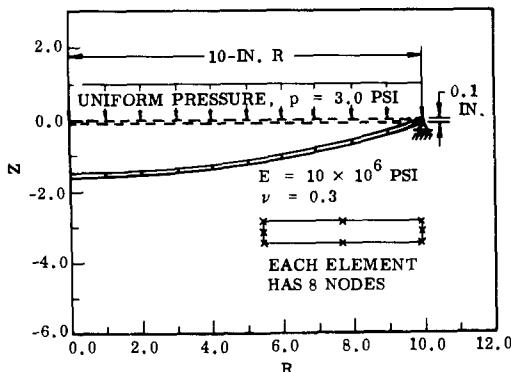
Fig. 43. Flat plate under uniform pressure modeled with 10 isoparametric 8-node finite elements (from Bushnell[35]).

tion of the total potential energy as was done in the previous sections on the analysis of elastic curved beams and thin shells.

Principle of virtual work

The first variation of a total energy functional H (analogous to H for the beam in eqn 12) is

$$\delta H = \int_{\text{Volume}} \lfloor \sigma \rfloor \{\delta \epsilon\} \, dV \qquad \text{(strain energy)}$$

$$- \int_{\text{Volume}} m \ddot{u} \quad dV \qquad \text{(kinetic energy)}$$

$$- \int_{\text{Volume}} \bar{F}_b \cdot \delta \bar{u} \, dV \qquad \text{(body forces)}$$

$$- \int_{\text{Area}} \bar{F}_s \cdot \delta \bar{u} \, dA \qquad \text{(surface tractions)}$$

$$- \int_{\text{Area}} \bar{F}_s{}' \cdot \delta [f(\bar{u})] \, dA \qquad \text{("following" pressure)}$$

$$- \int_{\theta} \bar{F}_L \cdot \delta \bar{u} r_L \, d\theta \qquad \text{(line loads)}$$

$$+ \sum_{l=1}^{m} \delta \lambda_l \left(\sum_{k=1}^{n_c} a_{lk} u_k + a_{l0} \right) + \sum_{l=1}^{m} \lambda_l \left(\sum_{k=1}^{n_c} a_{lk} \delta u_k \right)$$
$$\text{(constraint conditions)}$$

$$= 0 \qquad \text{(equilibrium condition)}.$$
$$\tag{209}$$

Strains are considered to be small but rotations may be moderately large. The material is elastic–plastic and primary or secondary creep are included in the analytical model. The strain components $\lfloor \epsilon \rfloor$ are nonlinear functions of the displacements $\bar{u}$. The displacements $\bar{u}$ anywhere in each finite element can be expressed in terms of nodal point values $\bar{q}$.

$$\bar{u} = \sum_{i=1}^{8} h_i(x,r) \bar{q}_i. \tag{210}$$

In eqn (210) $\bar{u}$ represents a displacement vector and $\bar{q}_i$ represents the value of $\bar{u}$ at the ith node of a finite element. For example, in Fig. 44(b) $\bar{u}$ has the components $u_1, u_2, u_3 = q_{i1}, q_{i2}, q_{i3}$.
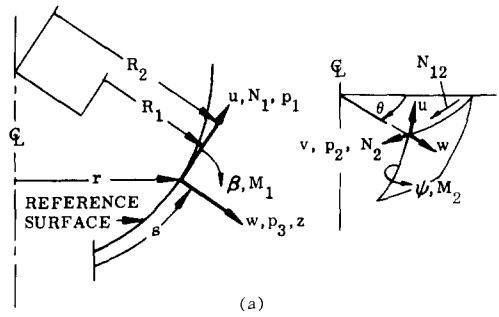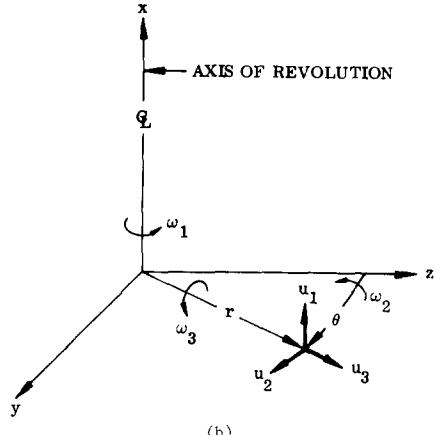
Fig. 44. Variables used in the analysis of (a) thin shell segments, (b) solids of revolution (from Bushnell[35]).

The variation δH is therefore given by

$$\delta H = \frac{\partial H}{\partial q} \cdot \delta q = \Psi \cdot \delta q = 0. \tag{211}$$

Since δq is arbitrary, the equilibrium condition is

$$\Psi_i = \int_V \left(\lfloor \sigma \rfloor \left\{ \frac{\partial \epsilon}{\partial q_i} \right\} - m \ddot{u} \cdot \frac{\partial \bar{u}}{\partial q_i} - \bar{F}_b \cdot \frac{\partial \bar{u}}{\partial q_i} \right) dV$$

$$- \int_A \left(\bar{F}_s \cdot \frac{\partial \bar{u}}{\partial q_i} + \bar{F}_s{}' \cdot \frac{\partial [f(\bar{u})]}{\partial q_i} \right) dA$$

$$- \int_{\theta} \bar{F}_L \cdot \frac{\partial \bar{u}}{\partial q_i} r_L \, d\theta$$

$$+ \sum_{l=1}^{m} \frac{\partial \lambda_l}{\partial q_i} \cdot \left(\sum_{k=1}^{n_c} a_{lk} u_k + a_{l0} \right)$$

$$+ \sum_{l=1}^{m} \lambda_l \left(\sum_{k=1}^{n_c} a_{lk} \frac{\partial u_k}{\partial q_i} \right) = 0 \tag{212}$$

$$i = 1, 2, 3, \ldots N.$$

Because the strains $\lfloor \epsilon \rfloor$ are nonlinear functions of the nodal point displacements q, eqn (212) represents a simultaneous set of nonlinear equations. These equations must be solved incrementally because the material is elastic–plastic creeping and hence its state is path-dependent. In addition to providing for an incremental procedure, one must provide for some kind of iterative or self-correcting technique at each load or time increment in order to prevent drifting from the correct solution path.

Appropriate use of the Newton–Raphson method with path-dependent material properties

Suppose that for some known starting vector q_0 of dimension N, we have $\psi_i(q_0) \neq 0$. We wish to determine Δq such that $\psi_i(q_0 + \Delta q) = 0$. A system of equations for the unknowns Δq can be generated by expansion of ψ_i about q_0 in a Taylor series. If only the linear terms in Δq are retained in this expansion, one obtains the following linear simultaneous equations:

$$\sum_{j=1}^{N} \frac{\partial \psi_i}{\partial q_j} \Delta q_j = -\psi_i \quad i = 1,2,3,\ldots N. \tag{213}$$

These equations are solved for Δq_i and a new estimate of the solution $q_i = q_0 + \Delta q$ becomes available. Iterations continue until Δq is smaller than a certain prescribed percentage of q. This is called the Newton–Raphson method. The short description above is a reiteration of the discussion associated with eqn (56) for the nonlinear analysis of the elastic curved beam.

A certain refinement in the solution strategy is required if large deflection effects and elastic–plastic material behavior are simultaneously present. The Newton–Raphson method can be used only if ψ_i can be expanded in a Taylor series about the known origins q_0 or q_1 or q_2, etc. The Taylor series expansion exists if and only if the gradient $\partial \psi / \partial q$ exists. In problems involving material which loads plastically but unloads elastically along a different path in stress–strain space, the existence of a unique $\partial \psi / \partial q$ depends on the use of a proper strategy for taking into account both geometric and material nonlinearity. One strategy is to establish a double iteration loop for each load or time increment: the tangent stiffness coefficients and plastic and creep strains are updated in the outer loop and the geometric nonlinearities are handled by the Newton–Raphson method in the inner loop. In the Newton–Raphson loop the tangent stiffness is *not* recomputed with each new estimate of the displacement vector q. While calculations are proceeding in this inner loop, it is as if the material were elastic, loading and unloading along the same path in stress–strain space. Therefore, a unique value of $\partial \psi / \partial q$ exists and the Newton–Raphson procedure is valid. It is important to be assured of this validity because the Newton method has certain favorable convergence properties which are well understood. If one is attempting to predict loads at which a structure collapses, it is important to know that failure of convergence of the iterations indicates failure of the structure and not simply failure of the algorithm to predict the behavior of the structure.

Details on various solution methods for nonlinear structural analysis, including methods for reliable prediction of collapse loads are given in Ref. [26]. More information is also given there on the double iteration loop and on the method used to update elastic–plastic material properties in the outer loop of the computational process.

Calculation of $\partial \psi_i / \partial q_j$

The stiffness matrix for each Newton–Raphson iteration is $\partial \psi / \partial q$, and the (i,j)th element of this matrix is $\partial \psi_i / \partial q_j$. From eqn (212), we can write:

$$\frac{\partial \psi_i}{\partial q_i} = \int_V \left(\lfloor \sigma \rfloor \left\{ \frac{\partial^2 \epsilon}{\partial q_i \partial q_j} \right\} + \lfloor \frac{\partial \sigma}{\partial q_j} \rfloor \left\{ \frac{\partial \epsilon}{\partial q_i} \right\} - m \frac{\partial \ddot{u}}{\partial q_i} \cdot \frac{d\ddot{u}}{\partial q_i} \right) dV$$

$$- \int_A \bar{F}'_s \cdot \frac{\partial^2 [f(\bar{u})]}{\partial q_i \partial q_j} dA + \sum_{l=1}^{m} \frac{\partial \lambda_l}{\partial q_i} \cdot \sum_{k=1}^{n_c} a_{lk} \frac{\partial u_k}{\partial q_j}$$

$$+ \sum_{l=1}^{m} \frac{\partial \lambda_l}{\partial q_j} \cdot \sum_{k=1}^{n_c} a_{lk} \frac{\partial u_k}{\partial q_i}. \tag{214}$$

Note that we have assumed by use of eqn (210) that the displacements $\bar{u}$ anywhere in the structure are linear functions of the nodal point displacements, q. This may be a questionable model for discrete rings attached to areas on the shell which undergo moderately large rotations. The displacements anywhere in the cross section of a discrete ring are expressed in terms of nodal points on the shell reference surface in the neighborhood of the attachment point of the ring to the shell. Since the cross section of the discrete ring is assumed to remain undeformed in "classical" ring theory, the displacements anywhere in that cross section involve sines and cosines of angles of rotation of the shell wall. If these angles are relatively large, retention of only the linear terms in the series expansions for their sines and cosines may not be very accurate. Hence, for the discrete ring analysis, the displacements $\bar{u}$ are considered for certain analysis branches to be nonlinear functions of q. (For example, see eqns (106) and related discussion.)

Equilibrium

Equilibrium is determined by iterative solution of eqns (213), with eqn (214) used on the l.h.s. and eqn (212) on the r.h.s. For statics problems $\bar{u} = 0$ and thus the last term on the first line of eqn (214) drops out.

Bifurcation buckling and eigenvibrations

The following discussion is a review of that associated with eqn (60) for the buckling of the beam. The calculation of bifurcation buckling loads and of modal vibration frequencies can be posed as a problem of determination of the values of a parameter for which the equilibrium solution is not unique. In bifurcation buckling problems the parameter is a load parameter, and in modal vibration problems it is a frequency.

If q_0 represents a solution of the equilibrium equations

$$\psi_i(q_0) = 0. \tag{215}$$

Then we need to know if

$$\psi_i(q_0 + q^b) = 0 \tag{216}$$

in which q^b is a non-trivial bifurcation buckling mode or vibration mode of infinitesimal amplitude. Following the Newton–Raphson iteration strategy, we can write

$$\sum_{j=1}^{M} \frac{\partial \psi_i}{\partial q_j} \bigg|_{q \to q_0} \cdot q_j^b = -\psi_i(q_0) = 0 \tag{217}$$

$$i = 1,2,3,\ldots M.$$

Equations (217) are linear and homogeneous. A nontrivial solution q^b exists only for certain discrete values of some parameter contained in the matrix $\partial \psi / \partial q^b$. These eigenvalues are the bifurcation buckling loads or modal vibration frequencies.

Variation of displacements in the circumferential direction

In nonlinear problems the loading and the structural

response are assumed to be axisymmetric. In cases involving bifurcation buckling or modal vibrations, the eigenvectors vary harmonically around the circumference with only one harmonic participating in each mode. Thus, the modal displacements are denoted $\bar{u}^b$,

$$\bar{u}^b = \begin{Bmatrix} u_1{}^b \\ u_2{}^b \\ u_3{}^b \end{Bmatrix} = \begin{Bmatrix} u_1^{b(n)} \sin n\theta \\ u_2^{b(n)} \cos n\theta \\ u_3^{b(n)} \sin n\theta \end{Bmatrix} \tag{218}$$

where $u_1{}^b$, $u_2{}^b$, $u_3{}^b$ are the axial, circumferential and radial displacement components, respectively. In linear nonsymmetric stress problems, the displacement field u_1, u_2, u_3 can be written as infinite series

$$u_1 = \sum_{n=1}^{\infty} u_1{}^{(n)} \sin n\theta + \sum_{n=0}^{-\infty} u_1{}^{(-n)} \cos n\theta$$

$$u_2 = \sum_{n=0}^{\infty} u_2{}^{(n)} \cos n\theta + \sum_{n=-1}^{-\infty} u_2{}^{(-n)} \sin |n|\theta \tag{219}$$

$$u_3 = \sum_{n=1}^{\infty} u_3{}^{(n)} \sin n\theta + \sum_{n=0}^{-\infty} u_3{}^{(-n)} \cos n\theta.$$

These equations are analogous to eqns (108) for the thin shell analysis.

Displacement components used for shells, rings, solids
   In the analysis of the thin shell segments, u_1, u_2, u_3 are written in terms of u, v, w the meridional, circumferential and normal displacement components of the shell reference surface. These components are shown in Fig. 44(a).
   In the analysis of a discrete ring the displacements anywhere in the ring cross section are ultimately expressed in terms of the displacements u, v, w of the point on the shell reference surface to which the ring is considered to be attached (see eqns 106 and 107). Further details on the elastic–plastic discrete ring analysis are given in Ref. [26].
   In the analysis of solids of revolution u_1, u_2, u_3 are the dependent variables. These are shown in Fig. 44(b).

STRAIN ENERGY

General equations
   The strain energy gradient is given by the first term in the integrand on the r.h.s. of eqn (212):

$$\frac{\partial U}{\partial q_i} = \int_V \overset{1 \times 6}{\lfloor \sigma \rfloor} \cdot \overset{6 \times 1}{\left\{ \frac{\partial \epsilon}{\partial q_i} \right\}} dV \tag{220}$$

where

$$\lfloor \sigma \rfloor = \lfloor \epsilon - \epsilon^p - \epsilon^c - \epsilon^T \rfloor \cdot \overset{6 \times 6}{[D]} \tag{221}$$

in which ϵ^p, ϵ^c, ϵ^T are the plastic, creep, and thermal strains, respectively, and $[D]$ is the constitutive matrix given later.
   The first two terms in the integrand on the r.h.s. of eqn (214) can thus be written

$$\frac{\partial^2 U}{\partial q_i \partial q_j} = \int_V \left(\lfloor \epsilon - \epsilon^p - \epsilon^c - \epsilon^T \rfloor [D] \left\{ \frac{\partial^2 \epsilon}{\partial q_i \partial q_j} \right\} \right.$$
$$\left. + \frac{\partial}{\partial q_j} \lfloor \epsilon - \epsilon^p - \epsilon^c - \epsilon^T \rfloor [D] \left\{ \frac{\partial \epsilon}{\partial q_i} \right\} \right). \tag{222}$$

In the discussion about the Newton–Raphson method, it was emphasized that within the inner iterative loop the material tangent stiffness is held constant. Since the solution corresponds to an instant in time, the creep strains $[\epsilon^c]$ and the thermal strains $[\epsilon^T]$ are also held constant. The plastic strains $[\epsilon^p]$ can be expressed in the form

$$\lfloor \epsilon^p \rfloor = \lfloor \epsilon_0{}^p \rfloor + \lfloor \epsilon - \epsilon_0 \rfloor [C_0{}^T] \tag{223}$$

in which $[C_0{}^T]$ is the transpose of a matrix which will be derived later. The subscript $(\ )_0$ in eqn (223) denotes "value obtained when the material properties were last updated". These values are held constant throughout the Newton–Raphson iterations. The total strain $\lfloor \epsilon \rfloor$ changes, of course, with each Newton–Raphson iteration. With the use of eqn (223) in eqn (222), and recognition that $\lfloor \epsilon_0{}^p \rfloor$, $\lfloor \epsilon^c \rfloor$ and $\lfloor \epsilon^T \rfloor$ are independent of q in the Newton–Raphson loop, we can write eqn (222) in the form:

$$\frac{\partial^2 U}{\partial q_i \partial q_j} = \int_V \left(\lfloor \epsilon \rfloor [D_{T0}] \left\{ \frac{\partial^2 \epsilon}{\partial q_i \partial q_j} \right\} + \left[\frac{\partial \epsilon}{\partial q_j} \right] [D_{T0}] \left\{ \frac{\partial \epsilon}{\partial q_i} \right\} \right.$$
$$\left. + \lfloor \epsilon_0 \cdot C_0{}^T - \epsilon_0{}^p - \epsilon^c - \epsilon^T \rfloor [D] \left\{ \frac{\partial^2 \epsilon}{\partial q_i \partial q_j} \right\} \right) dV \tag{224}$$

where $[D_{T0}]$ is a matrix which can be shown to be symmetric,

$$[D_{T0}] \equiv [I - C_0{}^T] \cdot [D]. \tag{225}$$

The expression (223) is also used in eqn (221) and eqn (220) so that,

$$\frac{\partial U}{\partial q_i} = \int_V \left(\lfloor \epsilon \rfloor [D_{T0}] \left\{ \frac{\partial \epsilon}{\partial q_i} \right\} + \lfloor \epsilon_0 \cdot C_0{}^T - \epsilon_0{}^p - \epsilon^c \right. \right.$$
$$\left. \left. - \epsilon^T \rfloor [D] \left\{ \frac{\partial \epsilon}{\partial q_i} \right\} \right) dV \tag{226}$$

Derivation of $C_0{}^T$
   This derivation follows Stricklin et al.[53]. The change in stress at an instant of time for a given temperature is

$$\{d\sigma\} = [D]\{d\epsilon - d\epsilon^p\}. \tag{227}$$

The stress and strain components are

$$\lfloor d\sigma \rfloor = \lfloor d\sigma_1, d\sigma_2, d\sigma_3, d\sigma_{13}, d\sigma_{12}, d\sigma_{23} \rfloor$$
$$\lfloor d\epsilon \rfloor = \lfloor d\epsilon_1, d\epsilon_2, d\epsilon_3, d\epsilon_{13}, d\epsilon_{12}, d\epsilon_{23} \rfloor. \tag{228}$$

The changes in plastic strain components $\{d\epsilon^p\}$, are related to the change in effective plastic strain by the flow law associated with the von Mises yield criterion:

$$\{d\epsilon^p\} = d\bar{\epsilon}^p \left\{ \frac{\partial \bar{\sigma}}{\partial \sigma} \right\} \tag{229}$$

where the effective stress $\bar{\sigma}$ is given by

$$\bar{\sigma} = \left\{ \frac{1}{2} [(\sigma_1 - \sigma_2)^2 + (\sigma_2 - \sigma_3)^2 + (\sigma_3 - \sigma_1)^2 \right.$$
$$\left. + 6(\sigma_{12}{}^2 + \sigma_{13}{}^2 + \sigma_{23}{}^2)] \right\}^{1/2} \tag{230}$$

and

$$\lfloor \partial \bar{\sigma} / \partial \sigma \rfloor \equiv \lfloor \partial \bar{\sigma} / \partial \sigma_1, \partial \bar{\sigma} / \partial \sigma_2, \ldots \text{etc.} \rfloor. \tag{231}$$

A change in effective plastic strain $d\bar{\epsilon}^p$ is related to a change in effective stress $d\bar{\sigma}$ by

$$d\bar{\sigma} = \frac{EE_T}{E - E_T}\, d\bar{\epsilon}^p = H'\, d\bar{\epsilon}^p \qquad (232)$$

and for small $d\bar{\sigma}$, we can write

$$d\bar{\sigma} = \lfloor \partial\bar{\sigma}/\partial\sigma \rfloor \{d\sigma\}. \qquad (233)$$

If we premultiply eqn (227) by $\lfloor \partial\bar{\sigma}/\partial\sigma \rfloor$ and make appropriate use of eqns (229) and (232) and (233), we obtain:

$$\lfloor \partial\bar{\sigma}/\partial\sigma \rfloor \{d\sigma\} = d\bar{\sigma} = H'\, d\bar{\epsilon}^p$$
$$= \lfloor \partial\bar{\sigma}/\partial\sigma \rfloor [D]\left(\{d\epsilon\} - d\bar{\epsilon}^p\left\{\frac{\partial\bar{\sigma}}{\partial\sigma}\right\}\right). \qquad (234)$$

We can solve eqn (234) for $d\bar{\epsilon}^p$,

$$d\bar{\epsilon}^p = \frac{\lfloor \partial\bar{\sigma}/\partial\sigma \rfloor [D]\{d\epsilon\}}{H' + \lfloor \partial\bar{\sigma}/\partial\sigma \rfloor [D]\left\{\dfrac{\partial\bar{\sigma}}{\partial\sigma}\right\}} \qquad (235)$$

and with the use of eqn (229) we obtain

$$\{d\epsilon^p\} \overset{6\times6}{=} [C_0]\{d\epsilon\} \qquad (236)$$

where

$$[C_0] = \frac{\left\{\dfrac{\partial\bar{\sigma}}{\partial\sigma}\right\} \lfloor \partial\bar{\sigma}/\partial\sigma \rfloor [D]}{H' + \lfloor \partial\bar{\sigma}/\partial\sigma \rfloor [D]\left\{\dfrac{\partial\bar{\sigma}}{\partial\sigma}\right\}}. \qquad (237)$$

The matrix $C_0{}^T$, used in eqn (223), is the transpose of $[C_0]$. In eqns (221)–(237) the quantity D or $[D]$ is given by

$$[D] \equiv \frac{E}{(1+\nu)(1-2\nu)}$$

$$\times \begin{bmatrix}
(1-\nu) & \nu & \nu & 0 & 0 & 0 \\
\nu & (1-\nu) & \nu & 0 & 0 & 0 \\
\nu & \nu & (1-\nu) & 0 & 0 & 0 \\
0 & 0 & 0 & \dfrac{1-2\nu}{2} & 0 & 0 \\
0 & 0 & 0 & 0 & \dfrac{1-2\nu}{2} & 0 \\
0 & 0 & 0 & 0 & 0 & \dfrac{1-2\nu}{2}
\end{bmatrix}$$

$$\hspace{8cm}(238)$$

Equations for thin shells, discrete rings, solids of revolution

The integration over the volume of the structure indicated in eqns (224) and (226) includes portions of the structure modeled as thin shell segments, discrete rings and solids of revolution. Each of these analytical models of the actual structure has its own kinematic law.

Thin shells

Each shell segment may contain a number of layers, each layer with its own orthotropic properties G, E_1, E_2, ν_{12} and each with its own stress–strain curve. A reference surface is selected; the strains anywhere in the wall are expressed in terms of the strains and changes in curvature of this reference surface as in eqns (82), and numerical integration is carried out through the thickness of each layer by Simpson's rule, with five integration points being used through the thickness of each layer.

For thin shells the stress and strain vectors given in eqns (228) reduce to

$$\lfloor d\sigma \rfloor \equiv \lfloor d\sigma_1, d\sigma_2, d\sigma_{12} \rfloor$$
$$\lfloor d\epsilon \rfloor \equiv \lfloor d\epsilon_1, d\epsilon_2, d\epsilon_{12} \rfloor \qquad (239)$$

in which "1" denotes meridional direction, "2" denotes circumferential direction, and "12" denotes in-plane shear. For isotropic materials the 6×6 elasticity matrix $[D]$ in eqn (238) reduces to

$$[D] = \frac{E}{(1-\nu^2)}\begin{bmatrix}
1 & \nu & 0 \\
\nu & 1 & 0 \\
0 & 0 & \dfrac{1-\nu}{2}
\end{bmatrix}. \qquad (240)$$

Equation (240) can be derived from eqn (238) by remembering that for shell theory the stress component σ_3 normal to the shell wall is zero. From the third row of the $[D]$ matrix in eqn (238) one can derive

$$\epsilon_3 = -\left(\frac{\nu}{1-\nu}\right)(\epsilon_1 + \epsilon_2). \qquad (241)$$

With use of eqn (241) and recalling that the transverse shear strains $\epsilon_{13} = \epsilon_{23} = 0$, one can condense the matrix in eqn (238) to that in eqn (240).

The 6×6 $[C_0]$ matrix given in eqn (237) for general three-dimensional plasticity analysis becomes a 3×3 matrix in shell analysis since the stress vector in eqn (239a) contains only three components. The effective stress in eqn (230) simplifies to

$$\bar{\sigma} = (\sigma_1{}^2 + \sigma_2{}^2 - \sigma_1\sigma_2 + 3\sigma_{12}{}^2)^{1/2}. \qquad (242)$$

Discretization in the meridional direction is by the finite difference method, as described previously. Figure 21 shows the arrangement of nodal points used for the discretized shell analysis. As already stated, the energy density is evaluated midway between adjacent "u" or "v" nodes. The u, v, w, displacement components in the neighborhood "E" $\pm l/2$ are expanded in a Taylor series about the point "E", where the independent variable is the meridional arc length s. Thus for portions of the structure being treated as thin shell segments, eqn (210) might be written in the form

$$u = \sum_{i=1}^{7} h_i(s)q_i \qquad (243)$$

in which the domain over which eqn (243) holds is the neighborhood "E" $\pm l/2$ and the q_i are the 7 nodal displacement components w_{i-1}, u_i, v_i, w_i, u_{i+1}, v_{i+1}, w_{i+1} indicated in Fig. 21 and eqn (115).

The $h_i(s)$ could be derived from consideration of the linear variation of u and v and the quadratic variation of w within each shell finite difference element as shown in Fig. 36. However, the $h_i(s)$ are not needed, since there is only one Gaussian integration point per element. Therefore, expressions such as given in eqns (110), (111), (113) and (116) are sufficient.

Discrete rings

If warping is neglected, the strain energy associated with a discrete ring arises from circumferential strain and torsion. The integrals over the volume indicated in eqns (224) and (226) have the form

$$\int_{x'}\int_{\theta}\int_{y'} f(x', y')(r_x + x')\, dy'\, dx'\, d\theta \qquad (244)$$

in which the (x',y') coordinate system has its origin at the ring shear center r_s and the limits of x' and y' define the shape of the ring cross section. The function $f(x',y')$ represents the integrand of eqns (224) or (226). The strain vector contains two elements

$$\lfloor \epsilon \rfloor = \lfloor \epsilon_{\text{hoop}}, \epsilon_{\text{twist}} \rfloor \qquad (245)$$

and the elastic matrix $[D]$ is given by

$$[D] = E_r \begin{bmatrix} 1 & 0 \\ 0 & \dfrac{1}{2(1+\nu)} \end{bmatrix}. \qquad (246)$$

The 6×6 C_0 matrix given in eqn (237) for general three-dimensional plasticity analysis becomes a 2×2 matrix in discrete ring analysis since we are only concerned with the two stress components $\sigma_{\text{hoop}}, \sigma_{\text{twist}}$.

Each discrete ring cross section can be modeled as if it consists of an assemblage of K straight segments of thickness T_k, length L_k, and orientation angle ϕ_k, $k = 1,2,\ldots,K$. Figure 45 shows an example. The material of each ring segment may have a different stress–strain curve and different creep properties. The temperature may vary along the length L_k of the ring segments but must be constant through the thickness T_k. The integrated ring properties are determined by Simpson's rule integration within each segment for all K segments.

Further details are given in Refs. [26, 54].

Solids of revolution

Isoparametric finite elements [52] are used to represent those portions of the hybrid body of revolution for which shell theory might be inadequate. The element geometry is given in Fig. 46. The independent variables are x, θ and r and the corresponding displacement components are u_1, u_2, u_3.

This element was chosen because it can adequately predict shell behavior as long as all eight nodes are present. Hence, it does not create spurious discontinuity stresses in the neighborhood of a junction with a finite difference shell element.

Within the element the displacement field u_1, u_2, u_3 and r,x coordinates can be expressed in terms of the nodal point values and interpolation formulas written in

Fig. 46. Isoparametric 8-node solid element of revolution used in hybrid computer program (from Bushnell[35]).

terms of the local coordinates s, t which vary from -1 to 1:

$$(x,r) = \sum_{i=1}^{8} h_i(s,t)(x^i,r^i)$$

$$(u_1,u_2,u_3) = \sum_{i=1}^{8} h_i(s,t)(u_1{}^i,u_2{}^i,u_3{}^i) \qquad (247)$$

in which the interpolation formulas $h_i(s,t)$ are given along with the kinematic expressions and other details in the following section. Integration over the x–r plane is performed by Gaussian quadrature in which the numbers of Gaussian points in the "s" and "t" directions are input variables. The circumferential variations of displacement components are given by eqns (219).

DETAILS OF THE ANALYSIS OF A TWO-DIMENSIONALLY DISCRETIZED (SOLID) REGION

In this section expressions will be derived for most of the components of the energy functional which appear in eqn (209).

Strain energy—general

The strain displacement relations valid for small strains and moderately large rotations are given by Novoshilov[55]:

$$\epsilon_1 = \frac{\partial u_1}{\partial x} + \frac{1}{2}(\omega_2{}^2 + \omega_3{}^2)$$

$$\epsilon_2 = \frac{1}{r}(u_3 - nu_2) + \frac{1}{2}(\omega_1{}^2 + \omega_3{}^2)$$

$$\epsilon_3 = \frac{\partial u_3}{\partial r} + \frac{1}{2}(\omega_1{}^2 + \omega_2{}^2)$$

$$\epsilon_{13} = \frac{\partial u_1}{\partial r} + \frac{\partial u_3}{\partial x} - \omega_1\omega_3 \qquad (248)$$

$$\epsilon_{12} = nu_1/r + \frac{\partial u_2}{\partial x} - \omega_1\omega_2$$

$$\epsilon_{23} = \frac{\partial u_2}{\partial r} + \frac{1}{r}(nu_3 - u_2) - \omega_2\omega_3$$

in which the rotation components ω_1, ω_2, ω_3, shown in

Fig. 45. Discrete ring as modeled in the hybrid program (from Bushnell[25]).

NOTE: Discrete ring attachment point is considered to be located on the shell reference surface.

Fig. 46, are given by

$$2\omega_1 = \frac{1}{r}(nu_3 - u_2) - \frac{\partial u_2}{\partial r}$$

$$2\omega_2 = \frac{\partial u_1}{\partial r} - \frac{\partial u_3}{\partial x} \tag{249}$$

$$2\omega_3 = \frac{\partial u_2}{\partial x} - nu_1/r.$$

In writing eqns (248) and (249) it has been assumed that

$$u_1 = u_1(x, r) \sin n\theta$$

$$u_2 = u_2(x, r)\cos n\theta \tag{250}$$

$$u_3 = u_3(x, r)\sin n\theta.$$

The kinematic relations (248) and (249) are consistent with those used for the shell analysis, eqns (90) and (91).

Within the element the displacement field u_1, u_2, u_3 and r, x coordinates can be expressed in terms of the nodal point values and interpolation formulas written in terms of the local coordinates s, t which vary from -1 to 1 as in eqns (247). In Ref. [42] the interpolation formulas $h_i(s,t)$ are given by:

Delete if node I is not included

	$I = 5$	$I = 6$	$I = 7$	$I = 8$
$h_1 = RS/4$	$-h_5/2$			$-h_8/2$
$h_2 = \bar{R}S/4$	$-h_5/2$	$-h_6/2$		
$h_3 = \bar{R}\bar{S}/4$		$-h_6/2$	$-h_7/2$	
$h_4 = R\bar{S}/4$			$-h_7/2$	$-h_8/2$
$h_5 = R^*S/2$				
$h_6 = \bar{R}S^*/2$				
$h_7 = R^*\bar{S}/2$				
$h_8 = RS^*/2$				(251)

in which

$$R = 1 + t \quad \bar{R} = 1 - t \quad R^* = 1 - t^2$$
$$S = 1 + s \quad \bar{S} = 1 - s \quad S^* = 1 - s^2 \tag{252}$$

and the numbered subscript refers to node point number in the 8-node isoparametric quadrilateral of revolution. The nodes are numbered as shown in Fig. 46.

The kinematic relations (248) and (249) contain derivatives with respect to x and r. These can be expressed in terms of derivatives with respect to s and t by means of

$$\begin{Bmatrix} \dfrac{\partial}{\partial x} \\[2mm] \dfrac{\partial}{\partial r} \end{Bmatrix} = \frac{1}{|J|} \begin{bmatrix} \dfrac{\partial r}{\partial t} & -\dfrac{\partial r}{\partial s} \\[2mm] -\dfrac{\partial x}{\partial t} & \dfrac{\partial x}{\partial s} \end{bmatrix} \begin{Bmatrix} \dfrac{\partial}{\partial s} \\[2mm] \dfrac{\partial}{\partial t} \end{Bmatrix} \tag{253}$$

where

$$|J| = \frac{\partial x}{\partial s}\frac{\partial r}{\partial t} - \frac{\partial r}{\partial s}\frac{\partial x}{\partial t}. \tag{254}$$

In terms of s and t the infinitesimal volume element dV in eqn (209) is

$$dV = |J| \, r \, ds \, dt \, d\theta. \tag{255}$$

Strain energy: nonlinear axisymmetric prebuckling analysis

The kinematic relations for axisymmetric deformations including moderate rotations are obtained by simplification of eqns (248) and (249):

$$\epsilon_1 = \frac{\partial u_1}{\partial x} + \frac{1}{2}\omega_2^2$$

$$\epsilon_2 = u_3/r$$

$$\epsilon_3 = \frac{\partial u_3}{\partial r} + \frac{1}{2}\omega_2^2 \tag{256}$$

$$\epsilon_{13} = \frac{\partial u_1}{\partial r} + \frac{\partial u_3}{\partial x}$$

in which the rotation component ω_2 is given by

$$2\omega_2 = \frac{\partial u_1}{\partial r} - \frac{\partial u_3}{\partial x}. \tag{257}$$

If we let

$$a_{11} = \frac{dx}{ds}; \quad a_{12} = \frac{\partial r}{\partial s}; \quad a_{21} = \frac{\partial x}{\partial t}; \quad a_{22} = \frac{\partial r}{\partial t} \tag{258}$$

then, using eqn (253), we obtain

$$\epsilon_1 = \frac{1}{|J|}\left(a_{22}\frac{\partial u_1}{\partial s} - a_{12}\frac{\partial u_1}{\partial t}\right) + \frac{1}{2}\omega_2^2$$

$$\epsilon_2 = u_3/r$$

$$\tag{259}$$

$$\epsilon_3 = \frac{1}{|J|}\left(-a_{21}\frac{\partial u_3}{\partial s} + a_{11}\frac{\partial u_3}{\partial t}\right) + \frac{1}{2}\omega_2^2$$

$$\epsilon_{13} = \frac{1}{|J|}\left(-a_{21}\frac{\partial u_1}{\partial s} + a_{11}\frac{\partial u_1}{\partial t} + a_{22}\frac{\partial u_3}{\partial s} - a_{12}\frac{\partial u_3}{\partial t}\right)$$

and

$$2\omega_2 = \frac{1}{|J|}\left(-a_{21}\frac{\partial u_1}{\partial s} + a_{11}\frac{\partial u_1}{\partial t} - a_{22}\frac{\partial u_3}{\partial s} + a_{12}\frac{\partial u_3}{\partial t}\right). \tag{260}$$

With use of eqn (247b), we can write eqns (259) in the form

$$\{\epsilon\} = \begin{Bmatrix} \epsilon_1 \\ \epsilon_2 \\ \epsilon_3 \\ \epsilon_{13} \end{Bmatrix} = \overset{4\times16}{[B]}\{q\} + \frac{1}{2}\begin{Bmatrix} \omega_2^2 \\ 0 \\ \omega_2^2 \\ 0 \end{Bmatrix} \tag{261}$$

in which

$$\lfloor q \rfloor \equiv \lfloor u_1^{\,1}, u_3^{\,1}, u_1^{\,2}, u_3^{\,2}, u_1^{\,3}, u_3^{\,3}, \ldots u_1^{\,8}, u_3^{\,8}\rfloor. \tag{262}$$

The superscripts in eqn (262) denote nodal point numbers

as shown in Fig. 46. The terms in the 4×16 matrix $[B]$ are

$$B(1,2I-1) = \frac{1}{|J|}\left(a_{22}\frac{\partial h_I}{\partial s} - a_{12}\frac{\partial h_I}{\partial t}\right)$$

$$B(2,2I-1) = 0$$

$$B(3,2I-1) = 0$$

$$B(4,2I-1) = \frac{1}{|J|}\left(-a_{21}\frac{\partial h_I}{ds} + a_{11}\frac{\partial h_I}{\partial t}\right)$$

Equation (268) is analogous to eqn (68) in the curved beam analysis.

$$B(1,2I) = 0$$

$$B(2,2I) = h_I/r$$

$$B(3,2I) = \frac{1}{|J|}\left(-a_{21}\frac{\partial h_I}{\partial s} + a_{11}\frac{\partial h_I}{\partial t}\right)$$

$$B(4,2I) = \frac{1}{|J|}\left(a_{22}\frac{\partial h_I}{\partial s} - a_{12}\frac{\partial h_I}{\partial t}\right) \qquad (263)$$

in which I is the local node point number, $I = 1,2,\ldots 8$. The rotation ω_2 may be written in the form

$$2\omega_2 = \lfloor\bar{R}\rfloor\{q\} \qquad (264)$$

in which

$$\bar{R}(2I-1) = B(4,2I-1) \quad \bar{R}(2I) = -B(4,2I) \qquad (265)$$

The h_I in eqns (263) are given by eqns (251).

Using eqns (255), (261) and (264), we can write eqn (224) in terms of the nodal point displacement components. The first and third terms in eqn (224) are expressed in the combined form

$$(\lfloor\Delta\epsilon\rfloor [D_{T0}] + \lfloor\sigma_0\rfloor)\left\{\frac{\partial^2\epsilon}{\partial q_i\partial q_j}\right\} \qquad (266)$$

where

$$\lfloor\Delta\epsilon\rfloor \equiv \lfloor\epsilon - \epsilon_0\rfloor = \lfloor\sigma_0\rfloor = \lfloor\epsilon_0 - \epsilon_0{}^P - \epsilon^c - \epsilon^T\rfloor [D] \quad (267)$$

in order to save computer storage space and to reduce the number of calculations required to obtain the stiffness matrix. Equation (224) thus becomes

$$\frac{\partial^2 U}{\partial q_i\partial q_j} = 2\pi \sum_{k_s=1}^{K_s} \Delta s_k \sum_{k_t=1}^{K_t} \Delta t_k \left[\left(\overset{1\times 4}{(\lfloor\Delta\epsilon\rfloor} \overset{4\times 4}{[D_{T0}]} + \overset{1\times 4}{\lfloor\sigma_0\rfloor)} \right. \right.$$

$$\times \begin{Bmatrix} \bar{R}_i\bar{R}_j \\ 0 \\ \bar{R}_i\bar{R}_j \\ 0 \end{Bmatrix}$$

$$+ \lfloor B_j\rfloor [D_{T0}]\{B_i\} + \lfloor B_j\rfloor [D_{T0}]\begin{Bmatrix} \omega_2\bar{R}_i \\ 0 \\ \omega_2\bar{R}_i \\ 0 \end{Bmatrix}$$

$$+ \lfloor \omega_2\bar{R}_j, 0, \omega_2\bar{R}_j, 0\rfloor [D_{T0}]\{B_i\} \qquad (268)$$

$$\left. \left. + \lfloor \omega_2\bar{R}_j, 0, \omega_2\bar{R}_j, 0\rfloor [D_{T0}] \begin{Bmatrix} \omega_2\bar{R}_i \\ 0 \\ \omega_2\bar{R}_i \\ 0 \end{Bmatrix} \right) |J|r \right]_{k_t, k_s}$$

in which Δs_k, Δt_k are Gaussian integration weights; K_s and K_t are the numbers of Gaussian integration points in the s and t directions; $\bar{R}_i$ is the ith member of the vector $\lfloor\bar{R}\rfloor$ given in eqn (265); $\lfloor B_j\rfloor$ is the transpose of the jth column of $[B]$; and $\{B_i\}$ is the ith column of $[B]$. All terms in eqn (268) are evaluated at s and t corresponding to the Gaussian integration points (s_{k_s}, t_{k_t}) in the element.

Equation (226) can be written in the form

$$\frac{\partial U}{\partial q_i} = 2\pi \sum_{k_s=1}^{K_s} \Delta s_k \sum_{k_t=1}^{K_t} \Delta t_k \left[\left((\lfloor\Delta\epsilon\rfloor [D_{T0}] + \lfloor\sigma_0\rfloor)\{B_i\} \right. \right.$$

$$\left. \left. + (\lfloor\Delta\epsilon\rfloor [D_{T0}] + \lfloor\sigma_0\rfloor)\begin{Bmatrix} \omega_2\bar{R}_i \\ 0 \\ \omega_2\bar{R}_i \\ 0 \end{Bmatrix} \right) |J|r \right]_{k_t, k_s} \qquad (269)$$

In the axisymmetric prebuckling analysis the terms in eqn (268) contribute to the l.h.s. of eqn (213) and those in eqn (269) contribute to the r.h.s. of eqn (213). Equation (268) represents a contribution to the (i,j)th term of the local stiffness matrix for a single solid element of revolution. The entire local stiffness matrix is obtained by variation of i and j to cover all 16 nodal degrees of freedom associated with that element. The stiffness matrix of the entire solid axisymmetric structural segment is obtained by assembly of other local matrices derived for other solid elements. Equation (269) represents the negative of an analogous contribution to the "loading" vector.

Strain energy: nonsymmetric analysis

Linear nonsymmetric stress analysis

The linear solution can be thought of as the solution obtained after one Newton–Raphson iteration with zero used for the starting vector. Thus, eqn (213) holds and Δq now represents the entire linear solution, not just a correction vector. The strain displacement relations (248) should be linearized. For each circumferential harmonic these relations have the form

$$\overset{6\times 1}{\{\epsilon\}} = \overset{6\times 24}{[B]}\{q\} \quad \begin{Bmatrix} \sin n\theta & \cos n\theta \\ \sin n\theta & \cos n\theta \\ \sin n\theta & \cos n\theta \\ \sin n\theta & or & \cos n\theta \\ \cos n\theta & \sin n\theta \\ \cos n\theta & \sin n\theta \end{Bmatrix} \qquad (270)$$

with $\lfloor\epsilon\rfloor$ given by eqn (228b) without the d's, and

$$\lfloor q\rfloor = \lfloor u_1{}^1, u_2{}^1, u_3{}^1, u_1{}^2, u_2{}^2, u_3{}^2, \ldots u_1{}^8, u_2{}^8, u_3{}^8\rfloor. \qquad (271)$$

Equation (224) becomes

$$\frac{\partial^2 U}{\partial q_i\partial q_j} = \pi \sum_{k_s=1}^{K_s} \Delta s_k \sum_{k_t=1}^{K_t} \Delta t_k [\lfloor B_j\rfloor \overset{6\times 6}{[D]}\{B_i\}|J|r]_{k_t, k_s} \qquad (272)$$

in which the subscripts $[\ ]_{k_t,k_s}$ signify "evaluated at the Gaussian integration station (s_{k_s}, t_{k_t})".

Equation (226) becomes

$$\frac{\partial U}{\partial q_i} = \pi \sum_{k_s=1}^{K_s} \Delta s_k \sum_{k_t=1}^{K_t} \Delta t_k \lfloor \lfloor -\epsilon^T \rfloor [D]\{B_i\}|J|r \rfloor_{k_t,k_s} \quad (273)$$

in which $[D]$ is given by eqn (238). If $n = 0$ the factor π should be replaced by 2π. The 6×24 matrix $[B]$ is given by

$$B(1,3I\text{-}2) = \frac{1}{|J|}\left(a_{22}\frac{\partial h_I}{\partial s} - a_{12}\frac{\partial h_I}{\partial t}\right)$$

$$B(1,3I\text{-}1) = 0 \qquad\qquad\qquad B(1,3I) = 0$$

$$B(2,3I\text{-}2) = 0 \qquad\qquad\qquad B(2,3I\text{-}1) = -nh_I/r$$

$$B(2,3I) = h_I/r$$

$$B(3,3I\text{-}2) = 0 \qquad\qquad\qquad B(3,3I\text{-}1) = 0$$

$$B(3,3I) = \frac{1}{|J|}\left(-a_{21}\frac{\partial h_I}{\partial s} + a_{11}\frac{\partial h_I}{\partial t}\right)$$

$$B(4,3I\text{-}2) = \frac{1}{|J|}\left(-a_{21}\frac{\partial h_I}{\partial s} + a_{11}\frac{\partial h_I}{\partial t}\right)$$

$$(274)$$

$$B(4,3I-1) = 0 \qquad\qquad B(4,3I) = \frac{1}{|J|}\left(a_{22}\frac{\partial h_I}{\partial s} - a_{12}\frac{\partial h_I}{\partial t}\right)$$

$$B(5,3I-2) = nh_I/r \qquad\qquad B(5,3I-1) = \frac{1}{|J|}\left(a_{22}\frac{\partial h_I}{\partial s} - a_{12}\frac{\partial h_I}{\partial t}\right)$$

$$B(6,3I\text{-}2) = 0 \qquad\qquad B(6,3I-1) = \frac{1}{|J|}\left(-a_{21}\frac{\partial h_I}{\partial s} + a_{11}\frac{\partial h_I}{\partial t}\right) - h_I/r$$

$$B(6,3I) = nh_I/r$$

in which $I = 1,2,3,\ldots8$, refers to the local node point number; h_I is given by eqn (251); and a_{11}, a_{12}, a_{21}, a_{22} are given by eqn (258) with use of eqn (247a).

The deformations due to a general nonsymmetric load are calculated by superposition of deformations of the form (250) or, if n is zero or negative, of the form

$$u_1 = u_1(x,r)\cos n\theta; \quad u_2 = u_2(x,r)\sin |n|\theta;$$
$$u_3 = u_3(x,r)\cos n\theta \quad (275)$$

corresponding to each harmonic of the Fourier series representation of the load.

Equation (272) represents the contribution in the nth circumferential harmonic to the (i,j)th term of the local stiffness matrix for a single solid element of revolution. The entire local stiffness matrix is obtained by variation of i and j to cover all 24 nodal degrees of freedom associated with that element. The stiffness matrix for the entire axisymmetric solid region is obtained by assembly of similar local matrices derived for other solid elements in the two-dimensionally discretized structural segment.

Nonsymmetric vibrations and bifurcation buckling

The starting point for this derivation is eqn (224) with eqn (266). The (i,j)th element of the stability or vibration stiffness matrix is given by

$$\left(\frac{\partial^2 U^b}{\partial q_i^b \partial q_j^b}\right)_{q=q_0} = \left(\int_\theta \int_s \int_t \left(\lfloor\sigma_0\rfloor\left\{\frac{\partial^2\epsilon}{\partial q_i^b \partial q_j^b}\right\}\right.\right.$$
$$\left.\left. + \lfloor\partial\epsilon/\partial q_i^b\rfloor [D_{T0}]\left\{\frac{\partial\epsilon}{\partial q_j^b}\right\}\right)|J|r\,ds\,dt\,d\theta\right)_{q=q_0} \quad (276)$$

In the bifurcation buckling and vibration analysis the term $\Delta\epsilon$ in eqn (266) is zero because the stiffness matrix is evaluated at $q = q_0$. Therefore, $\epsilon = \epsilon_0$ in the first term in eqn (266). The six-element vector $\lfloor\sigma_0\rfloor$ is given by

$$\lfloor\sigma_0\rfloor = \lfloor\sigma_{10},\sigma_{20},\sigma_{30},\sigma_{130},\sigma_{120},\sigma_{230}\rfloor \quad (277)$$

in which the first four components are calculated from eqn (267) and the last two components are zero if the axisymmetric prebuckled state is torsionless.

As in the shell analysis (eqn 125) the strain vector can be divided into three parts:

$$\lfloor\epsilon\rfloor = \lfloor\epsilon^{(0)}\rfloor + \lfloor\epsilon^{(1)}\rfloor + \lfloor\epsilon^{(2)}\rfloor \quad (278)$$

where superscripts$^{(i)}$, $i = 0,1,2$ indicate zeroth, first and second order in the infinitesimal buckling or vibration mode $q^b = u_1^b, u_2^b, u_3^b$. The zeroth order represents the axisymmetric prebuckled state. The first and second order terms, derived from eqns (248), are given by

$$\{\epsilon^{(1)}\} = $$

$$\left\{\begin{array}{c} \epsilon_1^{(1)} \\ \epsilon_2^{(1)} \\ \epsilon_3^{(1)} \\ \epsilon_{13}^{(1)} \\ \epsilon_{12}^{(1)} \\ \epsilon_{23}^{(1)} \end{array}\right\} = \left\{\begin{array}{c} \left(\dfrac{\partial u_1^b}{\partial x} + \omega_{20}\omega_2^b\right)\sin n\theta \\[2mm] (u_3^b/r - nu_2^b/r)\sin n\theta \\[2mm] \left(\dfrac{\partial u_3^b}{\partial r} + \omega_{20}\omega_2^b\right)\sin n\theta \\[2mm] \left(\dfrac{\partial u_1^b}{\partial r} + \dfrac{\partial u_3^b}{\partial x}\right)\sin n\theta \\[2mm] \left(nu_1^b/r + \dfrac{\partial u_2^b}{\partial x} - \omega_{20}\omega_1^b\right)\cos n\theta \\[2mm] \left(\dfrac{\partial u_2^b}{\partial r} + (nu_3^b - u_2^b)/r - \omega_{20}\omega_3^b\right)\cos n\theta \end{array}\right\}$$

$$(279)$$

$$\{\epsilon^{(2)}\} = \begin{Bmatrix} \epsilon_1^{(2)} \\ \epsilon_2^{(2)} \\ \epsilon_3^{(2)} \\ \epsilon_{13}^{(2)} \\ \epsilon_{12}^{(2)} \\ \epsilon_{23}^{(2)} \end{Bmatrix} = \begin{Bmatrix} \frac{1}{2}(\omega_2^{b2}\sin^2 n\theta + \omega_3^{b2}\cos^2 n\theta) \\ \frac{1}{2}(\omega_1^{b2} + \omega_3^{b2})\cos^2 n\theta \\ \frac{1}{2}(\omega_1^{b2}\cos^2 n\theta + \omega_2^{b2}\sin^2 n\theta) \\ -\omega_1^b\omega_3^b\cos^2 n\theta \\ -\omega_1^b\omega_2^b\sin n\theta \cos n\theta \\ -\omega_2^b\omega_3^b\sin n\theta \cos n\theta. \end{Bmatrix} \quad (280)$$

Equations (279) and (280) are based on the assumption that

$$u_1^b = u_1^b(x,r)\sin n\theta$$

$$u_2^b = u_2^b(x,r)\cos n\theta \quad (281)$$

$$u_3^b = u_3^b(x,r)\sin n\theta.$$

Two of the prebuckling rotation components ω_{10} and ω_{30} are zero because the prebuckled state is axisymmetric and torsionless. The prebuckling shear terms σ_{120} and σ_{230} are also zero. Hence, the circumferential coordinate θ can be separated from the other independent variables s, t in the usual way, thereby leading to reduction of a three-dimensional phenomenon to a numerically two-dimensional analysis.

It is clear that only $\lfloor\epsilon^{(2)}\rfloor$ will contribute terms to the vector $\lfloor\partial^2\epsilon/\partial q_i^b\partial q_j^b\rfloor$ and only $\lfloor\epsilon^{(1)}\rfloor$ will contribute terms to the vectors $\lfloor\partial\epsilon/\partial q_i^b\rfloor$ and $\lfloor\partial\epsilon/\partial q_j^b\rfloor$. As in the case of the thin shell theory, we can write eqn (279) in the form

$$\{\epsilon^{(1)}\} = (\overset{6\times24}{[B_1]} + \omega_{20}\overset{6\times24}{[B_2]})\{q^b\}\begin{Bmatrix} \sin n\theta \\ \sin n\theta \\ \sin n\theta \\ \sin n\theta \\ \cos n\theta \\ \cos n\theta \end{Bmatrix} \quad (282)$$

in which $[B_1]$ is given by eqns (274) and $\lfloor q^b\rfloor$ is

$$\lfloor q^b\rfloor = \lfloor u_1^{b1}, u_2^{b1}, u_3^{b1}, u_1^{b2}, u_2^{b2}, u_3^{b3}, \ldots u_1^{b8}, u_2^{b8}, u_3^{b8}\rfloor. \quad (283)$$

The matrix $[B_2]$ is derived from eqns (279), (249), (247) and (253):

$$B_2(1,3I-2) = \frac{1}{|J|}\left(-a_{21}\frac{\partial h_I}{\partial s} + a_{11}\frac{\partial h_I}{\partial t}\right) \quad B_2(1,3I-1) = 0$$

$$B_2(1,3I) = \frac{-1}{|J|}\left(a_{22}\frac{\partial h_I}{\partial s} - a_{12}\frac{\partial h_I}{\partial t}\right)$$

$$B_2(2,3I-2) = 0; \quad B_2(2,3I-1) = 0; \quad B_2(2,3I) = 0$$

$$B_2(3,3I-2) = B_2(1,3I-2); \quad B_2(3,3I-1) = 0$$

$$B_2(3,3I) = B_2(1,3I)$$

$$B_2(4,3I-2) = 0; \quad B_2(4,3I-1) = 0 \quad B_2(4,3I) = 0$$

$$B_2(5,3I-2) = 0$$

$$B_2(5,3I-1) = h_I/r + \frac{1}{|J|}\left(-a_{21}\frac{\partial h_I}{\partial s} + a_{11}\frac{\partial h_I}{\partial t}\right)$$

$$B_2(5,3I) = -nh_I/r$$

$$B_2(6,3I-2) = nh_I/r$$

$$B_2(6,3I-1) = \frac{-1}{|J|}\left(a_{22}\frac{\partial h_I}{\partial s} - a_{12}\frac{\partial H_I}{\partial t}\right)$$

$$B_2(6,3I) = 0. \quad (284)$$

After integration over θ in closed form and numerical integation with respect to s and t, we obtain eqn (276) in the form

$$\left(\frac{\partial^2 U^b}{\partial q_i^b\partial q_j^b}\right)_{q=q_0} = \pi\sum_{k_s=1}^{K_s}\Delta s_k\sum_{k_t=1}^{K_t}\Delta t_k$$

$$\times\left[\left(\sigma_{10}\left(\frac{\partial\omega_2^b}{\partial q_i^b}\frac{\partial\omega_2^b}{\partial q_j^b} + \frac{\partial\omega_3^b}{\partial q_i^b}\frac{\partial\omega_3^b}{\partial q_j^b}\right)\right.\right.$$

$$+ \sigma_{20}\left(\frac{\partial\omega_1^b}{\partial q_i^b}\frac{\partial\omega_1^b}{\partial q_j^b} + \frac{\partial\omega_3^b}{\partial q_i^b}\frac{\partial\omega_3^b}{\partial q_j^b}\right)$$

$$+ \sigma_{30}\left(\frac{\partial\omega_1^b}{\partial q_i^b}\frac{\partial\omega_1^b}{\partial q_j^b} + \frac{\partial\omega_2^b}{\partial q_i^b}\frac{\partial\omega_2^b}{\partial q_j^b}\right)$$

$$- \sigma_{130}\left(\frac{\partial\omega_1^b}{\partial q_i^b}\frac{\partial\omega_3^b}{\partial q_j^b} + \frac{\partial\omega_1^b}{\partial q_j^b}\frac{\partial\omega_3^b}{\partial q_i^b}\right)$$

$$+ \lfloor\partial q^b/\partial q_i^b\rfloor[B_1 + \omega_{20}B_2]^T[D_{T0}]$$

$$\left.\left.\times [B_1 + \omega_{20}B_2]\left\{\frac{\partial q^b}{\partial q_j^b}\right\}\right)|J|r\right]_{k_s,k_t}. \quad (285)$$

In eqn (285) ω_1^b, ω_2^b, ω_3^b are given in eqns (249) with superscript $(\ )^b$ added; σ_{10}, σ_{20}, σ_{30}, σ_{130} are the stresses associated with the x, θ, r, xr directions, respectively; $[D_{T0}]$ is the 6×6 constitutive matrix including effects of plasticity (eqn 225); and ω_{20} is the prebuckling rotation component analogous (but with opposite sign) to the meridional rotation β_0 of the shell. Note that eqn (285) is valid only if the terms D_{T015}, D_{T016}, D_{T025}, D_{T026}, D_{T035}, D_{T036}, D_{T045}, D_{T046} in the constitutive coefficient matrix $[D_{T0}]$ are zero. If these terms were nonzero, one would not be able to separate variables as has been done.

The terms in eqn (285) multiplied by σ_{10}, σ_{20}, σ_{30}, and σ_{130} can be expressed in the form

$$\lfloor\partial q^b/\partial q_i^b\rfloor\overset{24\times3}{[R]^T}\overset{3\times3}{[\sigma_0]}\overset{3\times24}{[R]}\left\{\frac{\partial q^b}{\partial q_i}\right\} \quad (286)$$

in which $[\sigma_0]$ is given by

$$\overset{3\times3}{[\sigma_0]} = \begin{bmatrix} (\sigma_{20}+\sigma_{30}) & 0 & -\sigma_{130} \\ 0 & (\sigma_{10}+\sigma_{30}) & 0 \\ -\sigma_{130} & 0 & (\sigma_{10}+\sigma_{20}) \end{bmatrix} \quad (287)$$

and $[\bar{R}]$ occurs in the transformation from the rotation vector

$$\lfloor\omega^b\rfloor = \lfloor\omega_1^b, \omega_2^b, \omega_3^b\rfloor \quad (288)$$

to the nodal degree of freedom vector, $\lfloor q^b \rfloor$:

$$\{\omega\} = [R]\,\{q^b\}. \qquad (289)$$

The matrix $[R]$ can be derived from eqns (249) with use of eqn (253). The derivatives of the nodal degree of freedom vectors $\lfloor \partial q^b/\partial q_j^b \rfloor$ and $\lfloor \partial q^b/\partial q_i^b \rfloor$ are simply

$$\overset{1\times24}{\lfloor \partial q^b/\partial q_j^b \rfloor} = \lfloor 0,0,0,\ldots 0,1,0,0 \quad \rfloor \qquad (290)$$

$$\underset{\substack{\text{corresponds to}\\ \text{d.o.f. number ``}j\text{''}}}{}$$

$$\overset{1\times24}{\lfloor \partial q^b/\partial q_i^b \rfloor} = \lfloor 0,0,\ldots 0,1,0,0,\ldots \rfloor \qquad (291)$$

$$\underset{\substack{\text{corresponds to}\\ \text{d.o.f. number ``}i\text{''}}}{}$$

so that

$$\overset{1\times24}{\lfloor \partial q^b/\partial q_j^b \rfloor}\; \overset{24\times3}{[R]^T} = \overset{1\times3}{\lfloor \bar{R}_j \rfloor}$$

$$\overset{3\times24}{[R]}\, \overset{24\times1}{\left\{\dfrac{\partial q^b}{\partial q_i^b}\right\}} = \overset{3\times1}{\{\bar{R}_i\}}. \qquad (292)$$

Similarly,

$$\overset{1\times24}{\lfloor \partial q^b/\partial q_j^b \rfloor}\; \overset{24\times6}{[B_1 + \omega_{20}B_2]^T} = \overset{1\times6}{\lfloor (B_1 + \omega_{20}B_2)_j \rfloor}$$

$$\overset{6\times24}{[B_1 + \omega_{20}B_2]}\, \overset{24\times1}{\left\{\dfrac{\partial q^b}{\partial q_i^b}\right\}} = \overset{6\times1}{\{(B_1 + \omega_{20}B_2)_i\}}. \qquad (293)$$

Using the expression (286) and eqns (292) and (293) in eqn (285), one obtains

$$\left(\frac{\partial U^b}{\partial q_i^b \partial q_j^b}\right)_{q=q_0} = \pi \sum_{k_s=1}^{K_s} \Delta s_k \sum_{k_t=1}^{K_t} \Delta t_k [(\lfloor \bar{R}_j \rfloor [\sigma_0]\{\bar{R}_i\}$$
$$+ \lfloor (B_1 + \omega_{20}B_2)_j \rfloor\, [D_{T0}]\{(B_1 + \omega_{20}B_2)_i\}) |J|r]_{k_s,k_t}. \qquad (294)$$

In modal vibration analysis eqn (294) represents a contribution to the local tangent stiffness matrix for a solid finite element of revolution that is loaded by stress components σ_{10}, σ_{20}, σ_{30}, σ_{130} and deformed by rotation ω_{20}. In bifurcation buckling analysis the loading is divided into two parts, as described earlier (see eqn 122):

$$p_{nb} = p^f + \lambda\Delta p \qquad (295)$$

and the prebuckling rotation $\Delta\omega_{20}$ associated with the load increment Δp is neglected. Assuming that the "fixed" part p^f gives rise to σ_0^f, ω_{20}^f and the increment Δp gives rise to $\Delta\sigma_0$, $\Delta\omega_{20}$, one can write eqn (294) in the form

$$\left(\frac{\partial^2 U^b}{\partial q_i^b \partial q_j^b}\right)^k = K_{ij}^k = \pi(K_{1ij}^k + \lambda K_{2ij}^k) \qquad (296)$$

in which k denotes finite element number. The (i,j)th

term of the stiffness matrix K_{1ij}^k is given by

$$K_{1ij}^k = \sum_{k_s=1}^{K_s} \Delta s_{k_s} \sum_{k_t=1}^{K_t} \Delta t_{k_t} |J(s_g,t_g)^k| r(s_g,t_g)^k \qquad (297)$$

$$\times (\lfloor (B_1 + \omega_0^f B_2)_j \rfloor\, [D_{T0}]\{(B_1 + \omega_0^f B_2)_i\}$$
$$+ \lfloor \bar{R}_j \rfloor\, [\sigma_0^f]\{\bar{R}_i\})_{s_g,t_g}^k$$

and the (i,j)th term of the load-geometric matrix K_{2ij}^k is given by

$$K_{2ij}^k = \sum_{k_s=1}^{K_s} \Delta s_{k_s} \sum_{k_t=1}^{K_t} \Delta t_{k_t} |J(s_g,t_g)^k| r(s_g,t_g)^k \qquad (298)$$

$$\times (\lfloor \bar{R}_j \rfloor\, [\Delta\sigma_0]\{\bar{R}_i\})_{s_g,t_g}^k$$

where superscript k indicates finite element number and s_g, t_g indicate the (s, t) coordinates of the Gaussian integration point. One can readily see the analogy between eqn (297) and (298) for the two-dimensionally discretized solid of revolution with eqns (136) and eqn (137) for the thin shell. The local stiffness and load-geometric matrices for the isoparametric quadrilateral 8-node elements of revolution are dimensioned 24×24, whereas those for finite-difference shell element are dimensioned 7×7.

Kinetic energy

The kinetic energy in eqn (209) has the general form

$$T = \frac{1}{2}\int_V m\dot{\bar{u}}^2\,dV \qquad (299)$$

in which m is the mass density and the total displacement vector $\bar{u}$ is the sum of the axisymmetric prestressed state $\bar{u}_0$ and the infinitesimal vibration mode $\bar{u}^b$:

$$\bar{u} = \bar{u}_0 + \bar{u}^b(x,r)\begin{pmatrix}\sin n\theta\\ \text{or}\\ \cos n\theta\end{pmatrix}e^{i\Omega t}. \qquad (300)$$

Since the prestressed state is static,

$$\dot{\bar{u}} = i\Omega\bar{u}^b(x,r)\begin{pmatrix}\sin n\theta\\ \text{or}\\ \cos n\theta\end{pmatrix}e^{i\Omega t}. \qquad (301)$$

For the calculation of vibration modes and frequencies one needs the matrix $[\partial^2 T/\partial q_i^b \partial q_j^b]$; $i,j=1,2,3,\ldots N$, where N is the number of degrees of freedom in the vibration problem. Recalling that $\bar{u}^b$ is a linear function of the nodal degrees of freedom q^b, one can write

$$\frac{\partial^2 T}{\partial q_i^b \partial q_j^b} = -\Omega^2\int_V m\frac{\partial \bar{u}^b}{\partial q_i}\cdot\frac{\partial \bar{u}^b}{\partial q_j}\begin{pmatrix}\sin^2 n\theta\\ \text{or}\\ \cos^2 n\theta\end{pmatrix}dV \qquad (302)$$

The displacement field in the quadrilateral isoparametric finite element is given by eqn (247b). Therefore, eqn (302) can be written in the form

$$\frac{\partial^2 T}{\partial q_i \partial q_j} = -\Omega^2\pi\int_s\int_t mh_i(s,t)h_j(s,t)|J|r\,ds\,dt. \qquad (303)$$

The integrals in eqn (303) are evaluated by Gaussian quadrature. The local mass matrix is dimensioned 24×24.

Body forces

The term in the energy functional (209) related to body forces is

$$\int_V \bar{F}_b \cdot \delta \bar{u} \, dV = \int_V \bar{F}_b \cdot \frac{\partial \bar{u}}{\partial q} \, dV \delta q. \qquad (304)$$

If the displacement vector $\bar{u}$ is a linear function of the nodal point degrees of freedom q, the body force term generates contributions only to the first variation ψ_i of the energy functional. It is assumed here that body forces are due to rigid body accelerations of the center of mass, angular accelerations about the center of mass, and angular rotation about the axis of revolution. Figure 47 shows a body of revolution with components of translational acceleration a_x, a_y, a_z and rotational acceleration $\dot{\omega}_x$, $\dot{\omega}_y$, $\dot{\omega}_z$. In order to transform eqn (304) into a form suitable for programming, one must have the local components of acceleration g_1, g_2, g_3 corresponding to u_1, u_2, u_3 at a point at a radius r from the axis of revolution and a distance d from the yz plane in which the center of mass is located. These components, in terms of a_x, a_y, a_z, ω_x, $\dot{\omega}_x$, $\dot{\omega}_y$, $\dot{\omega}_z$, are

$$g_1 = -a_x + r(\dot{\omega}_z \sin \theta - \dot{\omega}_y \cos \theta)$$

$$g_2 = r\dot{\omega}_x + (a_z - d\dot{\omega}_y) \sin \theta - (a_y + d\dot{\omega}_z) \cos \theta \quad (305)$$

$$g_3 = r\omega_x^2 - (a_y + d\dot{\omega}_z) \sin \theta - (a_z - d\dot{\omega}_y) \cos \theta$$

Equation (304) can be written in the form

$$\int_V \bar{F}_b \cdot \delta \bar{u} \, dV = \int_V (mg_1 \delta u_1 + mg_2 \delta u_2 + mg_3 \delta u_3) \, dV. \qquad (306)$$
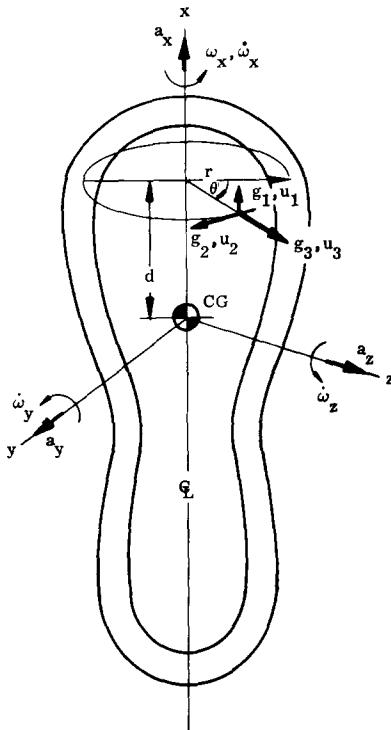
Fig. 47. Local accelerations g_1, g_2, g_3 due to rigid body translational (a_x, a_y, a_z) and angular $(\dot{\omega}_x, \dot{\omega}_y, \dot{\omega}_z)$ accelerations and angular velocity ω_x of and about the center of mass.

Since u_1, u_2, u_3 are functions of the nodal degrees of freedom q, eqn (306) can be written in the form

$$\int_V \bar{F}_b \cdot \frac{\partial \bar{u}}{\partial q} \, dV = \int_V m\left(g_1 \frac{\partial u_1}{\partial q} + g_2 \frac{\partial u_2}{\partial q} + g_3 \frac{\partial u_3}{\partial q}\right) dV \qquad (307)$$

after cancellation of δq.

In general the displacement field u_1, u_2, u_3 can be expanded in the trigonometric series as in eqn (219). Because g_1, g_2, g_3 contain only terms independent of θ and terms which vary as $\sin \theta$ and $\cos \theta$, only the terms in eqns (219) with $n = 0$ or $n = \pm 1$ contribute to eqn (307). After performing the integration with respect to θ, one obtains for the r.h.s. of eqn (307)

For $n = 0$:

$$2\pi \int_x \int_r m\left(-a_x \frac{\partial u_1^{(0)}}{\partial q} + r\dot{\omega}_x \frac{\partial u_2^{(0)}}{\partial q} + r\omega_x^2 \frac{\partial u_3^{(0)}}{\partial q}\right) r \, dx \, dr. \qquad (308)$$

For $n = +1$:

$$\pi \int_x \int_r m\left[r\dot{\omega}_z \frac{\partial u_1^{(1)}}{\partial q} - (a_y + d\dot{\omega}_z)\left(\frac{\partial u_2^{(1)}}{\partial q} + \frac{\partial u_3^{(1)}}{\partial q}\right)\right] r \, dx \, dr. \qquad (309)$$

For $n = -1$:

$$\pi \int_x \int_r m\left[-r\dot{\omega}_y \frac{\partial u_1^{(-1)}}{\partial q} + (a_z - d\dot{\omega}_y)\left(\frac{\partial u_2^{(-1)}}{\partial q} - \frac{\partial u_3^{(-1)}}{\partial q}\right)\right] r \, dx \, dr \qquad (310)$$

Thin shell segment body forces. The displacement components u_1, u_2, u_3 are assumed to be constant through the thickness. In terms of u, v, w (Fig. 44a), u_1, u_2, u_3 are

$$u_1 = u(r/R_2) - wr'; \quad u_2 = v \qquad (311)$$

$$u_3 = ur' + w(r/R_2).$$

Furthermore u, v, w can be written in terms of the nodal displacement quantities

$$\lfloor q \rfloor = \lfloor w_{i-1}, u_i, v_i, w_i, u_{i+1}, v_{i+1}, w_{i+1} \rfloor \qquad (312)$$

by means of eqns (114). The double integration indicated in Expressions (308)–(310) is replaced by single integration along the shell meridian, and the quantity m is interpreted as the mass per area of shell reference surface.

Solid of revolution body forces. The displacement components u_1, u_2, u_3 are written in terms of the nodal degrees of freedom by eqn (247b). If the r.h.s. of eqn (247) is used in eqns (308)–(310) and the (x, r) integration is transformed into (s, t) integration according to eqn (255), the contributions of the body forces to the loading vector of the discretized problem are obtained.

Surface tractions on solid of revolution

The term in the energy functional (209) related to constant-directional surface traction is

$$\int_{\text{Area}} \bar{F}_s \cdot \delta \bar{u} \, dA \quad \text{or} \quad \int_A \bar{F}_s \cdot \frac{\partial \bar{u}}{\partial q} \, dA \delta q. \qquad (313)$$

As with body forces, this term generates only contributions to Ψ_i.

The three components of external surface load p_t, p_c, p_n, acting on a solid region (one element in this example) are shown in Fig. 48. These positive values form a right-handed system.

The work done by the surface tractions acting over an elemental length dl (shown in Fig. 48) is

$$dW = (p_t dlu_t + p_c dlu_2 + p_n dlu_n)\, rd\theta \qquad (314)$$

in which the normal and tangential displacement components u_n and u_t are given by

$$u_n = -u_1\frac{dr}{dl} + u_3\frac{dx}{dl}$$

$$u_t = u_1\frac{dx}{dl} + u_3\frac{dr}{dl}. \qquad (315)$$

The elemental work done is therefore

$$dW = [p_t(u_1 dx + u_3 dr) + p_c dlu_2 + p_n(-u_1 dr + u_3 dx)]\, rd\theta \qquad (316)$$

The variables that appear in eqn (316) can be written in terms of the local coordinates (s, t) of the element by means of eqns (247) and the relationships

$$dr = \frac{\partial r}{\partial s}ds + \frac{\partial r}{\partial t}dt; \quad dx = \frac{\partial x}{\partial s}ds + \frac{\partial x}{\partial t}dt. \qquad (317)$$

The finite element depicted in Fig. 48 has four faces, labeled ①, ②, ③, ④. On each of the faces the work done by the surface tractions can be shown to be given by:

On Face ①: s = + 1.0, t varies

$$W① = \pi \sum_{k=1}^{K_t} r_k \Delta t_k \left[\sum_{i=1}^{8} h_i(+1, t_k)\{-p_t(u_1{}^i x_{,t} + u_3{}^i r_{,t}) \right.$$
$$\left. + p_c u_2{}^i (r_{,t}{}^2 + x_{,t}{}^2)^{1/2} + p_n(u_1{}^i r_{,t} - u_3{}^i x_{,t})\}_k \right]. \qquad (318)$$

On Face ②: s varies, t = − 1.0

$$W② = \pi \sum_{k=1}^{K_s} r_k \Delta s_k \left[\sum_{i=1}^{8} h_i(s_k, -1)\{-p_t(u_1{}^i x_{,s} + u_3{}^i r_{,s}) \right.$$
$$\left. + p_c u_2{}^i (r_{,s}{}^2 + x_{,s}{}^2)^{1/2} + p_n(u_1{}^i r_{,s} - u_3{}^i x_{,s})\}_k \right]. \qquad (319)$$

On Face ③: s = − 1.0, t varies

$$W③ = \pi \sum_{k=1}^{K_t} r_k \Delta t_k \left[\sum_{i=1}^{8} h_i(-1, t_k)\{p_t(u_1{}^i x_{,t} + u_3{}^i r_{,t}) \right.$$
$$\left. + p_c u_2{}^i (r_{,t}{}^2 + x_{,t}{}^2)^{1/2} + p_n(-u_1{}^i r_{,t} + u_3{}^i x_{,t})\}_k \right]. \qquad (320)$$

On Face ④: s varies, t = + 1.0

$$W④ = \pi \sum_{k=1}^{K_s} r_k \Delta s_k \left[\sum_{i=1}^{8} h_i(s_k, +1)\{p_t(u_1{}^i x_{,s} + u_3{}^i r_{,s}) \right.$$
$$\left. + p_c u_2{}^i (r_{,s}{}^2 + x_{,s}{}^2)^{1/2} + p_n(-u_1{}^i r_{,s} + u_3{}^i x_{,s})\}_k \right]. \qquad (321)$$
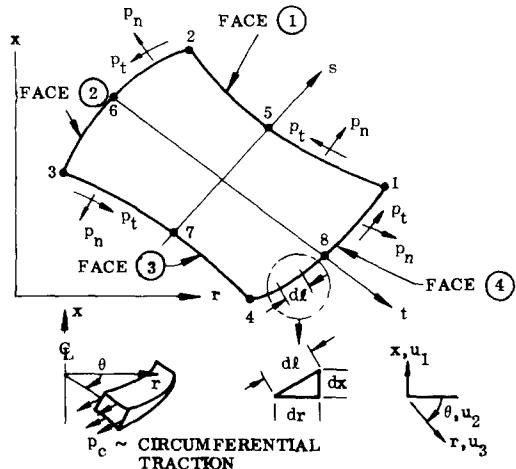
Fig. 48. Surface tractions on isoparametric quadrilateral finite element of revolution. p_t, p_c, p_n form a right-handed system.

In eqns (318)–(321) the factor π arises from integration of $\cos^2 n\theta$ or $\sin^2 n\theta$ from 0 to 2π. If $n = 0$ this factor should be 2π. The quantities Δt_k and Δs_k are the Gaussian integration weights and K_s, K_t are the numbers of integration points in the s and t directions, respectively. Subscript k here denotes a quantity evaluated at the kth Gaussian integration station. Subscripts $(\ )_{,s}$ and $(\ )_{,t}$ denote differentiation with respect to the local element coordinates s and t.

The contributions to the loading vector are obtained from eqns (318)–(321) by differentiation of $W①$ through $W④$ with respect to the nodal degrees of freedom.

Of course, in a solid region consisting of many finite elements, only those elements with faces exposed to external surface loads yield contributions to the global loading vector.

Following pressure for solid of revolution

The relevant term in the energy functional (209) is

$$\delta W' = -\int_{\text{Area}} \bar{F}_s' \cdot \delta[f(\bar{u})]\, dA. \qquad (322)$$

The term arises from the fact that the direction of the pressure may change as the structure deforms. As derived in the discussion associated with eqns (169)–(171), the so-called "live-load" terms in the energy functional are quadratic; they contribute to the stiffness and load-geometric matrices.

The expressions for each face of the isoparametric quadrilateral can be derived from the nonlinear terms in eqn (169) with $1/R_1 = 0$, with the meridional arc length element ds replaced by dl (see Fig. 48), and with use of the transformations (315), (247), and (317). For any of the four faces it can be shown that after integration with respect to θ, W' is given by

$$W' = \frac{\pi}{2}\int_{\text{face}} \left[p_n(x_{,s}\, ds + x_{,t}\, dt)\left(-u_1\frac{dr}{dl} + u_3\frac{dx}{dl}\right)^2 \right.$$
$$- p_n(x_{,s}\, ds + x_{,t}\, dt)u_2{}^2 - 2(p_{n,s}\, ds + p_{n,t}\, dt)r$$
$$\left. \times \left(u_1\frac{dx}{dl} + u_3\frac{dr}{dl}\right)\left(-u_1\frac{dr}{dl} + u_3\frac{dx}{dl}\right) \right]. \qquad (323)$$

Differentiating with respect to the nodal degrees of freedom q_i and q_j, one obtains

$$\frac{\partial^2 W'}{\partial q_i \partial q_j} = \pi \int_{\text{face}} \left\{ p_n(x_{,s} \, ds + x_{,t} \, dt) \left(-\frac{\partial u_1}{\partial q_i}\frac{dr}{dl} + \frac{\partial u_3}{\partial q_i}\frac{dx}{dl} \right) \right.$$

$$\times \left(-\frac{\partial u_1}{\partial q_j}\frac{dr}{dl} + \frac{\partial u_3}{\partial q_j}\frac{dx}{dl} \right) - p_n(x_{,s} \, ds + x_{,t} \, dt)\frac{\partial u_2}{\partial q_i}\frac{\partial u_2}{\partial q_j}$$

$$- (p_{n,s} \, ds + p_{n,t} \, dt)r\left[\left(\frac{\partial u_1}{\partial q_i}\frac{dx}{dl} + \frac{\partial u_3}{\partial q_i}\frac{dr}{dl}\right)\right.$$

$$\times \left(-\frac{\partial u_1}{\partial q_j}\frac{dr}{dl} + \frac{\partial u_3}{\partial q_j}\frac{dx}{dl} \right) + \left(\frac{\partial u_1}{\partial q_j}\frac{dx}{dl} + \frac{\partial u_3}{\partial q_j}\frac{dr}{dl}\right)$$

$$\left. \times \left(-\frac{\partial u_1}{\partial q_i}\frac{dr}{dl} + \frac{\partial u_3}{\partial q_i}\frac{dx}{dl} \right)\right]\right\}. \tag{324}$$

In analogy with eqns (318)–(221), the following conditions prevail on the four faces of the quadrilateral element:

On Face ①: $s = +1.0$, $ds = 0$, t varies, dt is negative

$$dr/dl = -r_{,t}/(r_{,t}^2 + x_{,t}^2)^{1/2}; \quad dx/dl = -x_{,t}/(r_{,t}^2 + x_{,t}^2)^{1/2}$$

On Face ②: s varies, ds is negative, $t = -1.0$, $dt = 0$

$$dr/dl = -r_{,s}/(r_{,s}^2 + x_{,s}^2)^{1/2}; \quad dx/dl = -x_{,s}/(r_{,s}^2 + x_{,s}^2)^{1/2}$$

On Face ③: $s = -1.0$, $ds = 0$, t varies, dt is positive

$$dr/dl = +r_{,t}^2/(r_{,t}^2 + x_{,t}^2)^{1/2}; \quad dx/dl = x_{,t}/(r_{,t}^2 + x_{,t}^2)^{1/2}$$

On Face ④: s varies, ds is positive, $t = +1.0$, $dt = 0$

$$dr/dl = +r_{,s}/(r_{,s}^2 + x_{,x}^2)^{1/2}; \quad dx/dl = +x_{,s}/(r_{,s}^2 + x_{,s}^2)^{1/2}.$$

The derivatives $\partial u/\partial q$ and $r_{,s}$, $r_{,t}$, $x_{,s}$, $x_{,t}$ can be obtained from eqns (247). The integration in eqn (324) is carried out by Gaussian quadrature as with eqns (318)–(321).

Constraint conditions for junctions between thin shells and two-dimensionally discretized regions

The relevant terms in the energy functional (209) are

$$\delta U_c = \sum_{l=1}^{m} \delta \lambda_l \left(\sum_{k=1}^{n_c} a_{lk} u_k + a_{l0} \right) + \sum_{l=1}^{m} \lambda_l \left(\sum_{k=1}^{n_c} a_{lk} \delta u_k \right). \tag{325}$$

These terms contribute to ψ_i (eqn 212) and $\partial \psi_i/\partial q_i$ (eqn 214):

$$\psi_{ic} = \sum_{l=1}^{m} \frac{\partial \lambda_l}{\partial q_i} \left(\sum_{k=1}^{n_c} a_{lk} u_k + a_{l0} \right) + \sum_{l=1}^{m} \lambda_l \left(\sum_{k=1}^{n_c} a_{lk} \frac{\partial u_k}{\partial q_i} \right) \tag{326}$$

$$\frac{\partial \Psi_{ic}}{\partial q_j} = \sum_{l=1}^{m} \frac{\partial \lambda_l}{\partial q_i} \sum_{k=1}^{n_c} a_{lk} \frac{\partial u_k}{\partial q_j} + \sum_{l=1}^{m} \frac{\partial \lambda_l}{\partial q_j} \sum_{k=1}^{n_c} a_{lk} \frac{\partial u_k}{\partial q_i}. \tag{327}$$

Figure 49 shows a junction AB between a thin shell segment and a two-dimensionally discretized region. At the junction u^*, v, w^*, and β at the end of the shell reference surface must be equal to $u_1(s_j, t_j)$, $u_2(s_j, t_j)$, $u_3(s_j, t_j)$ in the "solid" region and a rotation derived from the differences of u_n. (Subscript "n" denotes "normal to the junction line AB" and superscript "i" denotes "ith nodal point on the junction line AB".) The coordinates s_j and t_j coincide with the end of the thin shell reference surface on the line AB. In addition, all nodal points
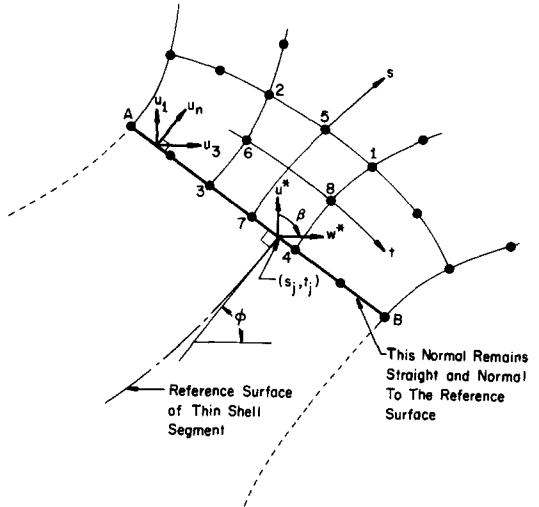
Fig. 49. Junction between thin shell segment and two-dimensional finite element region (from Bushnell[35]).

lying along the junction line AB must be constrained to remain on a straight line normal to the shell reference surface as the structure deforms. This is accomplished by imposition of appropriate constraints on differences of u_n for compatibility and uniformity of the meridional rotation β of AB and constraints on differences of u_2 for compatibility and uniformity of the rotation ψ of AB about an axis through s_j, t_j parallel to the meridional direction of the shell reference surface. The length of AB is free to change, of course, since there should not be any constraint preventing strain normal to the plane of the thin shell reference surface. Thus, typical constraint conditions at a junction line AB are:

$$u^* = u_1(s_j, t_j); \quad v = u_2(s_j, t_j); \quad w^* = u_3(s_j, t_j)$$

$$\beta = (u_n^7 - u_n^4)/L_{74}; \quad \psi = \pm (u_2^4 - u_2^7)/L_{74}$$

$$\beta = (u_n^3 - u_n^4)/L_{34}; \quad \psi = \pm (u_2^4 - u_2^3)/L_{34} \tag{328}$$

$$\vdots \qquad \vdots \qquad \vdots \qquad \vdots$$

$$\beta = (u_n^i - u_n^4)/L_{i4}; \quad \psi = \pm (u_2^4 - u_2^i)/L_{i4}$$

in which

$$u_n^i = u_1^i \sin\phi + u_3^i \cos\phi$$

$$L_{ij} = [(x_i - x_j)^2 + (r_i - r_j)^2]^{1/2}$$

$$\beta = w' - u/R_1 \left.\right\} \quad \text{Shell wall}$$
$$\left.\right\} \quad \text{rotations at}$$
$$\psi = (1/r)\partial w/\partial\theta - v/R_2 \left.\right\} \quad (s_j, t_j) \tag{329}$$

and superscript i denotes any node on the junction line AB. For each such junction, therefore, there are $3 + 2(k-1)$ constraint conditions, where k is the number of nodal points on the junction line AB. The sign for ψ in eqns (328) as well as the nodal indices in all of the equations depend on which end of the shell segment and which faces of the two-dimensional finite element are involved in the junction.

SECTION 5

LINEAR EQUATIONS FOR GENERAL SHELLS

The purpose of this section is to summarize certain aspects of the more widely used linear shell theories, to explain where the differences originate, and to comment on the significance of these differences to the engineer or designer of shell structures. Much of the material here is abstracted from Leissa's excellent survey given in chapter 1 of his monograph *Vibration of Shells* [56].

INTRODUCTION

Whereas in thin plate theory the differential equation of motion is universally agreed upon, the same cannot be said for thin shell theory. Differences arise from different simplifying approximations and different points in a derivation where a given approximation is introduced. The more commonly referred to shell theories are those by Donnell[57,58], Mushtari[59,60], Love[61,62], Timoshenko[63], Reissner[64], Naghdi and Berry[65], Vlasov[66,67], Sanders[68], Byrne[69], Flügge[70,71], Goldenveizer[72], Lur'ye[73], and Novoshilov[74]. All of these theories result from Love's "first approximation" and apply to shells of arbitrary curvature. For comparisons of various thin shell theories the reader is referred to the work of Leissa[56], Koiter[75], Goldenveizer[76], Klosner and Levine[77], Naghdi and Berry[65], Kraus[78], Naghdi[79], and Kalnins[80].

CONCEPTS FROM THE THEORY OF SURFACES NEEDED FOR SHELL THEORY

The essential feature of thin shell theory is the complete characterization of stress and deformation throughout the three-dimensional domain of the shell wall by knowledge of the deformation of a reference surface. The expressions for stress and deformation throughout the domain therefore depend on parameters of this surface, such as its original shape and the extent to which it has been stretched and bent.

Surface coordinates

In order to measure deformations of a surface, we must attach a two-dimensional coordinate system to it. Figure 50 shows such a coordinate system and its relationship to a three-dimensional system fixed in space. Any point on the undeformed surface may be located by a vector

$$\bar{r} = \bar{r}(\alpha, \beta) \qquad (330)$$

in which α and β are independent coordinates of the surface. A system of unit vectors $\bar{i}_\alpha$, $\bar{i}_\beta$, $\bar{i}_n$ parallel and normal to lines of constant $\beta = \beta_0$ and constant $\alpha = \alpha_0$ is depicted in Fig. 50. These so-called "base" vectors are given by

$$\bar{i}_\alpha = \bar{r}_{,\alpha}/A, \quad \bar{i}_\beta = \bar{r}_{,\beta}/B; \quad \bar{i}_n = (\bar{i}_\alpha \times \bar{i}_\beta)/\sin\gamma \qquad (331)$$

in which $(\ )_{,\alpha}$ and $(\ )_{,\beta}$ indicate differentiation with respect to α and β; $A \equiv |\bar{r}_{,\alpha}|$; $B \equiv |\bar{r}_{,\beta}|$; and γ is the angle between the surface coordinate lines.

First fundamental form

Three of the surface parameters needed for characterization of surface deformations are the three coefficients of the first fundamental quadratic form,
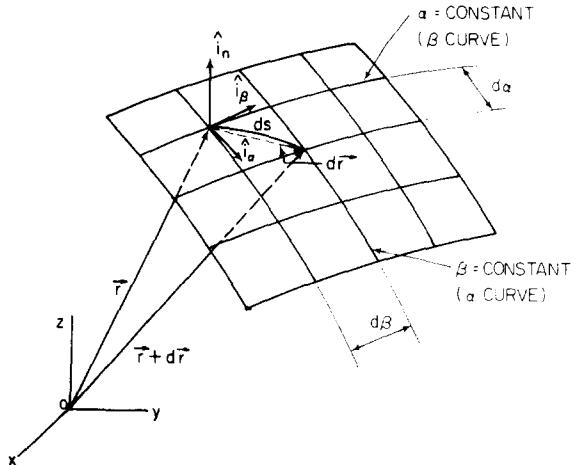
Fig. 50. Middle surface coordinates (from Leissa[56]).

which is derived from the square of the length of an infinitesimal arc

$$d\bar{r} = \bar{r}_{,\alpha}d\alpha + \bar{r}_{,\beta}d\beta = d\bar{s} \qquad (332)$$

lying in the surface. The square of $d\bar{r}$ is a scalar quantity obtained from the dot product $d\bar{r} \cdot d\bar{r}$:

$$d\bar{r} \cdot d\bar{r} = ds^2 = A^2 \, d\alpha^2 + 2AB \cos\gamma \, d\alpha d\beta + B^2 \, d\beta^2. \quad (333)$$

The three coefficients of the first quadratic form (333) are essential, for example, in the derivation of strain due to stretching of the surface. The engineering strain components expressed in terms of surface coordinates are found by comparing ds^2 for the undeformed surface with ds^{*2} for the deformed surface, with the location of the deformed surface $\bar{r}^* = \bar{r}^*(\alpha, \beta)$ being expressed in terms of that of the undeformed surface $\bar{r}$ plus displacement components u, v, w in the directions of the base vectors $\bar{i}_\alpha$, $\bar{i}_\beta$, $\bar{i}_n$:

$$\bar{r}^* = \bar{r} + u\bar{i}_\alpha + v\bar{i}_\beta + w\bar{i}_n. \qquad (334)$$

It can be shown [74] that for orthogonal coordinate lines these reference surface strains are given for linear theory by

$$e_\alpha = \frac{1}{A}\frac{\partial u}{\partial\alpha} + \frac{v}{AB}\frac{\partial A}{\partial\beta} + \frac{w}{R_\alpha}$$

$$e_\beta = \frac{u}{AB}\frac{\partial B}{\partial\alpha} + \frac{1}{B}\frac{\partial v}{\partial\beta} + \frac{w}{R_\beta} \qquad (335)$$

$$e_{\alpha\beta} = \frac{A}{B}\frac{\partial}{\partial\beta}\left(\frac{u}{A}\right) + \frac{B}{A}\frac{\partial}{\partial\alpha}\left(\frac{v}{B}\right)$$

in which e_α and e_β are the strains in the $\bar{i}_\alpha$ and $\bar{i}_\beta$ directions, respectively, and $e_{\alpha\beta}$ is the in-plane shearing strain, a measure of the change in angle between the α and β coordinate lines. All shell theoreticians agree on eqns (335).

There are differences of opinion, however, as to the expressions for the change in curvature and twist of the reference surface as it deforms. A derivation of these expressions requires what is called the second fundamental form.

Second fundamental form

The second fundamental form has to do with the curvature and torsion of the surface coordinate lines. Leissa[56] presents a derivation of an expression for the normal curvature $1/R$ of any line element lying in the reference surface

$$\frac{1}{R} = -\frac{Ld\alpha^2 + 2Md\alpha d\beta + Nd\beta^2}{A^2 d\alpha^2 + 2AB \cos \gamma d\alpha d\beta + B^2 d\beta^2} \quad (336)$$

in which the numerator on the r.h.s. is the second fundamental form with coefficients L, M, and N given by the dot products

$$L = \vec{r}_{,\alpha\alpha} \cdot \vec{i}_n; \quad M = \vec{r}_{,\alpha\beta} \cdot \vec{i}_n; \quad N = \vec{r}_{,\beta\beta} \cdot \vec{i}_n. \quad (337)$$

The normal curvatures of the α curves and β curves are obtained by setting either $d\beta$ or $d\alpha$ in eqn (336) equal to zero:

$$\frac{1}{R_\alpha} = -L/A^2; \quad \frac{1}{R_\beta} = -N/B^2. \quad (338)$$

By "normal curvature" is meant the curvature of the line formed by intersection of the surface with a plane normal to it at the point (α, β).

In the comparisons of shell theories given by Leissa[56] it is assumed that the α and β coordinate lines are lines of principal curvature of the undeformed surface, that is, they are characterized by $\cos \gamma = 0$ and $M = 0$.

A shell: a surface with finite thickness

The shell theories developed in Refs.[57–74] are formulated considering an element such as shown in Fig. 51. An infinitesimal slice of thickness dz located a constant distance z above the reference surface has the following geometrical properties:

Lengths of Edges:
$$ds_\alpha^{(z)} = A(1 + z/R_\alpha)d\alpha$$
$$ds_\beta^{(z)} = B(1 + z/R_\beta)d\beta. \quad (339)$$

Areas of Edge Faces:
$$dA_\alpha^{(z)} = ds_\alpha^{(z)}dz; \quad dA_\beta^{(z)} = ds_\beta^{(z)}dz \quad (340)$$

Volume:
$$dV^{(z)} = AB(1 + z/R_\alpha)(1 + z/R_\beta)\,d\alpha d\beta dz. \quad (341)$$

Inclusion or neglect of the terms z/R_α and z/R_β in eqns (339)–(341) gives rise to many of the differences in the various shell theories. Differences also arise between two theories both of which include these z/R effects initially but which use different simplifications involving neglect of z/R compared to unity later in their derivations.

LOVE'S FIRST APPROXIMATION

Love[61] made the following approximations in his classical linear theory of thin shells:

(1) The thickness of the shell is small compared with the smallest radius of curvature of its reference surface.

(2) Strains and displacements are small. Hence second-order terms in the strain-displacement relations may be neglected in comparison with first-order terms.
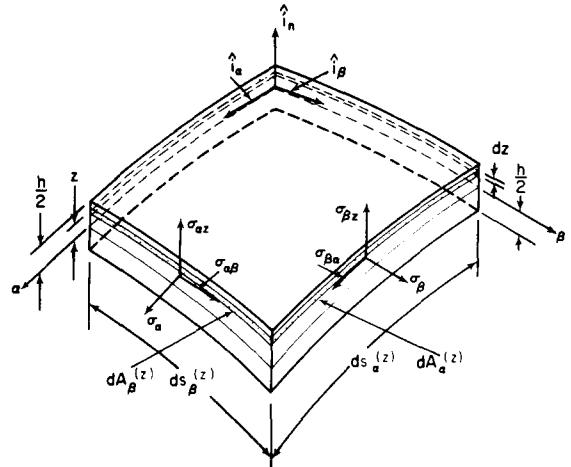

Fig. 51. Notation and positive directions of stress in shell coordinates (from Leissa[56]).

(3) The transverse normal stress is small compared with the other normal stress components and may be neglected.

(4) Normals to the undeformed middle surface remain straight and normal to the deformed middle surface and do not change in length.

These four assumptions constitute what Love called his "first approximation" shell theory. The approximations are almost universally accepted in the derivation of linear thin shell theories.

The first assumption gives the *raison d'être* for a discipline called "shell theory"; the second justifies linearization of the theory; the third restricts applications of shell theory to situations in which rates of change of phenomena and geometry with respect to surface coordinates α and β have characteristic lengths that are large compared to the shell thickness; the fourth permits the reduction of a fundamentally three-dimensional problem to one or two dimensions and is equivalent to neglect of transverse shearing strains. The fourth assumption, known as Kirchhoff's hypothesis, restricts the applications of shell theory in the same way as the third.

Several authors, including Leissa[56] point out the inconsistencies in the four assumptions with Hooke's law. For example, if the normal literally could not change in length at all, then for an isotropic material a considerable normal stress $\sigma_n = \nu(\sigma_\alpha + \sigma_\beta)$ would be generated by uniform biaxial stretching of a plate. This normal stress, arising from the Poisson effect, would not be negligible compared to the in-plane stress. Conversely, if the normal stress is small and the in-plane stress is not, then the normal must change length. Similarly, from Hooke's law, the Kirchhoff postulate implies zero transverse shear stress. However, the shell element cannot in general remain in equilibrium without transverse shear force resultants (which are the integrals of the transverse shear stresses over the wall thickness) acting along its edges.

These inconsistencies do not, of course, seriously diminish the value of shell theory as an engineering tool. Emphasis on them represents an unfair misinterpretation of the mathematical model. The inconsistencies can be deemphasized by introduction of the following two approximations to replace the third and fourth above:

(3a) The work done by the maximum normal stresses

acting through a distance equal to the maximum change in length of the normal and the work done by the maximum transverse shear stress acting through a distance equal to the maximum transverse shear strain times the thickness are negligible compared to the total change in strain energy during deformation.

(4) The displacements in planes parallel to the reference surface may be calculated *as if* the normal to the undeformed reference surface remains straight and normal and unextended during deformation of this surface.

The apparent inconsistencies can also be de-emphasized (as they deserve to be—at least by engineers) by introduction of a corollary rule stating that the average normal stresses and transverse shear stress resultants must be calculated from considerations of equilibrium rather than directly from the kinematics embodied in the Kirchhoff hypothesis.

As a result of the Kirchhoff hypothesis, the displacements U, V, W anywhere along the normal to the reference surface can be calculated from

$$U(\alpha,\beta,z) = u(\alpha,\beta) + z\theta_\alpha(\alpha,\beta)$$

$$V(\alpha,\beta,z) = v(\alpha,\beta) + z\theta_\beta(\alpha,\beta) \qquad (342)$$

$$W(\alpha,\beta,z) = w(\alpha,\beta)$$

in which Leissa[56] gives

$$\theta_\alpha = \frac{u}{R_\alpha} - \frac{1}{A}w_{,\alpha}; \qquad \theta_\beta = \frac{v}{R_\beta} - \frac{1}{B}w_{,\beta}. \qquad (343)$$

Differences in the kinematic relations for reference surface deformation

As stated above, all shell theoreticians agree on the expressions (335) for the strains of the reference surface. However, there are differences in the various theories for change in curvature κ_α, κ_β and twist $\kappa_{\alpha\beta}$. These expressions are listed in Tables 5 and 6.

Change in curvature κ_α, κ_β. Except for the expressions by Donnell and Mushtari, there is general agreement among the various theories concerning curvature changes κ_α and κ_β. The expressions of Vlasov in Table 5 differ from those of Byrne, Flügge, Goldenveizer, etc. only in terms of order e_α/R_α, e_β/R_β, this small difference arising from replacement of $1/(1 + z/R_\alpha)$ and $1/(1 + z/R_\beta)$ by their series expansions.

The Donnell–Mushtari expressions differ in a more fundamental way from the others in that they are obtained by neglect of terms containing tangential displacements u and v. A simple example will show that for certain commonly occurring cases of great engineering significance the Donnell–Mushtari expressions are not sufficiently accurate. Suppose that we consider inextensional deformations of an infinitely long cylindrical shell of radius R. For a cylinder the surface coordinate α can be identified with the axial coordinate x and the surface coordinate β with the circumferential coordinate θ. Then

$$A = |\bar{r}_{,\alpha}| = |\bar{r}_{,x}| = 1.0; \qquad B = |\bar{r}_{,\beta}| = |\bar{r}_{,\theta}| = R. \qquad (344)$$
$$R_\alpha = \infty; \qquad R_\beta = R$$

The displacement components, u, v, w are the axial, circumferential, and normal (outward) displacements of a

Table 5. Change in curvature of the middle surface

Theory	κ_α	κ_β
Byrne, Flügge, Goldenveizer, Lur'ye, Novozhilov, Love, Timoshenko, Reissner, Naghdi, Berry, Sanders	$\dfrac{1}{A}\dfrac{\partial\theta_\alpha}{\partial\alpha} + \dfrac{\theta_\beta}{AB}\dfrac{\partial A}{\partial\beta}$	$\dfrac{1}{B}\dfrac{\partial\theta_\beta}{\partial\beta} + \dfrac{\theta_\alpha}{AB}\dfrac{\partial B}{\partial\alpha}$
Vlasov[a]	$\dfrac{1}{A}\dfrac{\partial\theta_\alpha}{\partial\alpha} + \dfrac{\theta_\beta}{AB}\dfrac{\partial A}{\partial\beta} - \dfrac{1}{R_\alpha}\left(\dfrac{1}{A}\dfrac{\partial u}{\partial\alpha} + \dfrac{v}{AB}\dfrac{\partial A}{\partial\beta} + \dfrac{w}{R_\alpha}\right)$	$\dfrac{1}{B}\dfrac{\partial\theta_\beta}{\partial\beta} + \dfrac{\theta_\alpha}{AB}\dfrac{\partial B}{\partial\alpha} - \dfrac{1}{R_\beta}\left(\dfrac{u}{AB}\dfrac{\partial B}{\partial\alpha} + \dfrac{1}{B}\dfrac{\partial v}{\partial\beta} + \dfrac{w}{R_\beta}\right)$
Donnell, Mushtari	$-\dfrac{1}{A}\dfrac{\partial}{\partial\alpha}\left(\dfrac{1}{A}\dfrac{\partial w}{\partial\alpha}\right) - \dfrac{1}{AB^2}\dfrac{\partial A}{\partial\beta}\dfrac{\partial w}{\partial\beta}$	$-\dfrac{1}{B}\dfrac{\partial}{\partial\beta}\left(\dfrac{1}{B}\dfrac{\partial w}{\partial\beta}\right) - \dfrac{1}{A^2B}\dfrac{\partial B}{\partial\alpha}\dfrac{\partial w}{\partial\alpha}$

[a] Terms given for the Vlasov theory correspond only to the linear $(n = 1)$ terms of table 7

Table 6. Change in twist $\kappa_{\alpha\beta}$ of the middle surface

Byrne, Flügge, Lur'ye, Goldenveizer, Novozhilov, Timoshenko, Love	$\dfrac{A}{B}\dfrac{\partial}{\partial\beta}\left(\dfrac{\theta_\alpha}{A}\right) + \dfrac{B}{A}\dfrac{\partial}{\partial\alpha}\left(\dfrac{\theta_\beta}{B}\right) + \dfrac{1}{R_\alpha}\left(\dfrac{1}{B}\dfrac{\partial u}{\partial\beta} - \dfrac{v}{AB}\dfrac{\partial B}{\partial\alpha}\right) + \dfrac{1}{R_\beta}\left(\dfrac{1}{A}\dfrac{\partial v}{\partial\alpha} - \dfrac{u}{AB}\dfrac{\partial A}{\partial\beta}\right)$
Reissner, Berry, Naghdi	$\dfrac{A}{B}\dfrac{\partial}{\partial\beta}\left(\dfrac{\theta_\alpha}{A}\right) + \dfrac{B}{A}\dfrac{\partial}{\partial\alpha}\left(\dfrac{\theta_\beta}{B}\right)$
Vlasov[a]	$\left(\dfrac{1}{R_\alpha} - \dfrac{1}{R_\beta}\right)\left[\dfrac{A}{B}\dfrac{\partial}{\partial\beta}\left(\dfrac{u}{A}\right) - \dfrac{B}{A}\dfrac{\partial}{\partial\alpha}\left(\dfrac{v}{B}\right)\right] - \dfrac{B}{A}\dfrac{\partial}{\partial\alpha}\left(\dfrac{1}{B^2}\dfrac{\partial w}{\partial\beta}\right) - \dfrac{A}{B}\dfrac{\partial}{\partial\beta}\left(\dfrac{1}{A^2}\dfrac{\partial w}{\partial\alpha}\right)$
Sanders	$\dfrac{A}{B}\dfrac{\partial}{\partial\beta}\left(\dfrac{\theta_\alpha}{A}\right) + \dfrac{B}{A}\dfrac{\partial}{\partial\alpha}\left(\dfrac{\theta_\beta}{B}\right) + \dfrac{1}{2AB}\left(\dfrac{1}{R_\beta} - \dfrac{1}{R_\alpha}\right)\left(\dfrac{\partial Bv}{\partial\alpha} - \dfrac{\partial Au}{\partial\alpha}\right)$
Mushtari-Donnell	$-\dfrac{B}{A}\dfrac{\partial}{\partial\alpha}\left(\dfrac{1}{B^2}\dfrac{\partial w}{\partial\beta}\right) - \dfrac{A}{B}\dfrac{\partial}{\partial\beta}\left(\dfrac{1}{A^2}\dfrac{\partial w}{\partial\alpha}\right)$

[a] Terms given for the Vlasov theory correspond only to the linear $(n = 1)$ terms of table 7

point on the cylindrical reference surface. Suppose that for the infinite cylinder we have displacements $u = 0$ $v = v_n \cos n\theta$, and $w = w_n \sin n\theta$, in which v_n and w_n do not depend on x. From eqns (335)

$$e_\alpha = e_x = u' = 0; \quad e_\beta = e_\theta = \frac{1}{R}\dot{v} + \frac{w}{R}$$

$$= \frac{1}{R}(-nv + w_n) \sin n\theta$$

$$e_{\alpha\beta} = e_{x\theta} = \frac{1}{R}\dot{u} + v' = 0. \tag{345}$$

For inextensional deformations

$$e_\theta = \frac{1}{R}(-nv_n + w_n) \sin n\theta = 0 \tag{346}$$

which leads to

$$v_n = w_n/n. \tag{347}$$

From Table 5 and eqns (343) the curvature change expressions of Byrne, Flügge, etc. yield

$$\kappa_\alpha = \kappa_x = -w''; \quad \kappa_\beta = \kappa_\theta = \frac{1}{R^2}(\dot{v} - \ddot{w}). \tag{348}$$

With $v = v_n \cos n\theta$, $w = w_n \sin n\theta$ and no x-dependence, we have

$$\kappa_x = 0; \quad \kappa_\theta = \frac{1}{R^2}(-v_n n + w_n n^2) \sin n\theta \tag{349}$$

which, for inextensional deformation ($v_n = w_n/n$) yields

$$\kappa_x = 0; \quad \kappa_\theta = \frac{1}{R^2}(n^2 - 1)w_n \sin n\theta. \tag{350}$$

The expressions of Donnell in Table 5 yield

$$\kappa_\alpha = \kappa_x = -w'' = 0; \quad \kappa_\beta = \kappa_\theta = -\frac{1}{R^2}\ddot{w} = \frac{n^2}{R^2}w_n \sin n\theta. \tag{351}$$

For $n = 2$ the expression for κ_θ is 33% in error. This error occurs when, for example, one uses Donnell theory to calculate buckling loads of long cylindrical shells under external pressure, for which the buckling mode corresponds to $n = 2$. The buckling modal displacements correspond to nearly inextensional hoop strain, so that the relationship (347) holds with good accuracy. For shells which buckle with higher values of n, the Donnell–Mushtari theory is more accurate.

Twist, $\kappa_{\alpha\beta}$. Table 6 shows comparisons of the expressions for twist $\kappa_{\alpha\beta}$ of the reference surface. The Vlasov and the Donnell–Mushtari expressions differ from the others for the same reasons given in the discussion of κ_α and κ_β. The Reissner, Berry, Naghdi expression differs because of neglect of z/R_α, z/R_β compared to unity at an earlier stage in the derivation than in the Byrne, Flügge *et al.* formulation. Sanders' expression is derived through correction of that of Reissner *et al.* by addition of the term with the factor $(1/R_\beta - 1/R_\alpha)$ to eliminate non-zero $\kappa_{\alpha\beta}$ arising from rigid body rotation. Kraus[78] demonstrates that the kinematic relations of Byrne, Flügge, Goldenveizer, Lur'ye, and Novoshilov are consistent

with regard to rigid body motions. Kadi[81] found the same for the theories of Love, Timoshenko, and Vlasov, but that the Donnell–Mushtari theory gives non-zero curvature changes and twist due to rigid body translations.

DIFFERENCES IN RELATIONS INVOLVING STRESSES AND STRAINS THROUGH THE THICKNESS

Total strains

Table 7 shows differences in the expressions for total strain at any point z in the wall thickness. The total strain is always represented as the sum of stretching and bending components. The expressions of Byrne *et al.* are the most general and result from application of the Kirchhoff hypothesis to the kinematic relationships of the three-dimensional theory of elasticity. In the Love, Timoshenko *et al.* theory z/R_α and z/R_β are everywhere neglected compared to unity. The theory of Vlasov represents a sort of middle ground between the Byrne *et al.* and Love *et al.* formulations in that series expansions are used for $1/(1 + z/R_\alpha)$, $1/(1 + z/R_\beta)$.

Force and moment resultants

Since the strains are known functions of the thickness coordinate (Table 7) and, given Hooke's law, the stresses are known functions of the strains, the forces acting on the edges of the shell element shown in Fig. 51 can be derived by integration of the stresses over the thickness coordinate z. If the reference surface is chosen as the middle surface and if we rigorously note the dimensions (eqns 339–341) of the slice of thickness dz shown in Fig. 51, we can derive three force resultants acting on the face perpendicular to the α coordinate

$$\begin{Bmatrix} N_\alpha \\ N_{\alpha\beta} \\ Q_\alpha \end{Bmatrix} = \int_{-h/2}^{h/2} \begin{Bmatrix} \sigma_\alpha \\ \sigma_{\alpha\beta} \\ \sigma_{\alpha z} \end{Bmatrix} \left(1 + \frac{z}{R_\beta}\right) dz \tag{352}$$

and three more force resultants acting on the face perpendicular to the β coordinate

$$\begin{Bmatrix} N_\beta \\ N_{\beta\alpha} \\ Q_\beta \end{Bmatrix} = \int_{-h/2}^{h/2} \begin{Bmatrix} \sigma_\alpha \\ \sigma_{\beta\alpha} \\ \sigma_{\beta z} \end{Bmatrix} \left(1 + \frac{z}{R_\alpha}\right) dz. \tag{353}$$

The positive directions of the force resultants are shown in Fig. 52. These forces act at the reference surface and have units of force/length.
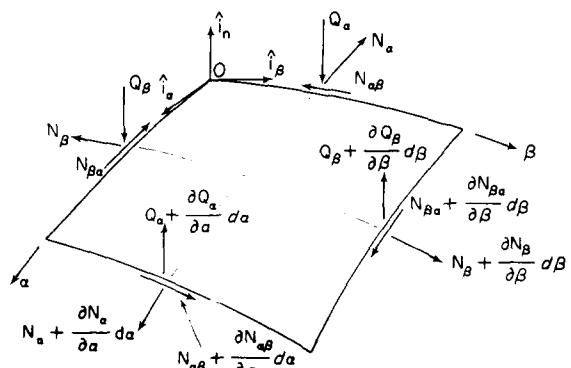
Fig. 52. Notation and positive directions of force resultants in shell coordinates.

Table 7. Total strains at any point in a shell

Theory	$\varepsilon_\alpha, \varepsilon_\beta$	$\varepsilon_{\alpha\beta}$
Byrne, Flügge, Goldenveizer, Lur'ye, Novoshilov	$\frac{1}{(1+z/R_\alpha)}\left(e_\alpha + z\kappa_\alpha\right)$ $\frac{1}{(1+z/R_\beta)}\left(e_\beta + z\kappa_\beta\right)$	$\frac{1}{(1+z/R_\alpha)(1+z/R_\beta)}\left[\left(1 - \frac{z^2}{R_\alpha R_\beta}\right)e_{\alpha\beta} + z\left(1 + \frac{z}{2R_\alpha} + \frac{z}{2R_\beta}\right)\kappa_{\alpha\beta}\right]$
Love, Timoshenko, Reissner, Naghdi, Berry, Sanders Donnell, Mushtari	$e_\alpha + z\kappa_\alpha$ $e_\beta + z\kappa_\beta$	$e_{\alpha\beta} + z\kappa_{\alpha\beta}$
Generalized Vlasov	$e_\alpha + \sum_{n=1} \kappa_{\alpha n} z^n$ $e_\beta + \sum_{n=1} \kappa_{\beta n} z^n$	$e_{\alpha\beta} + \sum_{n=1} \kappa_{\alpha\beta n} z^n$

Similar expressions for moment resultants can be derived

$$\left\{\begin{matrix} M_\alpha \\ M_{\alpha\beta} \end{matrix}\right\} = \int_{-h/2}^{h/2} \left\{\begin{matrix} \sigma_\alpha \\ \sigma_{\alpha\beta} \end{matrix}\right\} \left(1 + \frac{z}{R_\beta}\right) z \, dz$$

$$\left\{\begin{matrix} M_\beta \\ M_{\beta\alpha} \end{matrix}\right\} = \int_{-h/2}^{h/2} \left\{\begin{matrix} \sigma_\beta \\ \sigma_{\beta\alpha} \end{matrix}\right\} \left(1 + \frac{z}{R_\alpha}\right) z \, dz$$

(354)

which are shown in Fig. 53 and have dimensions moment/length. Note that even though $\sigma_{\alpha\beta} = \sigma_{\beta\alpha}$ from the symmetry of the stress tensor, the same does not hold for stress and moment resultants: $N_{\alpha\beta} \neq N_{\beta\alpha}$ and $M_{\alpha\beta} \neq M_{\beta\alpha}$ unless $R_\alpha = R_\beta$ because the areas over which the stresses $\sigma_{\alpha\beta}, \sigma_{\beta\alpha}$ act are different on the different edges of the shell element shown in Fig. 51.

Tables 8 and 9 show expressions for the stress and moment resultants in terms of middle surface strains and changes in curvature for an isotropic homogeneous shell wall. The theories of Love, Timoshenko, Reissner, Naghdi, Berry, Sanders, Mushtari, and Donnell are arrived at by indiscriminately neglecting z/R_α and z/R_β compared to unity. Novoshilov and Goldenveizer obtain resultants by taking variations of the strain energy functional and discarding selected terms. Byrne, Flügge, and Lur'ye simplify the z-integration by using series expansions for the quotients $1/(1 + z/R_\alpha)$, $1/(1 + z/R_\beta)$. Vlasov follows a similar procedure.

Fig. 53. Notation and positive directions of moment resultants in shell coordinates.

WHICH THEORY IS BEST?

In modern computerized structural analysis in which energy methods are almost universally applied to engineering shell problems it is most often advisable to avoid the use of Donnell–Mushtari theory or any theory in which rigid body motion generates finite reference surface strains or changes in curvature. The Donnell–Mushtari theory might still be applied profitably in computer-oriented optimization analyses for preliminary design. Such analyses usually involve sequential solution of many structural problems. The Donnell–Mushtari theory is computationally efficient because it permits the use of fewer unknowns in equilibrium and eigenvalue formulations. However, the analyst should be aware of the limitations illustrated by the above example of inextensional bending of a cylinder. The Donnell theory is accurate enough if the wavelength of the deformation pattern is small compared to a typical radius of curvature of the shell.

The differences attributable to retention of z/R_α, z/R_β are of little importance for most engineering problems, and it is best to choose the simplest theories in this

regard. In fact, retention of the z/R terms can lead to results that puzzle computer program users and cause them to distrust the programs they use. Two good examples have arisen in the writer's experience which caused him to remove terms involving z/R compared to unity in the BOSOR4 [18] and BOSOR5 [25] computer programs, which are now based on Sanders' equations. One example is a rather thick $(R/t = 10)$ isotropic hemispherical shell clamped at the equator and uniformly heated. Far away from the clamped boundary the stresses should be essentially zero. However, in the original versions of BOSOR4 and BOSOR5, which were based on total strain relations of the Byrne, Flügge, type in Table 7, the stresses did not die away but instead approached the values

$$\sigma(z) = \frac{E}{1 - \nu^2}\left[\frac{e_\alpha + z\kappa_\alpha}{(1 + z/R_\alpha)} + \nu\frac{e_\beta + z\kappa_\beta}{(1 + z/R_\beta)} - (1 + \nu)\alpha\Delta T\right]. \tag{355}$$

Far away from the clamped edge deformation of the uniformly heated hemisphere consists of a sum of a uniform radial (normal to surface) expansion plus a rigid body axial displacement. The rigid body displacement does not give rise to any strains or changes in curvature. From the first row of Table 5, the Byrne, Flügge *et al.* relations for κ_α and κ_β yield zero curvature change corresponding to uniform radial expansion. The strains e_α and e_β for uniform radial expansion are given, from eqns (335a,b), by

$$e_\alpha = e_\beta = w/R = \alpha\Delta T. \tag{356}$$

At the extreme fibers, $z = \pm t/2$, the stress $\sigma(z)$ in eqn (355) is therefore given by the spurious values

$$\sigma(\pm t/2) = \mp\frac{E}{1 - \nu}\alpha\Delta T(t/2R). \tag{357}$$

If $E = 10^7$ psi, $\nu = 0.3$, $\alpha = 10^{-5}$, $\Delta T = 300°$, $t/R = 0.1$ the maximum stresses are about -2000 psi at the outer fiber and $+2000$ psi at the inner fiber, values large enough to stimulate a program user to telephone the program developer. This error arises because actually the radial displacement due to uniform heating is not uniform throughout the thickness as the theory implies, but increases linearly with z as one moves radially outward from the reference surface. This linear variation of w with z gives rise to $1 + z/R$ terms in the numerators of the first two terms in eqn (355) which cancel the like terms in the denominators, resulting in a correct prediction of zero stress far from the clamped edge of the uniformly heated hemispherical shell. However, the same correct result is obtained simply by neglecting the z/R terms in eqn (355) and simultaneously ignoring the true nature of the linearly varying radial displacement, as the Kirchhoff hypothesis requires. This example demonstrates that it is inconsistent to include z/R terms compared to unity, as in the first row of Table 7, while neglecting the effect of extension of the normal to reference surface.

The second example in which "small" z/R terms proved troublesome in BOSOR4 involved the axisymmetric shell structure shown in Fig. 54(a) subjected to an axial load V. The shell is a wheel rim. Half of the wheel

Table 8. Force resultants according to the various theories[a]

Theory	$(1-\nu^2)N_\alpha/Eh$	$(1-\nu^2)N_\beta/Eh$	$2(1+\nu)N_{\alpha\beta}/Eh$	$2(1+\nu)N_{\beta\alpha}/Eh$
Byrne, Flügge, Lur'ye	$e_\alpha + \nu e_\beta - \frac{h^2}{12}\left(\frac{1}{R_\alpha}\right.$ $\left. - \frac{1}{R_\beta}\right)\left(\kappa_\alpha - \frac{e_\alpha}{R_\alpha}\right)$	$e_\beta + \nu e_\alpha - \frac{h^2}{12}\left(\frac{1}{R_\beta}\right.$ $\left. - \frac{1}{R_\alpha}\right)\left(\kappa_\beta - \frac{e_\beta}{R_\beta}\right)$	$e_{\alpha\beta} - \frac{h^2}{12}\left(\frac{1}{R_\alpha}\right.$ $\left. - \frac{1}{R_\beta}\right)\left(\frac{\tau}{2} - \frac{e_{\alpha\beta}}{R_\alpha}\right)$	$e_{\alpha\beta} - \frac{h^2}{12}\left(\frac{1}{R_\beta}\right.$ $\left. - \frac{1}{R_\alpha}\right)\left(\frac{\tau}{2} - \frac{e_{\alpha\beta}}{R_\beta}\right)$
Goldenveizer, Novozhilov	$e_\alpha + \nu e_\beta$	$e_\beta + \nu e_\alpha$	$e_{\alpha\beta} + \frac{h^2}{12R_\beta}\tau$	$e_{\alpha\beta} + \frac{h^2}{12R_\alpha}\tau$
Love, Timoshenko, Reissner, Berry, Naghdi, Mushtari, Donnell, Sanders	$e_\alpha + \nu e_\beta$	$e_\beta + \nu e_\alpha$	$e_{\alpha\beta}$	$e_{\alpha\beta}$
Vlasov	Same as Byrne, Flügge, Lur'ye	Same as Byrne, Flügge, Lur'ye	$e_{\alpha\beta} - \frac{h^2}{24}\left(\frac{1}{R_\alpha} - \frac{1}{R_\beta}\right)\tau$	$e_{\alpha\beta} - \frac{h^2}{24}\left(\frac{1}{R_\beta} - \frac{1}{R_\alpha}\right)\tau$

[a]Note: $\tau = \kappa_{\alpha\beta}$.

Table 9. Moment resultants according to the various theories[a]

| Theory	$12(1-\nu^2)M_\alpha/Eh^3$	$12(1-\nu^2)M_\beta/Eh^3$	$24(1+\nu)M_{\alpha\beta}/Eh^3$	$24(1+\nu)M_{\beta\alpha}/Eh^3$
Byrne, Flügge, Lur'ye	$\kappa_\alpha + \nu\kappa_\beta - \left(\frac{1}{R_\alpha} - \frac{1}{R_\beta}\right)e_\alpha$	$\kappa_\beta + \nu\kappa_\alpha - \left(\frac{1}{R_\beta} - \frac{1}{R_\alpha}\right)e_\beta$	$\tau - \frac{e_{\alpha\beta}}{R_\alpha}$	$\tau - \frac{e_{\alpha\beta}}{R_\beta}$
Goldenveizer, Novozhilov, Love, Timoshenko, Reissner, Naghdi, Berry, Mushtari, Donnell, Sanders	$\kappa_\alpha + \nu\kappa_\beta$	$\kappa_\beta + \nu\kappa_\alpha$	τ	τ
Vlasov	Same as Flügge, Byrne, Lur'ye	Same as Byrne, Flügge, Lur'ye	$\tau + \frac{e_{\alpha\beta}}{R_\beta}$	$\tau + \frac{e_{\alpha\beta}}{R_\alpha}$

[a]Note: $\tau = \kappa_{\alpha\beta}$.
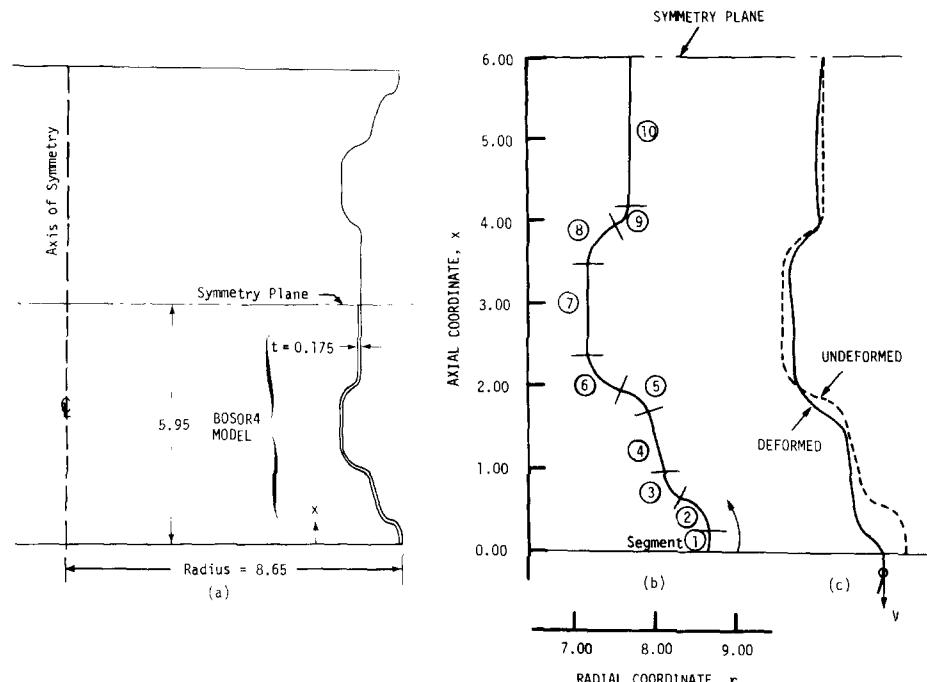
Fig. 54. Wheel rim modeled as shell with 10 segments: (a) dimensions; (b) model for analysis with BOSOR4; (c) deformation due to axial load V.
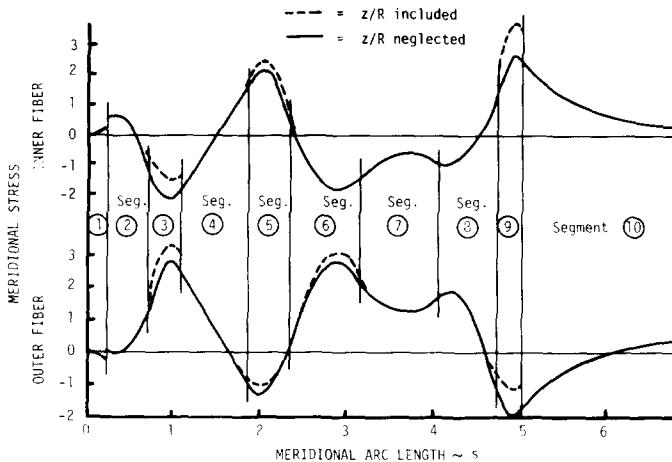

Fig. 55. Inner and outer fiber stresses along meridian of wheel rim predicted from theories including and neglecting z/R compared to unity (see eqn (339)).

rim is modeled as a shell with 10 segments as shown in Fig. 54(b). Some of these segments have small ratios of meridional curvature R_1 to thickness t. For example, in Segment ⑨ $R_1/t = 1.29$. In Segments ②, ③, ⑤, ⑥, and ⑧ $R_1/t = 2.14, 2.10, 2.42, 3.36$, and 3.36, respectively. Use of thin shell theory for prediction of stresses in these segments is questionable. Figure 54(c) shows how the wheel rim deforms under uniform axial load V. The extreme fiber stresses predicted in computer runs with and without the z/R terms are plotted in Fig. 55. The discontinuities in the "z/R included" curves are due to large discontinuities of z/R at segment boundaries. These discontinuities stimulated a program user to call the program developer, who decided to eliminate the offending z/R terms from the BOSOR4 and BOSOR5 computer programs permanently.

REFERENCES

1. G. A. Cohen, User document for computer programs for ring-stiffened shells of revolution, NASA CR-2086, 1973; Computer analysis of ring-stiffened shells of revolution, NASA CR-2085, 1973; Computer program for analysis of imperfection sensitivity of ring-stiffened shells of revolution," NASA CR-1801, 1971; National Aeronautics and Space Administration, Washington, D.C.

2. A. Kalnins, Users Manual for KSHEL Computer Programs (1970), available from Dr. Kalnins, Lehigh University, Pa. Also see Free vibration, static and stability analysis of thin elastic shells of revolution, AFFDL-TR-68-144, March 1969, Wright-Patterson Air Force Base, Ohio.

3. V. Svalbonas, Numerical analysis of stiffened shells of revolution, NASA CR-2273, 1973, National Aeronautics and Space Administration, Washington, D.C.

4. David Bushnell, Large deflection elastic–plastic creep analysis of axisymmetric shells. *Numerical Solution of Nonlinear Structural Problems*, ASME **AMD 6**, 103–138 (1973).

5. J. A. Stricklin, W. E. Haisler and W. A. von Riesemann, Formulation, computation, and solution procedures for material and/or geometric nonlinear structural analysis by the finite element method, SC-CR-72 3102, Sandia Laboratories, Albuquerque, New Mexico, July 1972.

6. R. M. Jones, *Mechanics of Composite Materials*. McGraw-Hill, New York (1975).

7. J. E. Ashton, J. C. Halpin and P. H. Petit, *Primer on Composite Materials*, Technomic, Connecticut (1969).

8. J. E. Ashton and J. M. Whitney, *Theory of Laminated Plates*. Progress in Materials Science Series, Vol. IV. Technomic, Connecticut (1970).

9. A. E. H. Love, *Phil. Trans., Roy. Soc.* (Ser. A), **179** (1888).

10. V. V. Novoshilov, *Foundations of the Nonlinear Theory of Elasticity*. Graylock Press (1953).

11. Sanders, J. Lyell, Jr., Nonlinear theories for thin shells. *Quart. Appl. Math.* **21**, 21–36 (1963).

12. R. H. Gallagher, Analysis of plate and shell structures. *Proc. Symp. Appl. Finite Element Methods in Civil Engng*, (Edited by Rowan, William H., Jr. and Robert M. Hackett), Vanderbilt University and the American Society of Civil Engineers (1969).

13. R. H. Gallagher, Applications of finite element analysis. *Advances in Computational Methods in Structural Mechanics and Design* (Proc. 2nd U.S.-Japan Seminar on Matrix Methods of Structural Analysis and Design), (Edited by J. T. Oden, R. W. Clough and Y. Yamamoto) University of Alabama Press, Huntsville, Alabama, pp. 641–678 (1972).

14. R. H. Gallagher, Geometrically nonlinear finite element analysis. *Specialty Conference on the Finite Element Method in Civil Engineering*. McGill University (1972).

15. J. L. Brombolich and P. L. Gould, Finite element analysis of shells of revolution by minimization of the potential energy functional. *Proc. Symp. on Appl. of Finite Element Methods in Civil Engng* (Edited by W. H. Rowan, Jr. and R. M. Hackett) Vanderbilt University and the ASCE, pp. 279–307 (1969).

16. E. L. Wilson, R. L. Taylor, W. P. Doherty and J. Ghaboussi, Incompatible displacement models. *Numerical and Computer Methods in Structural Mechanics* (Edited by S. J. Fenves, N. Perrone, A. R Robinson and W. C. Schnobrich), pp. 43-57. Academic Press, New York (1973).

17. D. E. Johnson, A difference based variational method for shells. *Int. J. Solids Structures* **6**, 699–724 (1970).

18. D. Bushnell, Stress, stability, and vibration of complex branched shells of revolution. *Comput. Structures* **4**, 399–435 (1974).

19. D. Bushnell, Finite-difference energy models versus finite element models: two variational approaches in one computer program. *Numerical and Computer Methods in Structural Mechanics* (Edited by S. J. Fenves, N. Perrone, A. R. Robinson and W. C. Schnobrich), pp. 291–336. Academic Press, New York (1973).

20. M. Khojasteh-Bakht, Analysis of elastic–plastic shells of revolution under axisymmetric loading by the finite element method. Ph.D. Dissertation, Department of Civil Engineering, University of California, Berkeley, CA 1967. (Also published as SESM Report 67-8.)

21. M. Baruch and J. Singer Effect of eccentricity of stiffeners on the general instability of stiffened cylindrical shells under hydrostatic pressure. *J. Mech. Engng Sci.* **5**, 23–27 (1963).

22. B. O. Almroth and F. A. Brogan, Bifurcation buckling as an approximation of the collapse load for general shells. *AIAA J.* **10**, 463–467 (1972).

23. D. Bushnell, B. O. Almroth and F. Brogan, Finite-difference energy method for nonlinear shell analysis. *Comput. Structures* **1**, 361–387 (1971).

24. W. Pilkey, K. Saczalski and H. Schaeffer (Eds), *Structural Mechanics Computer Programs: Surveys, Assessments, and Availability*. University Press of Virginia, Charlottesville (1974).

25. D. Bushnell, BOSOR5—Program for buckling of elastic-plastic complex shells of revolution including large deflections and creep. *Comput. Structures* **6**, 221–239 (1976).

26. D. Bushnell, *Plastic Buckling, Pressure Vessels and Piping: Design Technology–1982, A Decade of Progress*, (Edited by S. Y. Zamrik and D. Dietrich) pp. 47–117. ASME, New York (1982).

27. D. Bushnell Analysis of ring-stiffened shells of revolution under combined thermal and mechanical loading. *AIAA J.* **9**, 401–410 (1971).

28. D. Bushnell, Analysis of buckling and vibration of ring-stiffened, segmented shells of revolution. *Int. J. Solids Structures* **6**, 157–181 (1970).

29. G. A. Cohen, Conservativeness of a normal pressure field acting on a shell. *AIAA J.* **4**, 1886–1887 (1966).

30. J. J. Kotanchik, R. P. Yeghiayan, E. A. Witmer and B. A. Berg, The transient linear elastic response analysis of complex thin shells of revolution subjected to arbitrary external loadings, by the finite-element program, SABOR5-DRASTIC. SAMSO TR 70-206, ASRL TR 146-10, Aeroelastic and Struct. Res. Lab., MIT, April 1970.

31. P. M. Mebane and J. A. Stricklin, Implicit rigid body motion in curved finite elements. *AIAA J.* **9**, 344 (1971).

32. H. M. Adelman, D. S. Catherines and W. C. Jr. Walton, A method for computation of vibration modes and frequencies of orthotropic thin shells of revolution having general meridional curvature. NASA TN D-4972, Lengley Res. Center, Hampton, VA Jan. 1969.

33. M. Stein, The effect on the buckling of perfect cylinders of prebuckling deformations and stresses induced by edge support. NASA TN D-1510, p. 217. Langley Res. Center, Hampton, VA, Dec. 1962.

34. D. Bushnell, BOSOR4: program for stress, buckling, and vibration of complex shells of revolution. *Structural Mechanics Software Series*, (Edited by N. Perrone and W. Pilkey), Vol. 1, pp. 11–143. University Press of Virginia, Charlottesville, VA (1977).

35. D. Bushnell, Stress, buckling, and vibration of hybrid bodies of revolution. *Comput. Structures* **7**, 517–537 (1977).

36. G. E. Strickland, W. A. Loden and S. K. Ferriera, WASP—a digital computer program for the linear elastic analysis of hybrid symmetrically loaded bodies of revolution, Report 9-87-68-2, Lockheed Missiles & Space Co., Sunnyvale, CA, June 1968.

37. Z. Zudans, Analysis of elastically coupled shells on elastic foundation by hybrid method. *Nuclear Engng Design* **20**, 85–129 (1972).

38. J. Ergatoudis, B. M. Irons and O. C. Zienkiewicz, Curved, isoparametric, quadrilateral elements for finite element analysis. *Int. J. Solids Structures* **4**, 31–42 (1968).

39. S. Ahmad, B. M. Irons and O. C. Zienkiewicz, Curved thick shell and membrane elements with particular reference to axisymmetric problems. *Proc. 2nd Conf. on Methods in Structural Mechanics*, Wright-Patterson Air Force Base, OH (1968).

40. S. F. Pawsey, The analysis of moderately thick to thin shells by the finite element method. *UCSESM* 70-12, University of California, Berkeley, CA, Aug. 1970.

41. P. K. Larsen and E. P. Popov, Elastic–plastic analysis of axisymmetric solids using isoparametric finite elements. UCSESM 71-2, University of California, Berkeley, CA, Jan. 1971.

42. K. J. Bathe, E. L. Wilson and R. H. Iding, NONSAP—a structural analysis program for static and dynamic response of nonlinear systems. UCSESM 74-3, University of California, Berkeley, Feb. 1974.

43. R. S. Dunham and E. B. Becker, TEXGAP—the Texas grain analysis program. TICOM Rep. 73-1, The Texas Institute for Computational Mech., University of Texas at Austin, Aug. 1973.

44. P. Sharifi and D. N. Yates, Nonlinear thermo-elastic-plastic and creep analysis by the finite element method. *AIAA J.* **12**, 1210–1215 (1974).

45. G. Ferguson and N. Cyr, "DIAL-Structural Analysis System, User's Manual, Unnumbered Lockheed Missiles and Space Company Report, Sept. 20, 1982.
46. M. B. Marlow, FARSS User's Manual, unnumbered Lockheed Missiles & Space Company, Inc. Report, 1974.
47. J. C. Speare, Discrete-element static analysis of core-stiffened shells of revolution for asymmetric mechanical loading. ASRL TR 146-5, SAMSO TR 68-400, Aeroelastic & Structures Research Laboratory, M.I.T., Cambridge, Mass, Sept. 1968.
48. A. P. Cappelli, G. L. Agrawal and V. E. Romero, EPAD, a computer program for the elastic plastic analysis of domed structures and arbitrary solids of revolution subjected to asymmetrical loadings. Service Bureau Corporation, Inglewood, California, AFWL-TR-69-146, Air Force Weapons Laboratory, Kirtland AFB, New Mexico, Feb. 1970.
49. S. Ghosh and E. Wilson, Dynamic stress analysis of axisymmetric structures under arbitrary loading. Earthquake Engineering Res. Center Rep. EERC/69-10, Sept. 1969.
50. F. C. P. Yin, Discrete element analysis of core-stiffened shells of revolution. M.I.T. Aeroelastic & Structures Research Lab., TR 139-8, Feb. 1967.
51. B. M. Irons, Numerical integration applied to the finite element method. *Int. Symp. on the Use of Electronic Digital Computers in Structural Engineering*, Working Session No. 4, Paper No. 19, University of Newcastle (July 1966).
52. O. C. Zienkiewicz, Isoparametric and applied numerically integrated elements, a review. *Numerical and Computer Methods in Structural Mechanics* (Edited by S. J. Fenves, N. Perrone, R. Robinson and W. C. Schnobrich), pp. 13-41. Academic Press, New York (1973).
53. J. A. Stricklin, W. E. Haisler and W. A. von Riesemann, Formulation, computation, and solution procedures for material and/or geometric nonlinear structural analysis by finite element method. SC-CR-72-3102, Sandia Labs., Albuquerque, NM, July 1972.
54. D. Bushnell, Stress, buckling, and vibration of hybrid bodies of revolution, Vol. I. Analysis, LMSC Report D501503, Lockheed Missiles & Space Co., Inc., Palo Alto, CA (March 1976).
55. V. V. Novoshilov, *Foundations of the Nonlinear Theory of Elasticity*, Chap. 1. Graylock Press, Rochester, NY (1953).
56. A. W. Leissa, Vibration of shells. NASA SP-288, Chap. 1, 1973.
57. L. H. Donnell, Stability of thin walled tubes under torsion. NACA Rep. 479, 1933.
58. L. H. Donnell, A discussion of thin shell theory. *Proc. 5th Int. Congr. Appl. Mech.* (1938).
59. Kh. M. Mushtari, On the stability of cylindrical shells subjected to torsion. *Trudy Kaz. avais, in-ta*, Vol. 2, in Russian (1938).
60. Kh. M. Mushtari, Certain generalizations of the theory of thin shells. *Izv. Fiz. Mat. ob-va. Pri Kaz., un-te* 11, in Russian (1938).
61. A. E. H. Love, *A Treatise on the Mathematical Theory of Elasticity*, 1st Edn. Cambridge University Press (1892);, 4th Edn. Dover Pub., Inc. New York (1944).
62. A. E. H. Love, The small free vibrations and deformations of a thin elastic shell. *Phil. Trans. Roy. Soc.*, London, ser. A, 179, 491-549 (1888).
63. S. Timoshenko, *Theory of Plates and Shells*. McGraw-Hill, New York (1959).
64. E. Reissner, A new derivation of the equations of the deformation of elastic shells. *Am. J. Math.* 63, 177-184 (1941).
65. P. M. Naghdi and J. G. Berry, On the equations of motion of cylindrical shells. *J. Appl. Mech.* 21, 160-166 (1964).
66. V. Z. Vlasov, Osnovnye differentsialnye Uravnenie obshche teorii uprugikh obolochek. *Prikl. Mat. Metkh.* 8 (1944). (English translation: NACA TM 1241, Basic Differential Equations in the General Theory of Elastic Shells, Feb. 1951.)
67. V. Z. Vlasov, Obshchaya teoriya obolochek; yeye prilozheniya v tekhnike. *Gos. Izd. Tekh.-Teor. Lit.*, Moscow-Leningrad (1949). (English translation: NASA TT F-99, General Theory of Shells and Its Applications in Engineering, April 1964.)
68. J. L. Sanders, Jr., An improved first approximation theory for thin shells. NASA TR-R24, 1959.
69. R. Byrne, Theory of small deformations of a thin elastic shell. *Seminar Reports in Math.*, University of California Pub. in Math, N.S. vol. 2, No. 1, pp. 103-152 (1944).
70. W. Flügge, *Statik und Dynamik der Schalen*. Julius Springer, Berlin (1934). Reprinted by Edwards Brothers, Inc., Ann Arbor, Michigan (1943).
71. W. Flügge, *Stresses in Shells*. Springer-Verlag, Berlin (1962).
72. A. L. Goldenveizer, *Theory of Thin Shells*. Pergamon Press, New York (1961).
73. A. I. Lur'ye, General theory of elastic shells. *Prikl. Mat. Mekh* 4, 7-34 (1940), in Russian.
74. V. V. Novozhilov, *The Theory of Thin Elastic Shells*. Noordhoff, Groningen, The Netherlands (1964).
75. W. T. Koiter, A consistent first approximation in the general theory of thin elastic shells. *Proc. Symp. on Theory of Thin Elastic Shells*, I.U.T.A.M., Delft, 24-28 Aug. 1959, North Holland Pub. Co., Amsterdam, pp. 12-33 (1960).
76. A L. Goldenveizer, Method for justifying and refining the theory of shells (survey of recent results). *Appl. Math. Mech.* (transl. of *Prikl. Mat. Mekh.*), 32, 704-718 (1968).
77. J. M. Klosner and H. S. Levine, Further comparison of elasticity and shell theory solutions. *AIAA J.* 4, 467-480 (1966).
78. H. Kraus, *Thin Elastic Shells*. Wiley, New York (1967).
79. P. M. Naghdi, A survey of recent progress in the theory of elastic shells. *Appl. Mech. Rev.* 9, 365-367 (1956).
80. A. Kalnins, Dynamic problems of elastic shells. *Appl. Mech. Rev.* 18, 867-872 (1965).
81. A. S. Kadi, A study and comparison of the equations of thin shell theories. Dissertation, Ohio State University, June 1970.